DETERMINATION OF DISSOLUTION RATES OF ROCKS/MINERALS BY LABORATORY EXPERIMENTS

A THESIS

Submitted in partial fulfilment of the requirements for the award of the degree of

DOCTOR OF PHILOSOPHY

in

EARTH SCIENCES

By

SRI KRISHAN YADAV

DEPARTMENT OF EARTH SCIENCES
INDIAN INSTITUTE OF TECHNOLOGY ROORKEE
ROORKEE-247 667 (INDIA)

JULY, 2007

INDIAN INSTITUTE OF TECHNOLOGY ROORKEE
ROORKEE

CANDIDATE'S DECLARATION

I hereby certify that the work which is being presented in this thesis entitled **DETERMINATION OF DISSOLUTION RATES OF ROCKS/MINERALS BY LABORATORY EXPERIMENTS** in partial fulfilment of the requirements for the award of the Degree of Doctor Of Philosophy, submitted in the Department of Earth Sciences of the Indian Institute of Technology Roorkee, Roorkee is an authentic record of my own work carried out during the period from January, 2004 to July, 2007 under the supervision of Dr. G. J. Chakrapani, Associate Professor, Department of Earth Sciences, Indian Institute of Technology Roorkee, Roorkee.

The matter presented in this thesis has not been submitted by me for the award of any other degree of this or any other Institute.

Sri Krishan Yadav 17/7/07

(SRI KRISHAN YADAV)

This is to certify that the above statement made by the candidate is correct to the best of my knowledge.

G. J. Chakrapani

Date: July, 2007

(Dr. G. J. Chakrapani) 17/7/07
Associate Professor

The Ph.D Viva Voce Examination of **Mr. Sri Krishan Yadav**, Research Scholar has been held on 17th October 2007.

G. J. Chakrapani
Signature of Supervisor 17/10/07

Signature of External Examiner 17/10/07

ABSTRACT

Rocks and minerals on the Earth's surface weather at differential rates and are primarily responsible for the geochemistry of natural waters. Rock weathering is important in causing weakened surfaces of rock strata, thereby causing landslides and associated hazards. Qualitative understanding of rates of rock/mineral weathering is essential for many aspects of geologic phenomena including crust evolution, soil formation, river bank stabilisation etc. Determination of dissolution rates of rocks, minerals and soils in laboratory simulated conditions help in quantifying the data, which may be used in weathering models.

In the present study, organic and inorganic buffer solutions have been used in batch experiments (rocks and minerals) and column dissolution experiments (soils) at 5^0 and 25^0C. A few representative rock samples and soil columns were collected from the Alaknanda-Bhagirathi river basins in the Himalayas. The samples invariably underwent differential dissolution rates controlled primarily by pH and temperature. Water samples (sampled weekly) collected over one year at two locations, one from the Alaknanda river and the other from the Bhagirathi river were analyzed to observe possible temporal and spatial variations in concentration of dissolved phases and elemental flux rates were estimated. High Ca/Si flux ratio in both Alaknanda and Bhagirathi rivers indicates dominance of carbonate weathering. Laboratory derived dissolution rates of representative lithologies at pH 8.4 and temperature 25^0C is much lower compared to the average Ca - and SiO_2 -flux rates, whereas carbonate dissolution ($\sim 10^{-12}$ $molm^2s^{-1}$) is higher compared to the dissolution rates of rock types determined in the laboratory. At lower pH (2.2 and 4.2), acidity dominates over temperature in regulating dissolution rates of rocks whereas, in alkaline

condition (pH = 8.4), temperature is the dominant factor over pH. At pH 8.4 and temperature 25^0C, dissolution rate of soils is >20 times slower compared to carbonate dissolution rate. At pH 8.4, activation energy (E_a) is highly controlled by change in temperature, whereas at pH 2.2 and 4.2, it has negligible effect on temperature change.

The thesis is presented in five chapters. Chapter 1 presents the background of the chemical weathering process with special emphasis on dissolution reactions of carbonate and silicate rocks/minerals, major dissolution reactions occurring on the earth's surface, their mechanism and controlling factors, and its significance on watershed to global scale. It also highlights major work done by various workers on laboratory simulated dissolution rates of rocks and minerals and also on the chemical weathering of Alaknanda and Bhagirathi river basins. The primary objectives of the thesis are also enumerated. Chapter 2 deals with the geological details and sampling locations of the rocks, soil and water undertaken in the present study. Sample characteristics in terms of its mineralogical and chemical compositions have also been discussed using various parameters. Chapter 3 deals with the methodology followed for sample collection of rocks, soil and water in the field; preparation of buffers (pH of 8.4, 4.2 and 2.2) using different standard salts and preparation of samples (rocks/soil) and experimental set-up (batch and column) for carrying out dissolution experiment in the laboratory. The various instruments which have been used during the course of experimentation have also been discussed in this chapter. Chapter 4 presents the results and discussion segment of the thesis. Temporal and spatial variations in the geochemistry of the Alaknanda and Bhagirathi river water at two locations have been discussed and elemental flux rates calculated.

Laboratory simulated dissolution rates of representative samples of carbonates, silicate rocks and soil are calculated and the role of temperature, pH, ligands and surface dislocation sites regulating dissolution rates have been discussed. Chapter 5 outlines the major conclusions derived from the present study. The thesis is endowed with 32 figures, 11 tables, references and appendices.

ACKNOWLEDGEMENTS

I would like to express my deepest thanks and gratitude to my supervisor **Dr. Govind Joseph Chakrapani** for his guidance, support, fruitful suggestions, constructive criticism and his independence oriented supervision that has given me more insight into the field of scientific research and writing of this thesis and research manuscripts.

I would also like to thank to **Prof. V.N. Singh,** former Head of the Department of Earth Sciences and **Prof. R.P. Gupta**, present Head of the Department of Earth Sciences for their continuous administrative support, recommendations and useful suggestions in every possible way that helped me accomplish the thesis work as per the drawn schedule. I deeply appreciate the facilitation of successive Deans (Post Graduate Studies and Research), **Prof. R.N.Goyal and Prof. Hari Om Gupta** and **Mr. Salim Ahmed and the office staff at Dean PGS&R.**

I wish to express my special thanks and appreciation to the Ministry of Human Resource Development (MHRD), Government of India (GoI) for providing me financial help in the form of research fellowship and contingent grant for the study.

I thank all the other members of my thesis advisory committee, **Prof. C.S.P. Ojha, Dr. A.K. Sen, Prof. R.G.S. Sastry and Prof. Sri Niwas**.

I am extremely thankful to **Prof. Kailash Chandra and Prof. A.K. Choudhary,** Institute Instrumentation Centre (IIC) IITR, for their suggestions and cooperation regarding instrumentation and analysis. My sincere thanks also go to Mr. **Rajiv**

Juyal and Saini *ji* for helping me in analyzing the samples with Atomic Absorption Spectrophotometer (AAS) and X-ray diffractometer (XRD).

I express my sincere thanks to **Dr. N.K. Saini**, Wadia Institute of Himalayan Geology (WIHG) Dehradun; **Sushanta Pal and S. Karthikeyan**, Advanced Centre for Material Science (ACMS) IITK for their help in analysis of samples for Major oxides, BET surface area and BJH pore volume distribution measurement, grain surface morphology with estimation of surface chemistry respectively. **Dr. Oleg. S. Pokrovsky**, LMTG-Toulouse was very kind in providing calcite and dolomite samples.

The help extended by the technical and non-technical staffs of the Department especially **Nair *ji*, Rakesh *ji*, Saini *ji*, Mishra *ji*, Agrawal *ji*, Kamesh *ji* , Rahil *ji*, Najim *ji*, Babu Ram *ji*, Ram Karan *ji*, *Vijay and all others*** is duly acknowledged.

I am also deeply thankful to my lab mates, **Puru, Preetam, Ravi, Narendra Meena, Harish Gupta and Manoj Gupta,** for their gracious criticism, valuable discussions and assistance in giving final shape to my thesis. I express my sincere appreciation to my seniors and friends, **Rajeev Kumar, Rakhi-Ranjan, Suman *Bhai*, Vinay Sharma, Ritu, Saravanan, Rajan Choudhary, Diku, Devashish, Ajanta, Param, Deepak Tyagi, Krishna, Ramesh, and Rawat ji** for their continuous support, cooperation and encouragement.

For their immeasurable support and encouragement for as long as I can remember, I thank my **parents and my brother.** A special thanks to my wife **Preetam**, who is also my colleague and labmate, for her invaluable critical feedback during the entire period of my Ph.D work.

A final salutation is extended to Lord Shiva for inducing me with self determination, patience and a rightful mind in the entire phase of this research work.

Sri Krishan Yadav 17/7/07

(SRI KRISHAN YADAV)

CONTENTS

LIST OF TABLES

LIST OF FIGURES

ACRONYMS USED IN THE THESIS

R = dissolution rate

E_a = activation energy

T = temperature

t = time

R = Boltzmann gas constant

OH^- = hydroxyl ions

H^+ = hydrogen ion

pH = hydrogen ion concentration

kcal/mol = kilo calorie *per* mole

mmol/L = milli mole *per* litre

µmol/L = micro mole *per* litre

$mol/m^2/s$ = moles *per* square meter *per* second

mM = milli mole

mg/L = milligram *per* litre

m^2/g = square meter *per* gram

kg/yr = kilogram *per* year

$mol/km^2/yr$ = moles *per* square kilometer *per* year

wt % = percent weight

Ca = calcium ion

Mg = magnesium ion

Si = dissolved silica

TDS = total dissolved solids

CC = calcite

DM = dolomite

LG = leucogranite

GN = gneiss

CQ = quartzite

PY = phyllite

KS = shale

BET = Brunauer–Emmett-Teller

BJH = Barret-Joyner-Halenda

XRF = X-ray flouroscence

XRD = X-ray diffraction

SEM = Scanning electron microscope

EDX = Energy dispersive X-ray

AAS = Atomic absorption spectrophotometer

IC = Ion Chromatograph

ln = natural logarithm

w.r.t. = with respect to

CHAPTER 1

INTRODUCTION

1.1 BACKGROUND

Rocks and its framework minerals in the Earth's crust are rarely found in equilibrium, because of the continuous operation of weathering processes. Even a minor change in any part of the earth's lithosphere disturbs the geochemical cycle, which consequently renovates the chemical weathering reaction rates of the major rock types - the carbonates and silicates. The major source of dissolved species in natural waters is the rock-water interactions. Immediately after the rocks come in contact with water, water-rock interaction (dissolution and/or precipitation) commences and moves forward towards equilibrium by dissolution or leaching of bedrock minerals into the solution or in the opposite direction during precipitation reactions. By this mechanism, major cations, anions, silica, trace elements and other essential nutrients are released into the hydrosphere. The solute concentrations in aquatic bodies are proportional to the reactivity of the bedrock minerals (volume and ease) constituting the catchment area and thereby the chemical composition of the natural waters adopts the chemistry of catchment lithology.

Dissolution reactions are dependent mainly on pH, temperature, organic acids and ligands present in the reacting solution. Dislocation sites (steps and kinks) and density can be considered as precursors of the dissolution reactions (Wollast, 1967; Berner, 1981; Berner and Berner, 1987; Lasaga *et al.* 1994; Drever, 1994,1997; Gautlier, *et al.* 1999; Chen and Brantley, 1997,2000; Welch and Ullman, 2000; Pokrovsky and Schott, 2000; Cama *et al.* 2002; Brantley,

2003; Arvidson *et al.* 2003; Appelo and Postma, 2005; Pokrovsky et al., 2005; Wellman et al., 2006). In general, dissolution rate is controlled primarily by two processes, transport and surface reactions. If the dissolution is transport controlled, rapid diffusion of ions to and from the site of reaction will take place, resulting in general rounding of the mineral grains. When surface reaction is rate-controlled, adsorption and desorption of ionic-species occur at the mineral surface resulting in well-developed etch-pits (Berner, 1981; Drever, 1997; Velbel, 2004; Appelo and Postma, 2005). Salt minerals (highly soluble) undergo transport-controlled dissolution, whereas major framework minerals (feldspars, quartz, etc.) which are sparingly soluble undergo surface-reaction controlled dissolutions (Appelo and Postma, 2005). It has been observed that field-weathering rates are slower by a few orders of magnitude as compared to those determined in the laboratory, the possible reasons for the discrepancies have been explained in terms of differences in dissolution mechanism, lack of steady-state attainment, variability in pH and temperature conditions, differences in reactive surface area and time of reactivity (Brantley, 2003; White and Brantley, 2003).

Dissolution kinetics of rocks and minerals are important in understanding different rates of chemical weathering of various lithologies, development of soils, production of secondary porosity in the rocks, triggering of landslides and sequestration of atmospheric carbon dioxide. Dissolution kinetics refer to the measurement of rates of chemical weathering reactions. Kinetics also provide information on the mechanism of complex reactions involving rock-water interactions. Dissolution of carbonate and silicate minerals act as an important CO_2 sink, thus regulating global carbon cycle and hence climate (Dupre, *et al.*

2003; Huh, 2003). It is the primary mechanism of neutralizing acidity in aquatic systems by contributing HCO_3^- ions. A few common representative dissolution reactions are,

(1.1) $CaCO_{3(s)} + H_2O_{(l)} + CO_{2(g)} = Ca^{2+}_{(aq)} + 2HCO_3^-{}_{(aq)}$

Calcite

(1.2) $(Ca,Mg)(CO_3)_{2(s)} + 2CO_{2(g)} + 2H_2O_{(l)} = Ca^{2+}_{(aq)} + Mg^{2+}_{(aq)} + 4HCO_3^-{}_{(aq)}$

Dolomite

(1.3) $2KAlSi_3O_{8(s)} + 2CO_{2(g)} + 11H_2O_{(l)} = Al_2SiO_5(OH)_{4(s)} + 2K^+_{(aq)} + 4H_4SiO_{4(aq)} + 2HCO_3^-{}_{(aq)}$

Orthoclase/Microcline Kaolinite

(1.4) $2NaAlSi_3O_{8(s)} + 2CO_{2(g)} + 11H_2O_{(l)} = Al_2SiO_5(OH)_{4(s)} + 2Na^+_{(aq)} + 4H_4SiO_{4(aq)} + 2HCO_3^-$

Albite Kaolinite

(1.5) $2KMg_3AlSi_3O_{10}(OH)_{2(s)} + 2CO_{2(g)} + 9H_2O_{(l)} = Al_2Si_2O_5(OH)_{4(s)} + 6Mg^{2+}_{(aq)} + 2K^+_{(aq)} +$

Biotite Kaolinite

$2HCO_3^-{}_{(aq)} + 4H_4SiO_{4(aq)} + 3O_2{}^{\uparrow}{}_{(g)}$

(1.6) $CaAl_2Si_2O_{8(s)} + 2CO_{2(g)} + 3H_2O_{(l)} = Al_2Si_2O_5(OH)_{4(s)} + Ca^{2+}_{(aq)} + 2HCO_3^-{}_{(aq)}$

Anorthite Kaolinite

(1.7) $CaSiO_{3(s)} + 2CO_{2(g)} + 3H_2O_{(l)} = Ca^{2+}_{(aq)} + 2HCO_3^-{}_{(aq)} + H_4SiO_{4\ (aq)}$

Wollastonite

(1.8) $MgSiO_{3(s)} + 2CO_{2(g)} + 3H_2O_{(l)} = Mg^{2+}_{(aq)} + 2HCO_3^-{}_{(aq)} + H_4SiO_{4(aq)}$

Enstatite

(1.9) $FeSiO_{3(s)} + 2CO_{2(g)} + 3H_2O_{(l)} = Fe^{2+}_{(aq)} + 2HCO_3^-{}_{(aq)} + H_4SiO_{4(aq)}$

Ferrosilite

(1.10) $(Mg,Fe)SiO_{3(s)} + 2CO_{2(g)} + 3H_2O_{(l)} = Mg^{2+}_{(aq)} + Fe^{2+}_{(aq)} + 2HCO_3^-{}_{(aq)} + H_4SiO_{4(aq)}$

Hypersthene

(1.11) $(Mg,Fe)_2SiO_{4(s)} + 4CO_{2(g)} + 8H_2O_{(l)} = 2Mg^{2+}_{(aq)} + 2Fe^{2+}_{(aq)} + 4HCO_3^-{}_{(aq)} + H_4SiO_{4(aq)}$

Olivine

(1.12) $SiO_{2(s)} + 2H_20_{(l)} = H_4SiO_{4(aq)}$

Quartz

(1.13) $Al_2Si_2O_5(OH)_{4(s)} + 6H^+_{(aq)} = 2Al^{3+}_{(aq)} + 2H_4SiO_{4(aq)} + H_2O_{(l)}$

Kaolinite

Calcite and dolomite are the primary carbonates, whereas quartz, feldspars (orthoclase/microcline, albite, anorthite), micas (biotite, muscovite), pyroxenes (wollastonite, ferrosilite, enstatite, hypersthene), amphiboles and olivines are the chief aluminosilicate minerals forming the majority of crustal rocks. Silicate weathering aid in greater drawdown of atmospheric-CO_2 as compared to carbonate weathering (Berner and Berner, 1987; Raymo and Rudiman, 1992). The rock types undergoing weathering and the reaction rates play an important role in atmospheric consumption of CO_2. In high relief areas with fluctuating climatic conditions and undergoing frequent neotectonic activities, chemical weathering gets pronounced. Thus, understanding the mechanism and quantification of the rate of rock/mineral dissolution rates in laboratory simulated conditions help to understand natural weathering rates.

Chemical weathering in Alaknanda and Bhagirathi river basins dominantly control the geochemistry of Ganga River and the Bay of Bengal (Handa, 1970; Abbas and Subramanian, 1984; Sarin and Krishnaswami, 1984; Pande *et al.*

1994). Chemical weathering in the basin is significantly controlled by geographic, geologic, climatic and tectonic factors. Numerous studies have indicated that the headwaters of the Ganga river (Alaknanda and Bhagirathi rivers) are enriched in radiogenic U, Sr, and Os (Krishnaswami *et al.* 1992; Pegram *et al.* 1992; Sarin *et al.* 1992; Singh *et al.* 1999; Dalai *et al.* 2002). Considering the important role of the lithologies in the Alaknanda and Bhagirathi rivers in controlling the geochemistry of Ganga river, the present thesis work aims at studying the dissolution of representative lithologies in the basin by studying chemical composition of the river in the field and carrying out laboratory simulated experiments.

1.2 DISSOLUTION KINETICS

Wollast (1967) was one of the first workers on chemical weathering kinetics, who experimented with the dissolution of ground K-feldspar placed in buffered aqueous solutions and measurement of release of silica with time. He observed that the rate of release of silica to the solution declined over time and explained it in terms of the formation of a protective layer on the surface of the feldspars by inhibiting the migration of dissolved species to and from the surface of K-feldspar. The protective layer was assumed to be either a precipitate of aluminium hydroxide and /or clay minerals or "feldspar" in which the cations have been replaced by hydrogen (or hydronium) ions. Later on, subsequent workers expanded Wollast's theory and described the release of silica from alkali feldspar in terms of "parabolic" kinetics where the concentration of solute in solution builds up in direct proportion to the square root of time according to the relationship (Lasaga and Kirkpatrick, 1981; Drever, 1997),

$$Q=kt^{1/2} \qquad (1.14)$$

where, Q is amount in solution, k is a constant and t is time (in hours). After a sufficiently long time, the increase in concentration may become linear, as shown in Figure 1.1.

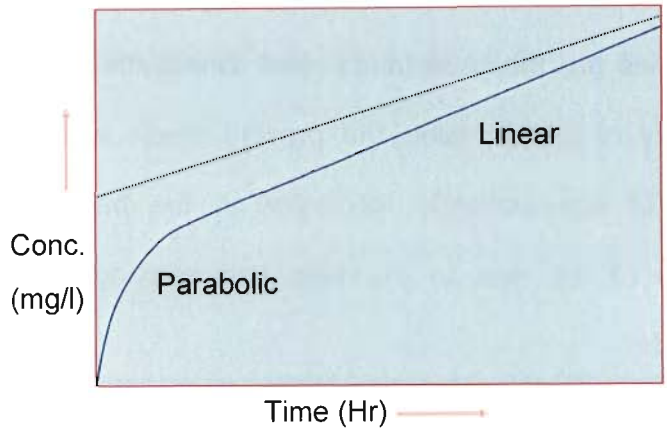

Figure 1.1 Illustration of dissolution rate showing parabolic curve which becomes linear after a long time (Drever, 1997)

In the laboratory, experiments to determine dissolution rates of rocks and/or minerals are generally carried out at "far from equilibrium" conditions (Lasaga *et al.* 1994; Chen and Brantley, 1997; Drever, 1997). By definition, for a simple reaction A↔B, at equilibrium, $R^+ = R^-$, where R^+ is the rate of forward reaction (dissolution), and R^- is the rate of backward reaction (precipitation). When a reaction approaches chemical equilibrium, the dependence of dissolution rate on the chemical affinity is derived in terms of the 'Transition State Theory' (TST) (Lasaga and Kirkpatrick, 1981), which states that dissolution rate is controlled by the desorption kinetics of an activated complex formed at the surface. For a simple, elementary dissolution reaction, TST shows,

$$R_{net} = k_{+} [1- \exp (\Delta G_R/\sigma RT)] \qquad (1.15)$$

where, R_{net} denotes the overall dissolution rate (mol/surface area /time), k_{+} is the apparent forward rate constant for dissolution at a given temperature and pressure, σ is a "stoichiometric number", conventionally set equal to 1, R is the gas constant and T is temperature in Kelvin. ΔG_R is *chemical affinity* or free energy difference with a unit of kcal/mol or kJ.

In dissolution reactions, the dissolving solid is called the *substrate*, the compound responsible for the dissolution of the substrate is the *solutant*, and the solution carrying both the solutant and the products of the dissolution is the *solvent*. Solutants can be divided into reductants, oxidants, ligands, complex-formers and chelators. This classification is based on the adsorption mechanism of the solutant and/or the type of reaction between solutant and substrate prior to dissolution (Hering and Stumm, 1990). Dissolution represents undersaturation of the bulk solution, in other words, where $\Omega<1$ (the parameter Ω is defined as the actual ion activity product divided (IAP) by the equilibrium or solubility product (K_{eq}) i.e. $\Omega = IAP/K_{eq}$). IAP in excess of K_{eq} leads to precipitation and $IAP < K_{eq}$ denotes dissolution reaction (Lasaga, 1984; Drever, 1994). The dissolution of a mineral is the sum of a series of chemical and physical reaction steps (Hering and Stumm, 1990). The first step in the dissolution reaction is the diffusion of the solutant through the solvent to the substrate. The second step in the reaction is of the solutant adsorbed to the substrate surface. The third step involves migration of combined solutant and surface ion over the substrate surface. The final step involves the release of solutant with the attached substrate-ion into the solvent. A

typical dissolution mechanism involves all the above steps in sequence (Morel and Hering, 1993; Cornell and Schwertmann, 1996).

Dissolution mechanism can be distinguished according to the most important step in the dissolution process, usually rate-limiting step is the slowest step in the entire process. Based on the rate-limiting step, two types of dissolutions are possible, *diffusion controlled dissolution* and *surface controlled dissolution* (Morel and Hering, 1993; Cornell and Schwertmann, 1996). In *diffusion-controlled dissolution*, the charged ions in the surface attract or repel water molecules. The attracted water molecules are bound to the surface ions in a solvation complex. When the bonds between the surface ions and its neighbouring ions in the solid are weak, the solvation complex detach from the solid and is accompanied by the transport of water molecules to the substrate surface (Sposito, 1989). In *surface-controlled dissolution* mechanisms, the first step (diffusion of the solutant to the substrate) is rapid whereas the detachment of the solvation complex is rate limiting. The detachment rate of exchangeable ions adsorbed to the mineral surface is different from the atoms of the mineral. Exchangeable ions are easily released from the solid surface, whereas the release of atoms from within the crystal structure requires a more powerful solvation complex (Morel and Hering, 1993).

Selective dissolution of the surface results in the formation of large, well developed etch pits, which result because majority of the dissolution originates only at specific points of excess energy on the surface such as dislocation outcrops. The dislocations normally include "steps" and "kinks". Kinks have three "sides" exposed to the solution, steps have two, and planar surfaces have only

one (Figure1.2, Berner and Berner, 1987; Arvidson *et al.* 2003). Because kinks are points of high surface energy, they are favored locations for the adsorption of species from the solution.

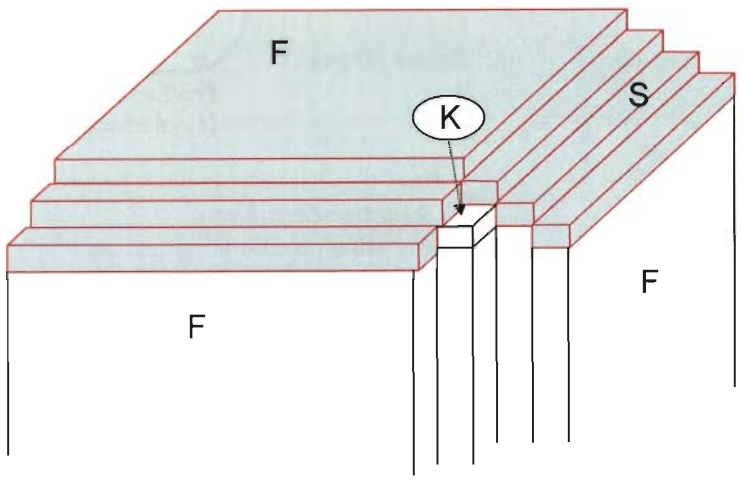

Figure 1.2 Cubical model of a crystal surface illustrating dislocation-type: face (F), step (S), and kink (K) (Arvidson *et al.* 2003)

Dissolution rate increases exponentially with increasing temperature as furnished by the Arrhenius equation (Welch and Ullman, 2000; Lasaga *et al.* 1994; Cama *et al.* 2002):

$$k = A \cdot e^{(-Ea/RT)} \qquad (1.16)$$

where, k is the dissolution rate constant, A is the temperature independent pre-exponential factor, E_a(kcal/mol) is the activation energy, R is gas constant and T is the absolute temperature in Kelvin. Transformation of reactants to products usually passes through some intermediate stage of higher energy compared to the reactants. E_a is the minimum amount of energy required to ensure a reaction to happen. The "energy hump" defines the limit of E_a (Figure 1.3).

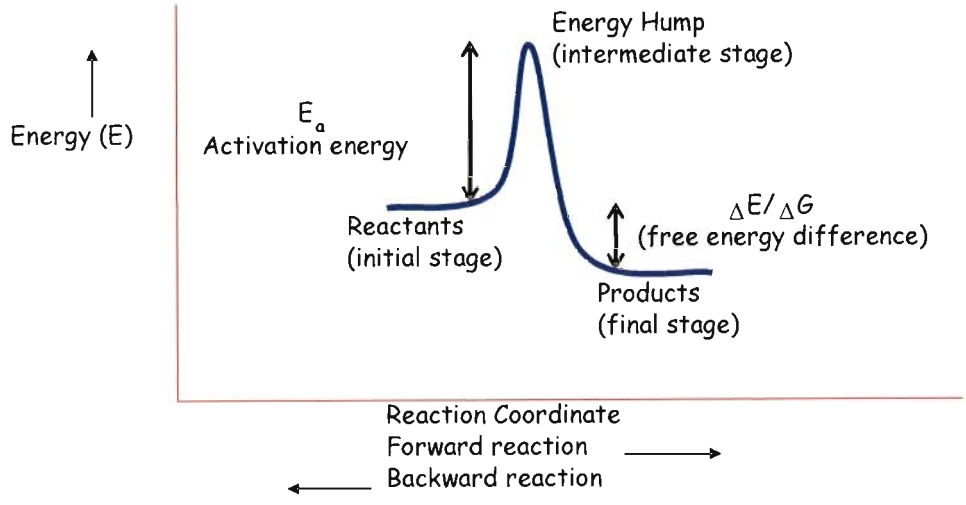

Figure 1.3 Diagram showing Activation Energy (E_a) of a reaction (Lasaga *et al.* 1994; Cama *et al.* 2002)

The activation energy E_a for the rate constant k of an overall reaction is the sum of all elementary reactions constituting the reaction mechanism. Activation energy (E_a) of the overall reaction, which is dependent on temperature, can also be defined by the equation (Lasaga and Kirkpatrick, 1981; Chen and Brantley, 1997),

$$E_a = -R \{d \ln k / d (1/T)\} \qquad (1.17)$$

Hence, values of E_a can be determined from the slope of the straight line obtained by plotting ln k versus 1/T. E_a (in kcal/mol) for diopside, enstatite, augite, forsterite, calcite and quartz (crystalline) are 12-36, 12, 19, 9.1, 8.4 and 16-18 respectively (Lasaga, 1984).

Far from equilibrium, the dissolution rates of most silicate minerals have the form as shown in Figure 1.4 (Taken from Drever, 1994; Drever and Stillings, 1997; Chen and Brantley, 2000).

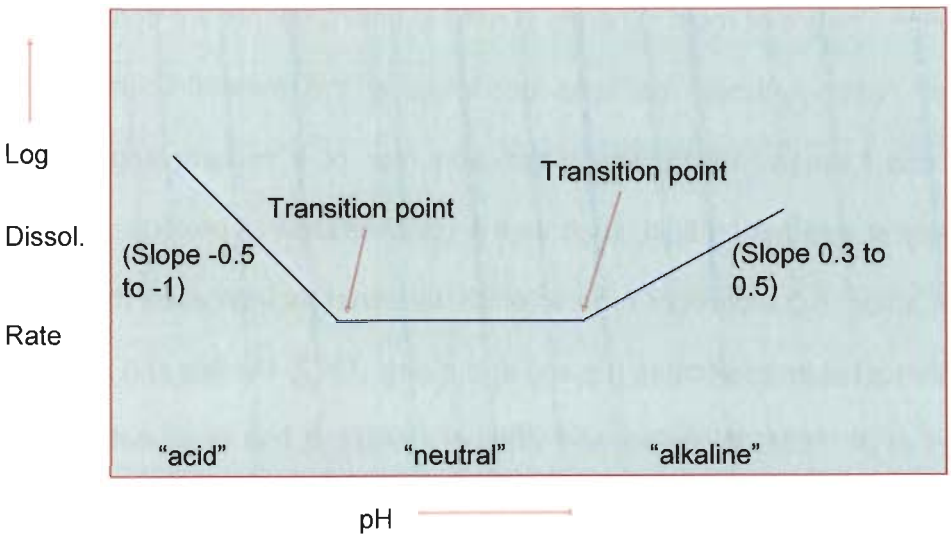

Figure 1.4 Silicate dissolution rates (far from equilibrium) as a function of pH.

The total dissolution-rate can be expressed as the sum of the individual rates,

$$(\text{Rate})_{\text{total}} = k_H [H^+]^n + k_N + k_{OH} [OH^-]^m \qquad (1.18)$$

where, $k_H [H^+]^n$ refers proton promoted dissolution in acidic region (1-5), k_N refers dissolution in neutral region (5-8), and $k_{OH} [OH^-]^m$ refers hydroxyl promoted dissolution in alkaline region (8-14), *n* and *m* are exponents, having values different for different minerals and typically the former has a value between 0.3 to 1, whereas the later has a value of about 0.3 to 0.5 (Berner and Berner, 1987; Appelo and Postma, 2005).

It is commonly accepted that dissolution rates of most primary and secondary minerals are promoted by the presence of proton and complex forming ligands (Zhang and Bloom, 1999) and the rate controlling steps in the dissolution of most oxides and aluminosilicates are surface transport processes (e.g. Stumm and Furrer, 1987). Aluminosilicate dissolution is generally considered to be controlled by reactions at mineral surfaces (Blum and Lasaga, 1991). The

dissolution kinetics of most minerals in natural environments are controlled by the rates of heterogeneous reactions occurring at the mineral-solution interface (Blum and Lasaga, 1991). The dissolution rate of a mineral depends on the chemistry of weathering fluid, such as the concentration of protons, hydroxyl and organic acids. Adsorption of organic acids by minerals increases the dissolution rates of most aluminosilicates (Huang and Kiang, 1972; Manley and Evans, 1986; Bennett *et al.* 1988; Wogelius and Walther, 1992). It has been established that organic ligands have direct effect on dissolution through surface-complexation reactions (Wogelius and Walther, 1991; Welch and Ullman, 1996; Stillings *et al.* 1998) by which, the strength of the ligand-cation interaction is thought to polarize and weaken the bonds between the cation and mineral lattice (Furrer and Stumm, 1986). It has been proposed that ligand promoted dissolution occurs in conjunction with proton promoted dissolution and the rates of each are additive (Furrer and Stumm, 1986). Surface complexation found in organic acids promotes dissolution of anorthite (Amrhein and Suarez, 1988), multioxide minerals such as kaolinite, feldspars (Wieland *et al.* 1988) and microcline (Nater and Huang, 1988). Chin and Mills (1991) observed low molecular weight organic ligands markedly increase the dissolution rates of both Al and Si from kaolinite in the order, oxalate > malonate = salicyclate > O-phthalate. Mast and Drever (1987), however, found no significant effects of oxalate (0.5 and 1 mM) on the dissolution rate of tremolite or on the steady state release of silica from oligoclase. More recent works have emphasized the importance of adsorbed complexes at the mineral-fluid interface on the overall kinetics of dissolution reactions. Surface chemists have developed theoretical and experimental techniques to describe the surface coordination, adsorption, and exchange

reactions at oxide surfaces in aqueous solutions (Stumm *et al.* 1985; Blum and Lasaga, 1991).

Field weathering rates are generally observed to be up to five orders of magnitude slower than laboratory dissolution-rates, and there are no definitive reasons for the deviations (Brantley, 2003). However, possible explanations for the deviations include, (i) differences in dissolution mechanism between lab and field; (ii) lack of steady-state attainment; (iii) differences in solution chemistry (inhibition in the field or acceleration in the lab); (iv) differences in solution chemistry (chemical affinity effects); (v) improper estimation of reactive surface area; (vi) differences or variability in temperature and (vii) biological effects and may be many others (Brantley, 2003; White and Brantley, 2003).

It is often possible to simulate field conditions in the laboratory and study rock/mineral dissolution rates at different pH and temperature conditions. The importance of Himalayan rivers is very significant in the context of global carbon cycle. Rock weathering consumes CO_2 from atmosphere, a greenhouse gas and hence modifies global temperature (climate) over geologic time (Velbel, 1993). Previous studies have indicated the source waters of Ganga river, namely Alaknanda and Bhagirathi rivers to show high chemical and physical denudation rates. These basins are characterised by lithologies, which release highly radiogenic U, Sr and Os to the river waters (Krishnaswami *et al.* 1992; Pegram *et al.* 1992; Sarin *et al.* 1992; Singh *et al.* 1999; Dalai *et al.* 2002), although the river water composition is mostly derived from carbonate rock weathering (Krishnaswami *et al.* 1992; Palmer and Edmond, 1992; Blum *et al.* 1998). The rapid rise in $^{187}Os / ^{188}Os$ in the world's oceans has been attributed to an increase

in the bulk silicate weathering rates resulting from the rise of the Himalayas and/or selective weathering and erosion of highly radiogenic black shales. The Lesser Himalayan lithology is characterised by occurrences of black shales, which are far more radiogenic compared to the presently eroding continental crust. Dalai *et al.* (2002), estimated that ~ 6-9 x 10^8 kg yr^{-1} of black shales are being weathered in the Ganga and Yamuna river basins in the Himalayas leading them to suggest that, If weathering results in the conversion of organic carbon in the black shales to CO_2, it would release ~ 2 x 10^5 moles of CO_2 km^{-2} yr^{-1} in the Yamuna and Ganga river basins. The CO_2 consumption rates by silicate and carbonate weathering in the six large rivers of Himalayas namely, Indus, Ganga, Brahmaputra, Mekong, Chang Jiang and Irrawady is about 4 x 10^{12} mol yr^{-1}, about four times higher compared to the Amazon river basin and accounts for nearly one-sixth of the global CO_2 consumption by continental weathering (Sarin, 2001). The high uranium mobilisation most likely results from the intense chemical weathering of biotite-rich granitoids and gneisses exposed in Higher Himalayas. According to Blum *et al.* (1998), 82% of bicarbonate in Raikhot watershed is derived from weathering of carbonate minerals and only 18% is derived from silicate weathering even though the bedrock is predominantly quartzo-felspathic gneiss and granite with only ~1% carbonate in the watershed. They further suggest that, the flux of Sr with a high $^{87}Sr/^{86}Sr$ ratio from the major Himalayan rivers may be derived in large part from the weathering of trace amounts of calcite within the largely silicate Higher Himalayan Crystalline Series.

The study of dissolution-behavior of individual rock types in laboratory simulated conditions could provide insight into the understanding of field weathering and flux rates. Thus, the present study area, which is a multilithologic

terrain provides a unique opportunity to conduct dissolution experiments on a variety of lithologies and soil columns under different pH and temperature conditions. Most of the studies have focused on monolithologic catchments to understand independently the role of lithology in regulating river water chemistry (Meybeck, 1987; Bluth and Kump, 1994). Meybeck (1987) studied 320 monolithologic terrains mostly in Europe, in order to understand the contribution of different lithologies to the dissolved load components by combining water chemical characteristics with their relative outcrop proportions on the surface. He showed the importance of a minor lithology such as evaporites (1.25% outcrops), contributing 17.2% of the dissolved river load as compared to the minor influence of crystalline rocks. Chemical erosion rates relative to granite weathering followed the sequence, granite (relative weathering = 1), gneiss and mica-schist (1), gabbro (1.3), sandstone (1.3), volcanic rocks (1.5), shales (2.5), serpentine and amphibolite (5), carbonate rocks (12), gypsum (40) and rock salt (80). On this basis, a relatively smaller outcrop of gypsum or rock salt can have large influence on the ensuing river water composition and flux rates.

1.3 OBJECTIVES

The primary objectives of the present study are to,

(1) Estimate flux rates of Ca, Mg and Si at two locations, Maneri along Bhagirathi river and Srinagar along Alaknanda river in Himalayas, to understand the field weathering rates.

(2) Calculate dissolution rates of representative lithologies, leucogranite, gneiss, quartzite, phyllite and shale constituting a part of the Alaknanda-Bhagirathi river basin and two pure minerals (calcite and dolomite) at different pH and

temperature conditions through laboratory simulated dissolution experiments using batch reactors (for rocks and minerals) and column reactors (for soil).

(3) Investigate the role of temperature, pH, organic acids and ligands in dissolution processes.

(4) Assessment of morphochemical alterations of treated rock/mineral/soil samples to figure out the effect of dissolution.

CHAPTER 2

SAMPLE CHARACTERISTICS

2.1 SAMPLING LOCATIONS

Fresh rock samples of Leucogranite (LG), Gneiss (GN), Quartzite (CQ), Phyllite (PY) and Shale (KS) were collected during December 2005 from the Garhwal Himalayan range of Alaknanda-Bhagirathi river basins (Figure 2.1). The minerals, Calcite (CC) and Dolomite (DM) were obtained from the collection of Oleg S. Pokrovsky (LMTG, Toulouse, France). Soil profile from which the soil core was taken for soil column leaching experiment, is located on the right bank of the Ganga river flowing downstream near Laxmanjhula (Rishikesh)(Figure 2.2). Daily river-water samples were collected for one year (July 2004-July 2005) to estimate elemental flux rates in field from two locations, Maneri (on Bhagirathi river) and Srinagar (on Alaknanda river) (Figure 2.1).

2.2 SAMPLE DESCRIPTION

2.2.1 Leucogranite (LG)

"Leucogranite" or "Gangotri Granite" was collected from the upper reaches of Bhagirathi river basin near Gangotri temple in the Higher Himalayan Crystalline Zone (HHCZ). It is generally believed that the Himalayan Leucogranites are generated intermittently as a result of crustal thickening associated with continental collision during Tertiary Period (Braun *et al.*1996). The leucogranite (LG) is peraluminous (Al_2O_3> Na_2O + K_20) and alkali rich, as revealed from its chemical formula derived from its chemical composition (Table 3.1). The cationic composition of LG is $(Na_{0.08}K_{0.103}Ca_{0.01})$ $(Fe_{0.0076}Mg_{0.01}Mn_{0.0001}Ti_{0.0004})$ $(Si_{1.19}Al_{0.302})$. Auden (1949) described it as fine

grained granite with tourmaline, muscovite, biotite and garnet. Powder XRD analysis of pretreated LG confirms the presence of quartz, microcline, plagioclase, biotite (Mg-rich), muscovite, and tourmaline (Na, Ca, Mg, Fe, Al, and Li- rich).

2.2.2 Gneiss (GN)

Gneiss (GN) was collected from the Vaikrita Group of Higher Himalayan Crystalline Zone (HHCZ). It constitutes a major lithology of HHCZ and exposed along both Alaknanda and Bhagirathi river basins. XRD analysis of pre-treated GN indicates quartz, orthoclase, plagioclase, garnet, biotite (Mg-rich), muscovite, (Al, Ca, Fe) – oxides are the primary phases constituting the rock. The cationic composition of GN is $(Na_{0.03}K_{0.0013}Ca_{0.068})$ $(Fe_{0.031}Mg_{0.0047}Mn_{0.0017}Ti_{0.0004})$ $(Si_{1.345}Al_{0.178})$.

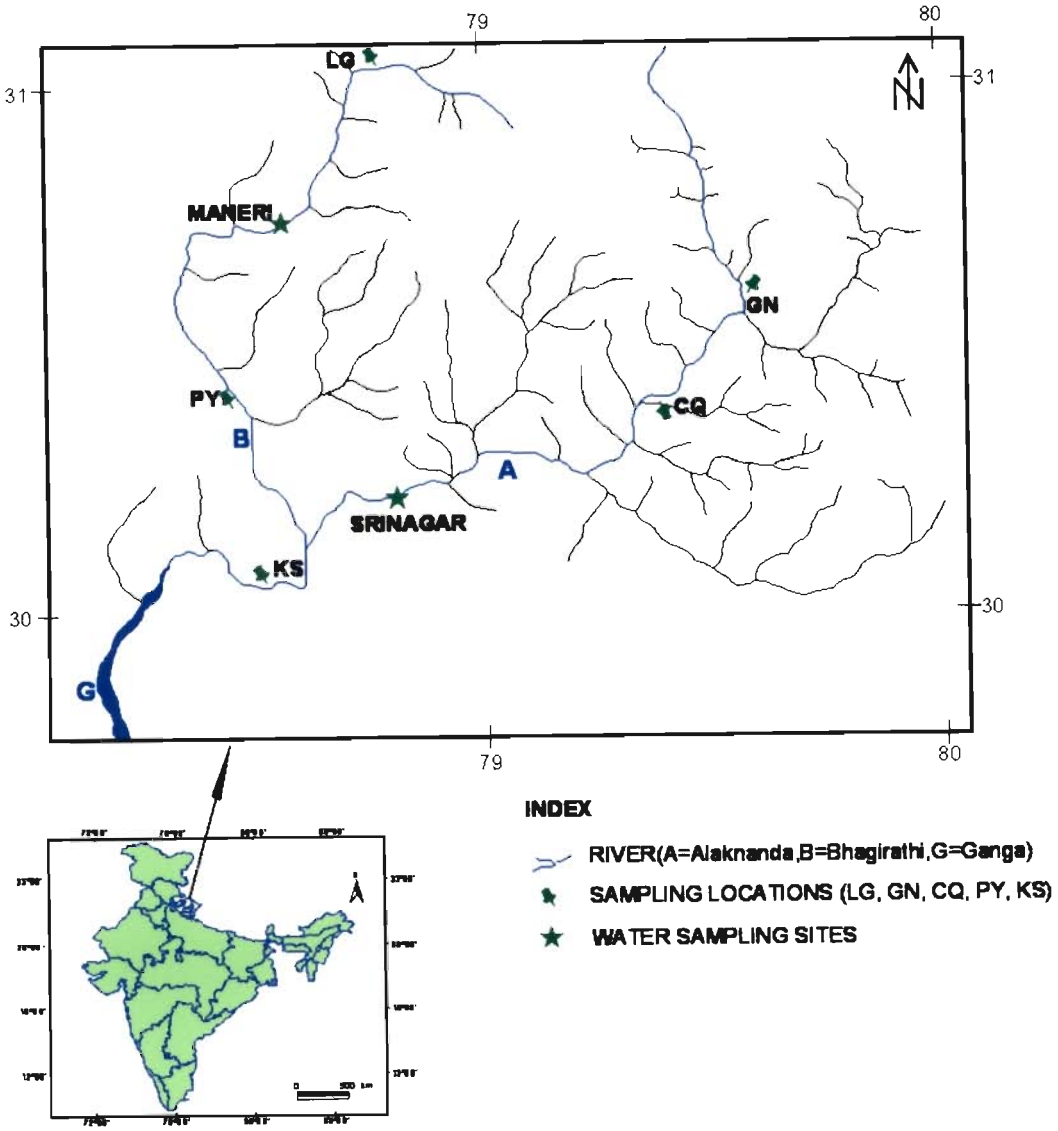

Figure 2.1 Rock and water sampling location map (digitized from National Atlas and Thematic Mapping Organisation)

Figure 2.2 Soil sampling site (modified from 'Google Earth')

2.2.3 Quartzite (CQ)

Quartzite (CQ) was collected from Chamoli and forms a major and distinct lithology of Higher Himalayan Crystalline Group exposed in and around Alaknanda and Bhagirathi river basins. The lithology is massive and milky white in color with minor stains of iron-oxide. XRD analysis of pre-treated CQ indicates that, it is composed almost of quartz. Cation composition of CQ is $(Na_{0.0002}K_{0.01}Ca_{0.0012})(Fe_{0.0005}Mg_{0.0007}Mn_{0.00014}Ti_{0.0005})(Si_{1.59}Al_{0.045})$.

2.2.4 Phyllite (PY)

Phyllite (PY) was collected from Chandpur Group, which forms a major lithostratigraphic unit of Alaknanda-Bhagirathi river basin. In literature, PY is described as Chandpur Phyllite, named after the type locality. The sample has been collected from road cuts along Bhagirathi river on Tehri-Uttarkashi highway. PY forms a major rock type of Garhwal Himalaya and constitutes the foundation rock of the Tehri earthfill dam, one of the largest hydropower projects in India. PY is foliated and greenish grey to khaki in colour. XRD analysis of pre-treated PY indicates its composition is primarily of quartz, chlorite, and chamosite. Cationic composition of PY is $(Na_{0.0002}K_{0.01}Ca_{0.0012})(Fe_{0.0005}Mg_{0.0007}Mn_{0.00014}Ti_{0.0005})(Si_{1.59}Al_{0.045})$.

2.2.5 Shale (KS)

Shale (KS) belongs to the Lower Tal Formation, which is exposed near Kauriyala. It is grayish black to black in color, laminated and easily friable. In literature, KS is referred to as black shale and is considered highly radiogenic (e.g. Singh et al, 1999; Dalai *et al.* 2002). Black shales are not a major lithology

of the Himalayas, although their occurrence has been reported in the Infra Krol, Lower Tal, Deoban, and the Mandhali Formations (Gansser, 1964; Valdiya, 1980). In the Outer Lesser Himalya, black shales are present in the Infra Krol, Krol, and Tal formations. Black shales are generally more abundant in the Tal formation as compared to Infra-Krol and Krol formations (Valdiya, 1980). XRD analysis of pre-treated KS indicates, quartz, illite and kaolinite are the primary minerals and with minor amounts of albite, gypsum and iron-oxides. The cationic composition of KS is $(Na_{0.0045}K_{0.0857}Ca_{0.0023})(Fe_{0.046}Mg_{0.0235}Mn_{0.00046}Ti_{0.007})(Si_{1.15}Al_{0.318})$.

Table 2.1 Geological details of rock-samples (*as in* Gopendra Kumar, 2005) used for dissolution experiment

Sample Code	Lithology	Group/Formation	Place
LG	Leucogranite	-	Gangotri
GN	Gneiss	Vaikrita	Vishnuprayag, Chamoli
CQ	Quartzite	Higher Himalaya Crystalline Group	Chamoli
PY	Phyllite	Chandpur	Tehri
KS	Shale	Krol/Tal	Kauriyala, Tehri Garhwal

2.2.6 Calcite (CC) and Dolomite (DM)

Calcite is large (100-200 μm), with transparent cleavage crystals of Icelandic spar collected from the hydrothermal veins in basaltic traps of Central Siberia. The crystals (130-200 μm) of DM were obtained from Ward Scientific Co. by Oleg Pokrovsky. Electron microprobe analysis show the samples to contain <0.5% impurities (Pokrovsky *et al.* 2005).

2.2.7 Soil Sample

The soil profile from which the soil core was collected, is developed along the right bank of the Ganga river flowing downstream near Laxmanjhula (Rishikesh). The geographical position of the site is 30^0.8' N; 78^0.19' W at an elevation of 1157 ft. from mean sea level (Figure 2.2). The soil-profile is developed at about 50 m on the inner side of the gently meandering Ganga river. XRD analysis of pre-treated soil indicates quartz, illite, biotite, muscovite, kaolinite, orthoclase, and albite are the major minerals. BET (Brunauer-Emmett-Teller) surface area and BJH (Barret-Joyner-Halenda) pore size distribution of different segments of the soil column are presented in Figure 2.3. The grain size distribution in the soils are, >170μm (48%), 80-120μm (26.5%),120-170 μm (13%), 60-80 μm (7.2%) and 45-60 μm (3.6%).The BJH pore volume distribution at different intervals in the soil show homogeneity (Table 2.2, Fig.2.3).

Table 2.2 BJH pore-diameter range distribution in soil at different depths

Pore Diameter Range(nm)	0-15 cm depth (%)	15-30 cm depth (%)	30-45 cm depth (%)	45-60 cm depth (%)	60-75 cm depth (%)
Below 6	25.24	28.93	24.22	26.94	25.16
6-8	11.25	12.43	10.52	12.15	11.31
8-10	7.81	8.65	7.15	8.39	7.89
10-12	6.79	7.41	6.24	7.15	6.95
12-16	7.30	8.06	7.02	7.38	7.48
16-20	5.86	6.24	5.39	6.56	6.08
20-80	22.52	19.21	24.25	22.02	21.96
Over 80	13.23	9.06	15.22	9.41	13.17

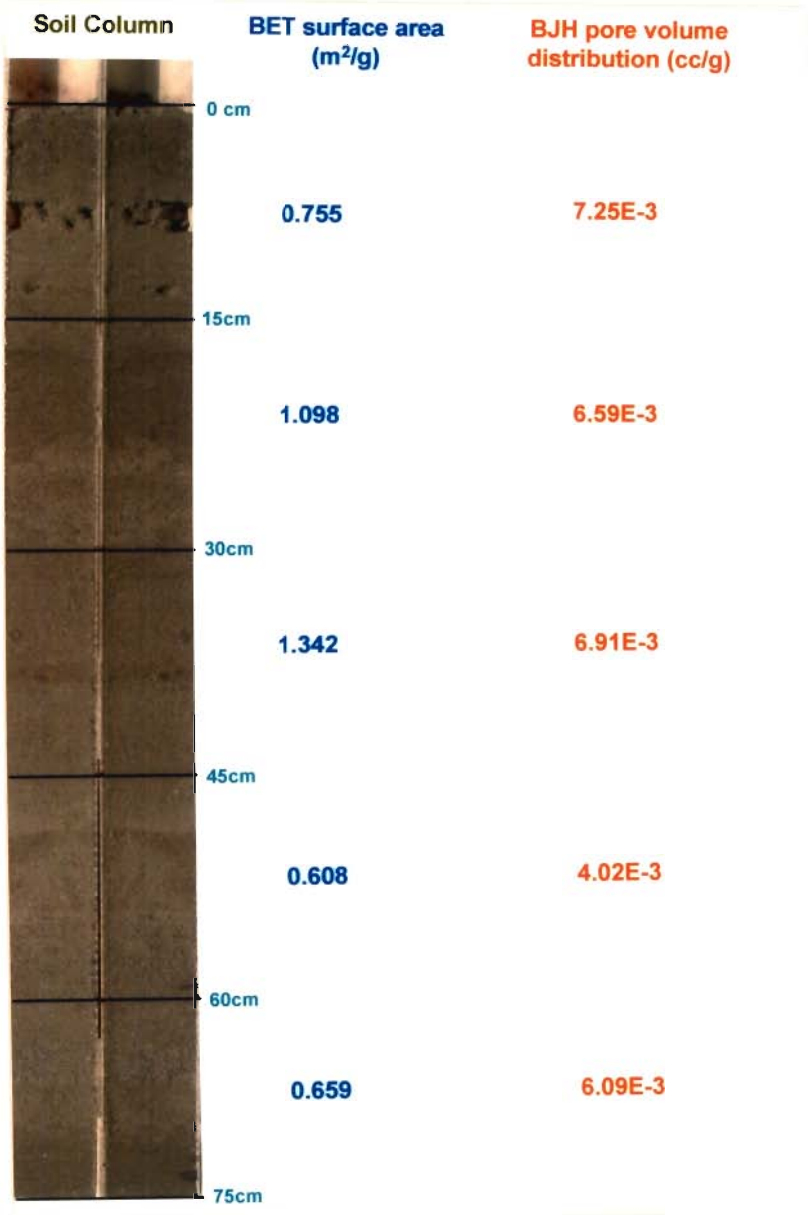

Figure 2.3 Vertical section of soil column and its characteristics

CHAPTER 3

METHODOLOGY

3.1 INTRODUCTION

Daily water samples of Alaknanda and Bhagirathi rivers collected daily over one year period during July 2004-July 2005 were analysed to estimate elemental flux rates. Laboratory experiments were carried out continuously for 30-35 days for each of the samples at 25^0C and 5^0C in three different buffer solutions of pH 2.2, 4.2 and 8.4 to calculate dissolution rates of the two minerals calcite (CC) and dolomite (DM) and five rocks, leucogranite (LG), gneiss (GN), quartzite (CQ), phyllite (PY) and shale (KS) collected from the Alaknanda-Bhagirathi river basins in the Himalayas. In addition, a soil-column collected from the soil-profile developed along the Ganga river at Rishikesh has been studied to estimate dissolution behavior under the same experimental solutions at room temperature. Analytical instruments such as COULTER SA3100 BET Surface Area Analyzer, GBC AVANTA M Atomic Absorption Spectrophotometer (AAS), pH-electrode (THERMO ORION 420), THERMO UV Spectrophotometer, SIEMENS SRS 3000 Sequential X-ray Spectrometer, BRUKER AXS D8 ADVANCE Diffractometer, FEI QUANTA 200 HV Scanning Electron Microscope (SEM) attached with TSL Energy Dispersive X-ray Analyser (EDX) and METROHM 792 Basic Ion Chromatograph (IC) were used for the various analyses. Dissolution experiments were carried out using batch reactors, mixed flow reactors (for rocks and minerals) and column reactors (for soils).

3.2 SAMPLE COLLECTION

The river water samples at Maneri (along Bhagirathi) and Srinagar (along Alaknanda) were collected daily during July 2005 through July 2006 in pre-cleaned plastic (high density polypropylene) bottles of 1 liter volume from midstream from an approximate depth of 0.6 m from the surface level. Extreme care was maintained to fill the sample containers completely to avoid any gas exchange with the atmosphere. pH and alkalinity were measured immediately after the sample collection. The water samples were filtered within 24 hours of the sampling through 0.45 μm pore size cellulose nitrate membrane filters. The filtered water samples were analysed for Ca, Mg and dissolved silica within two weeks of collection of water samples. All the water samples were kept at refrigerated condition (4^0C) before analysis and were equilibrated with ambient temperatures prior to analysis.

The rock samples were broken into loose fragments using hammer and chisel from the geological formations exposed on the roadside along the Alaknanda and Bhagirathi rivers. Due care was taken to collect unweathered and fresh rock samples. Four cylindrical undisturbed and intact cores of soil profile up to a depth of 75 cm from the surface were collected with the help of four identical (length=81cm, internal diameter=5.4cm) UPVC (Unplasticized Poly Vinyl Chloride) pipes. The vertical section of the soil-core shows the soil with no identifiable horizons and is mostly comprised of well sorted very fine grained alluvial sediments (refer Figure 2.3). The uppermost organic layer of the soils contains decomposed litter with grass roots extending up to a depth of 4-5 cm. The pipes with soil cores were sealed at the top and bottom and transported to the laboratory.

3.3 SAMPLE PREPARATION

In the sample processing laboratory, the rock-samples were hand sorted to remove macroscopic impurities and then washed with ultra pure water (milliQ) to remove dust and other impurities. After drying the samples in an oven at approximately 80^0C for 5 days, the fresh rock fragments were crushed mechanically using a jaw-crusher to get fractions of approximately 1-5 cm^3 in size, followed by gentle grinding and dry sieving to recover grains of 150-300 μm. The fractions were immersed in ultra pure water and manually agitated for 10 minutes until the cloudy supernatant is collected on the surface, which was decanted and replaced with fresh ultra pure water. The process was repeated until all the supernatant liquid became very transparent. Subsequently, ultrasonic cleaning in acetone medium was done to remove any more remaining ultra fine particles. To avoid rapid initial dissolution, the ultrasonic cleaned powdered samples were kept in polypropylene bottles with ultra pure water (1:10 sample to water ratio) for 7 days at 25^0C. Periodically, the bottles were agitated by electronic shaker for 1-2 hours. Finally, the samples were rinsed with fresh ultra pure water and kept in an oven at 60^0C, and stored in a dessicator until the resumption of dissolution experiments.

In the laboratory, one of the soil cores was cut longitudinally into two parts. One half has been preserved for any future requirements and the other half was divided into five equal parts from top to bottom. Soil samples were taken from each of the five parts and prepared for BET surface area measurement, BJH pore volume distribution, XRD analysis and grain size analysis. Post-experiment soil cores were also cut vertically to collect the treated soil samples for XRD analysis at respective intervals.

3.4 SAMPLE CHARACTERIZATION

Major oxides of the powdered rock/mineral samples were analyzed using SIEMENS SRS 3000 Sequential X-ray Flourescence (XRF) spectrometry to ascertain the chemical composition. The specific surface area of the experimental samples was calculated using COULTER SA3100 BET surface area analyzer. Table 3.1 and Figure 2.3 show the details of chemical composition (wt %) and BET surface area (m^2/g) of the untreated rock/mineral samples and untreated soil-samples respectively, whereas Table 3.2 shows the chemical formula of the experimented rocks/minerals. Table 2.2 presents adsorption BJH pore-diameter range distribution in untreated soil sample at different depth intervals. Surface topology and chemical composition characterization of the fresh and experimental powdered samples were also carried out using SEM attached with EDX. Powder XRD studies were carried out to determine the mineral phases present in the rock and soil samples. Table 3.3 and Figure 3.5 present various instruments which have been used in the present study for various analyses.

Table 3.1 Chemical composition (wt %) and BET surface area (m^2/g) of experimental rocks/minerals

Mineral /Rock	SiO_2	Al_2O_3	Fe_2O_3	MnO	MgO	CaO	Na_2O	K_2O	TiO_2	P_2O_5	Total (wt %)	BET surface area (m^2/g)
CC	-	-	-	-	-	55.56	-	-	-	-	55.56	0.037
DM	-	-	-	-	21.40	30.23	-	-	-	-	51.63	0.322
LG	72.75	15.41	0.61	0.01	0.43	0.50	5.46	4.86	0.03	0.22	100.28	0.491
GN	82.04	9.09	2.49	0.12	0.19	3.83	2.04	0.06	0.03	0.02	99.91	0.770
CQ	97.06	2.3	0.04	0.01	0.03	0.07	0.01	0.05	0.04	0.03	99.64	1.102
PY	70.34	16.1	3.7	0.03	0.94	0.13	0.27	4.0	0.61	0.08	96.20	0.443
KS	70.22	16.24	3.69	0.03	0.94	0.13	0.28	4.03	0.62	0.08	96.26	6.972

Table 3.2 Chemical composition of the samples used for dissolution experiment

Rocktype	Chemical Formula
LG	$(Na_{0.08}K_{0.103}Ca_{0.01})\ (Fe_{0.0076}Mg_{0.01}Mn_{0.0001}Ti_{0.0004})\ (Si_{1.19}Al_{0.302})$
GN	$(Na_{0.03}K_{0.0013}Ca_{0.068})\ (Fe_{0.031}Mg_{0.0047}Mn_{0.0017}Ti_{0.0004})\ (Si_{1.345}Al_{0.178})$
CQ	$(Na_{0.0002}K_{0.01}Ca_{0.0012})(Fe_{0.0005}Mg_{0.0007}Mn_{0.00014}Ti_{0.0005})(Si_{1.59}Al_{0.045})$
PY	$(Na_{0.0043}K_{0.085}Ca_{0.0023})(Fe_{0.046}Mg_{0.023}Mn_{0.0004}Ti_{0.0076})(Si_{1.153}Al_{0.316})$
KS	$(Na_{0.0045}K_{0.0857}Ca_{0.0023})(Fe_{0.046}Mg_{0.0235}Mn_{0.00046}Ti_{0.007})(Si_{1.15}Al_{0.318})$

Table 3.3 The various instruments used for the study of samples

Instrument Used	Performance	Purpose
BET surface area analyser	Based on gas (nitrogen/krypton) sorption method with a precision within ± 10%.	Measurement of specific surface area (m^2/g) of the powdered rock/mineral samples
BJH pore-volume analyzer	Based on gas (nitrogen/krypton) sorption method with a precision within ± 10%.	Measurement of pore-volume distribution (cc/g) of pretreated soil samples
X-ray Flourescence (XRF) Spectrometry	Based on emission intensity of particular radiation with suitable X-ray spectrometer using known international reference standards.	To determine major element oxide abundance of the samples
Powder X-ray diffraction (XRD)	X-rays are generated with CuK_α radiation, 30kV, 100mA and mineral phases are detected using Bragg's law.	To determine major mineral phases present in the fresh and treated rock/soil samples.
Scanning Electron Microscope (SEM) attached with Energy Dispersive X-ray Analyser (EDX)	SEM is capable of scanning images of magnifications 500x -2000x, while EDX operates using electron beam spot size < 50 nm and the spectra obtained for 100s live time.	To take photographs of surfaces of pretreated and treated samples and to measure quantitatively its elemental composition
Atomic Absorption Spectrophotometer (AAS)	Works on the principle that atomized samples (aqueous) absorb wavelengths characteristic of the elements present in the sample and absorbance is calculated using Lambert- Beer Law.	Measurement of major cations Ca and Mg (in rock/mineral dissolution experiment)
UV Spectrophotometer	Works on the principle of colorimetric spectrophotometry. Dissolved silica is measured at 410nm.	Measurement of dissolved silica
Ion Chromatograph	Based on the principle of chromatographic separation and detection methods.	Measurement of major cations Ca and Mg (in soil dissolution experiment and river water)
Ultrasonic cleaner	Works on the principle of ultrasonic cavitation.	For ultrasonic cleaning of the samples for dissolution experiment

3.5 EXPERIMENTAL SOLUTIONS

Buffer solutions of pH 8.4, 4.2, and 2.2 at 25^0C were used in the present experiment to facilitate the role of pH independently over the dissolution rate. The experimental solutions were prepared using reagent grade chemicals and ultra pure water. Buffer solution (alkaline) of pH 8.4 was prepared from 0.01M $NaHCO_3$. Fixed proportions of 0.2M CH_3COOH and 0.2M CH_3COONa; and 0.2M HCl and 0.2 M KCl was added to ultra pure water to obtain buffer solutions of pH 4.2 (organic buffer) and 2.2 (acidic buffer) respectively. For soil dissolution experiment, organic buffer (pH 4.2) was prepared from $KHC_8H_4O_4$ salt (1.021 g/100 ml ultra pure water).

3.6 EXPERIMENTAL DESIGNS AND ANALYSIS

3.6.1 Batch and Mixed Flow Reactors

Mineral/rock dissolution rate experiments were carried out in batch and mixed flow through reactors. Figure 3.3 represents simplified flow chart for dissolution experiment

Mixed flow reactors offer more options for temperature conditions and also a continuous and regulated flow of the solutions. One such reactor devised and manufactured for the present study is shown in Figure 3.1. In the mixed flow through reactor, 200 ml polyethylene reaction vessel with desired solution was kept inside the reactor and was continuously stirred with a floating teflon coated magnetic stirrer. Approximately, 5-10 gm of the powder (100-150 μm) sample was put into the reaction vessel and was constantly fluidized by the input solution at a fixed rate. The input solution was kept in a 5 litre glass-beaker placed outside the reactor and was injected into the reaction-vessel using a peristaltic pump with flow rates ranging from 0.01-1 ml min^{-1}. Approximately, 10% of the reacted

solution comes out of the reactor at regular intervals through a 5 μm pore size Ti filter and subsequently filtered through a 0.45 μm acetate filter. A pH electrode was dipped through the reactor to measure in-situ pH at different time intervals. The electrode was periodically calibrated with standard pH solution at 25 ^{0}C. Dissolution rates were calculated from the Ca, Mg or Si concentrations of the output solution.

In batch reactor experiments (Figure 3.2), dissolution experiments were conducted in acid washed 250 ml polypropylene bottles at temperatures of 5^0 and 25^0C and in aqueous solutions buffered at pH's of 8.4, 4.0, 2.2. Approximately, 10-20 grams of samples were placed in 100-200 ml buffer solutions of known pH values. Periodically, 5-10 ml aliquots were removed from the bottles and the same amount of fresh buffer solutions were added after each sampling to maintain constant ratio of the mineral (solid) and solution. The aliquots were filtered through 0.45μm membrane filters of 25mm size and analyzed for calcium, magnesium and silica as a function of time. The pH of the aliquots of initial buffering solutions was determined using a combination pH-electrode. The electrode was calibrated against NIST buffers (4.008, 6.865, and 9.18 at 25^0C) using a common combination pH-electrode. The precision of pH measurement was ± 0.002 units. Ca and Mg concentrations were measured by Atomic Absorption Spectrophotometer (AAS) within ± 5% uncertainty in the measurement, whereas total silica concentrations were determined by UV Spectrophotometer using the Blue Molybdate Method (APHA), within ± 3% uncertainty and detection limit of 0.5 μmol.

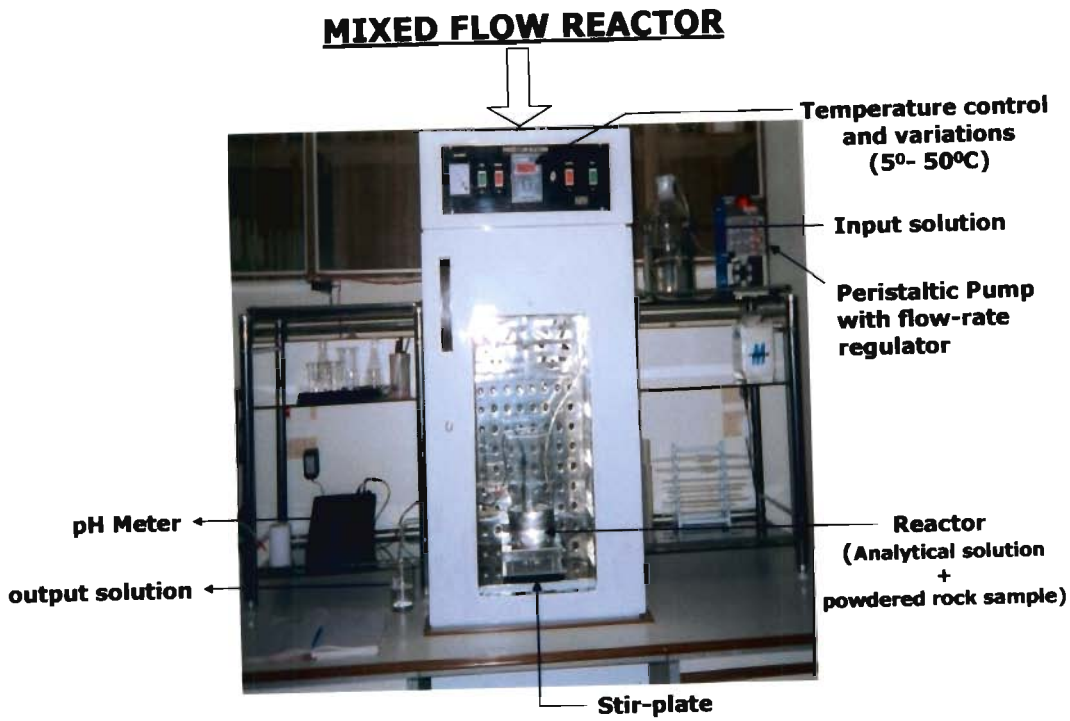

Figure 3.1 Photograph of Mixed Flow Reactor manufactured in the laboratory

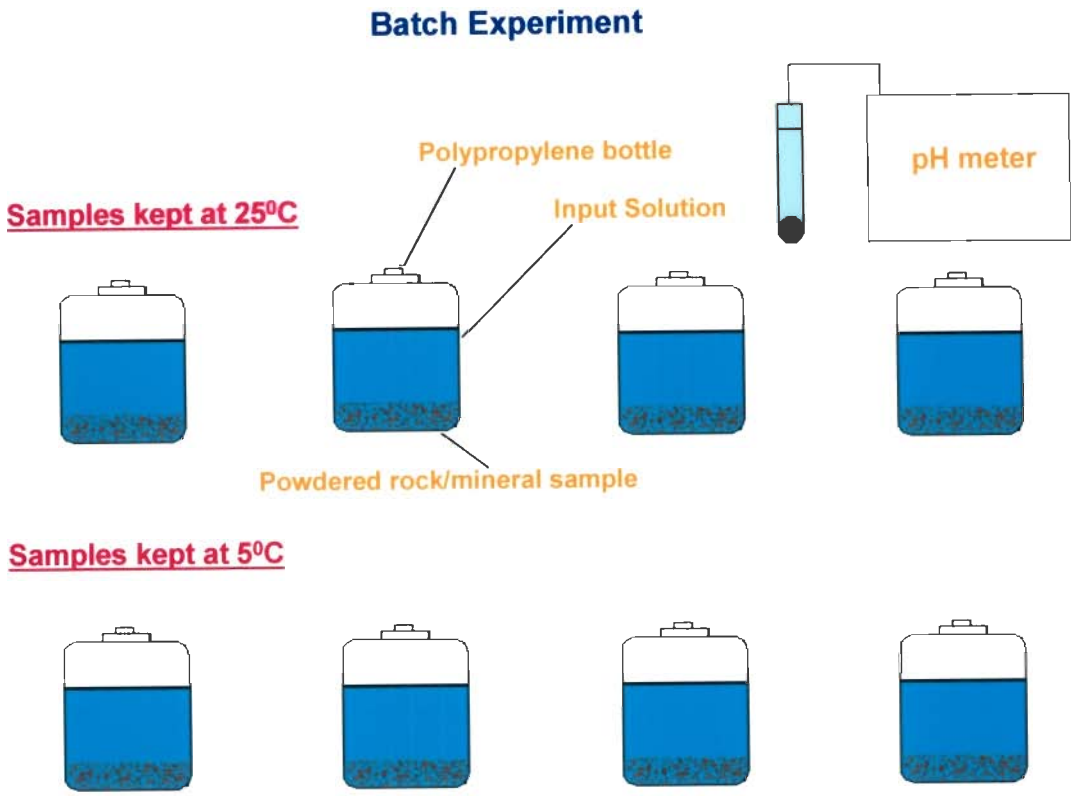

Figure 3.2 Design of Batch-Reactors

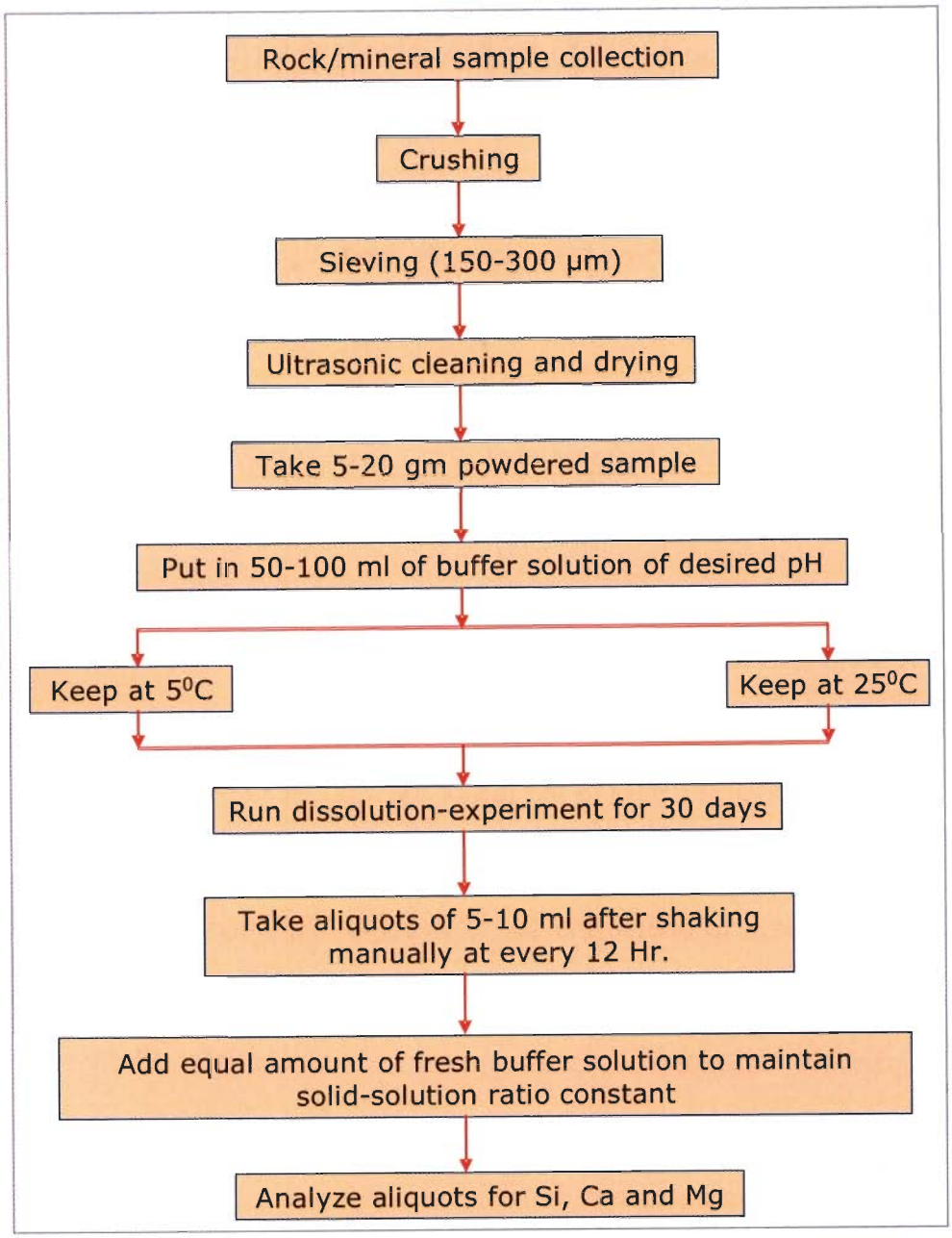

Figure 3.3 Simplified flow chart for dissolution experiment

3.6.2 Soil Column Reactor

The soil columns encased in UPVC pipes recovered from the sampling location was transported to the laboratory and air dried for removal of moisture content. The open end of the core was wrapped with nylon mesh, to enable the soil materials to remain packed and to prevent from falling down. After drying of the soil columns, three core samples were tightly fixed vertically to 3 different stationary stands as depicted in the Figure 3.4. Three different solvents (buffers) of pH 8.4, 4.2 and 2.2 were used to carry out the experiment at 3 different pH conditions at room temperatures (20^0-25^0 C). Analytical solutions were prepared at 25^0 C using 0.01 M $NaHCO_3$, $KHC_8H_4O_4$, and 0.2 M HCl plus 0.2 M KCl buffered at pH 8.4, 4.2, and 2.2 respectively. The pH of the solvents remained constant throughout the experiment with very minor fluctuations. Input solutions were passed automatically at a flow rate of 6-9 ml hr^{-1} by manually adjusting the flow regulator attached to the tap of the input solution container placed vertically above the soil column-stand (Figure 3.4). No leachates were collected for the initial 3 days to enable the soil to become fully saturated with the experimental solvents. Thereafter, everyday the leachate was collected twice at 12 hours interval. The experiment was repeated continuously for 30 days. The leachates were filtered through 0.45 μm size filter paper and analyzed for Ca^{2+} and Mg^{2+} using Ion Chromatograph (IC).

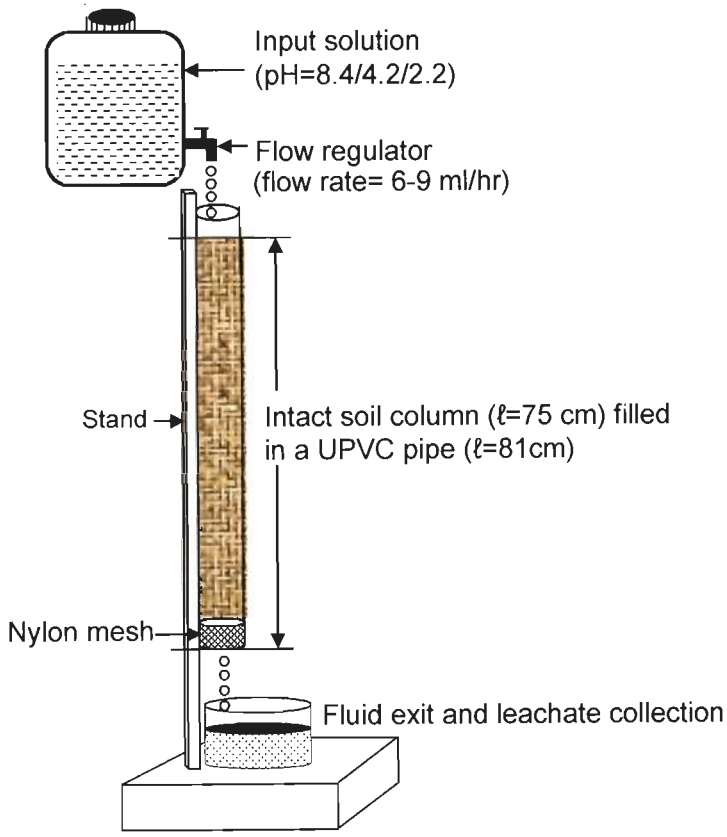

Figure 3.4 Schematic diagram of the soil-column reactor

3.7 FORMULAE USED

Elemental release data versus time were used to plot graphs to get a trend line, which defines the slope. The value of the slope was used in the equation to estimate the dissolution rates (R, mol/m^2/s) (as in Pokrovsky and Schott, 2000),

$$R = \text{slope}/ [(w/v) \times SSA] \qquad (3.1)$$

where, R = dissolution rate (mol/m^2/s)

W = weight of sample (g)

V = volume of solution (ml)

SSA = specific surface area (m^2 /g)

The temperature dependence of the dissolution rate generally follows the Arrhenius relationship, which describes the change in the ratio of reaction rates r_1 and r_2 (in moles/m^2/s) over a temperature range of T_1 and T_2 (^{0}K) such that (e.g. Brady and Carroll, 1994; White et al., 1999),

$$\ln (r_2/ r_1) = E_a/R(T_2 - T_1/ T_1.T_2) \qquad (3.2)$$

Where, E_a is the activation energy (kcal/mol) and R is the Boltzmann gas constant (kcal/mol/K). However, the values of E_a, determined for multimineralic rock do not necessarily define the temperature dependent rate constants for unique phases or reactions as required by the Arrhenius equation (White et al., 1999). Also, recent studies have shown that experimental activation energies for silicate dissolution are dependent on solution composition at a particular pH (Brady and Walter, 1992; Chen and Brantley, 1996; White et al., 1999). The effect of such variables is also considered in the present study. To obtain the apparent activation energy, experiments have been conducted at two different temperatures, keeping the pH constant.

(A)

(B)

(C)

(D)

(E)

(F)

Figure 3.5 Photograph of instruments used for various analyses (A) UV Spectrophotometer, (B) Ion Chromatograph (IC), (C) Scanning Electron Microscope attached with Energy Dispersive X-ray (SEM-EDAX), (D) Atomic Absorption Spectrophotometer (AAS), (E) X-ray Diffractometer (XRD), (F) BET Surface Area and BJH Pore volume Analyser

CHAPTER 4

RESULTS AND DISCUSSION

4.1 MAJOR IONS AND ELEMENTAL FLUX RATES IN ALAKNANDA AND BHAGIRATHI RIVERS

The objective of the present sub-chapter has been to understand, if there have been any temporal and spatial variations in the river water chemistry and if it does, then whether rock dissolutions play an important role in the resulting chemical composition of water in Alaknanda and Bhagirathi rivers.

4.1.1 Major Ions

Data on the major ion composition of the source waters of the Alaknanda and Bhagirathi rivers are presented in Table 4.1, which show significant seasonal and temporal variations (Figure 4.4). The major cations, which make up more than 42% of the total dissolved solids (TDS) in the Alaknanda-Bhagirathi rivers are Ca^{2+}, Mg^{2+}, Na^{+} and K^{+}. Among the cations, Ca^{2+} is the most dominant, contributing on average 55% of total cationic composition followed by Mg^{2+} (22%), Na^{+} (17%) and K^{+} (6%) (Figure 4.1).

Calcium (Ca^{2+}) in river water is derived largely from the weathering of carbonates (calcite, dolomite and aragonite), sulfates (gypsum and anhydrite) and silicates (feldspars, ca-pyroxenes). The Alaknanda mainstream shows mean annual concentration of Ca^{2+} ~ 560 $\mu molL^{-1}$, at Srinagar; whereas Ca^{2+} ranges from 342 $\mu molL^{-1}$ (High flow) to 714 $\mu molL^{-1}$ (Low flow). The Bhagirathi mainstream also shows similar trend. The average annual Ca^{2+} concentrations were observed to be 354 $\mu molL^{-1}$ at Maneri on Bhagirathi river.

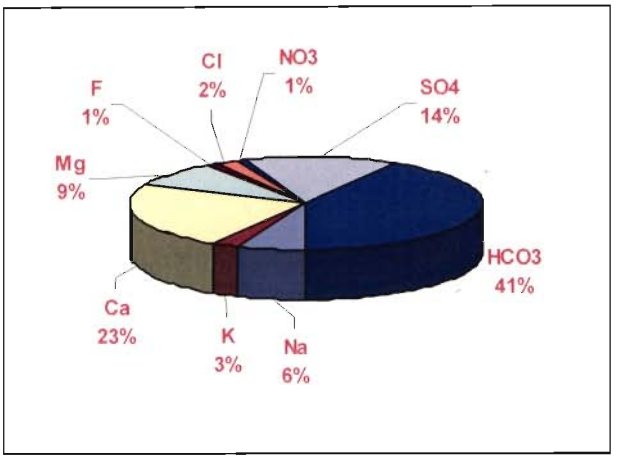

Figure 4.1 The average percentage of relative abundances of major cations and anions in Alaknanda-Bhagirathi river water

The Alaknanda mainstream shows average annual concentration of Mg^{2+} of approximately 230 $\mu molL^{-1}$, at Srinagar; and ranges from 83 $\mu molL^{-1}$ (High flow) to 445 $\mu molL^{-1}$ during low flow (January 2005). The Bhagirathi mainstream shows high concentrations during the lean period (winter). Mean annual Mg^{2+} concentrations were observed to be 143 $\mu molL^{-1}$ at Maneri. Mg-silicate minerals, chiefly amphiboles, pyroxenes, olivines and biotites, as well as dolomites constitute the major source of Mg^{2+}. Sodium and Potassium together accounted for 23% of the total cations and 8% of the dissolved solids, which show Na and K source minerals are being weathered in very less quantities. The Alaknanda mainstream shows mean annual concentration of Na^{+} of approximately 124 $\mu molL^{-1}$, at Srinagar, and ranges from 49 $\mu molL^{-1}$ (High flow) to 563 $\mu molL^{-1}$ during low flow (January 2005). The Bhagirathi mainstream also shows similar trend. The average annual Na^{+} concentrations were observed to be 110 $\mu molL^{-1}$ at Maneri village.

Ternary diagrams for cations for the Alaknanda and Bhagirathi mainstream (Figure 4.2) shows Ca^{2+} and Mg^{2+} are the dominant cations. Among the anions, the dominant species are HCO_3^- and SO_4^{-2} constituting approximately 57% of the dissolved solids. The bicarbonate contributions vary from 55 to 92%. The major source of HCO_3^- in river water is from carbonate and silicate weathering, which together account for >95% of global river water composition (Berner and Berner, 1987). Dominance of carbonate in the Highland rivers of Himalaya has also been reported by Sarin *et al.* (1992) and English *et al.* (2000).

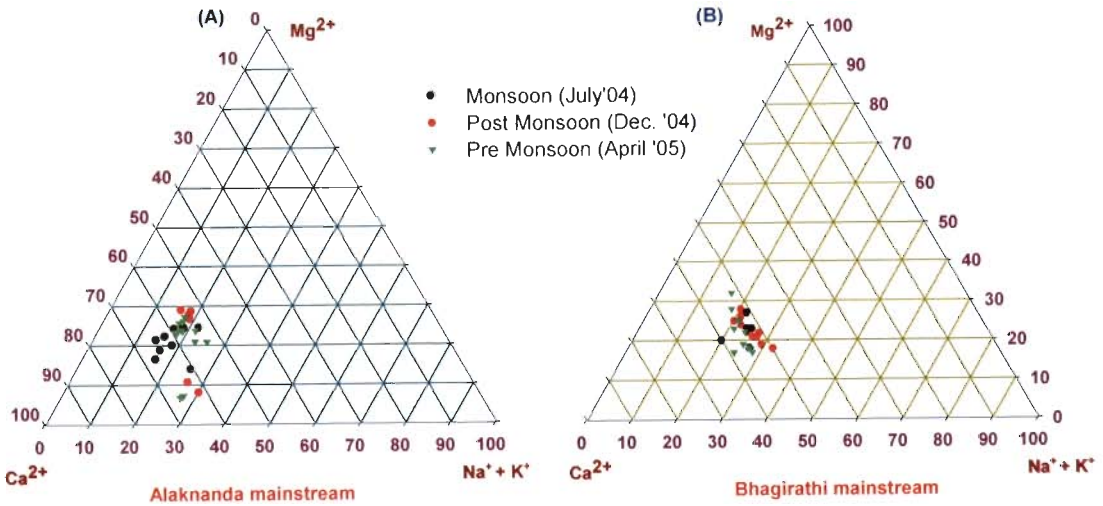

Figure 4.2 Ternary diagram for cations for the (A) Alaknanda and (B) Bhagirathi river

Among the anions, sulfate (SO_4^{-2}) constitutes ~ 14% of total anionic charge in the Alaknanda-Bhagirathi rivers. The annual average sulfate concentrations are 160 (64-303) $\mu molL^{-1}$ and 218 (44-371) $\mu molL^{-1}$ for the Alaknanda and Bhagirathi mainstreams respectively. These variations are in concurrence with the data of Sarin *et al.* (1992) and Bickle *et al.* (2003). After HCO^-_3, SO_4^{2-} is the next dominant anion in the Alaknanda and Bhagirathi river basins. The rocks which contain abundant sulfur are pyrites (FeS_2), gypsum

($CaSO_4.H_2O$) and anhydrite ($CaSO_4$). River sulfate results mainly from dissolution of gypsum or oxidation of pyrites. Gypsum weathers faster because it goes into solution quickly and also gypsum beds occur as discrete beds, thus enabling selective removal during weathering. On the other hand, pyrite occurs as disseminated forms and requires breakdown of surrounding rocks before sulfate is released by oxidation (Sarin et al. 1992).

Silica in river water is present largely as H_4SiO_4 derived from the weathering of silicate minerals. Dissolved silica at pH values less than 9 is present as silicic acid (H_4SiO_4). At pH values above 9, H_4SiO_4 dissociates to $H_3SiO_3^-$ and $H_2SiO_4^{2-}$. All the water samples analyzed in present study and data of previous studies indicate that pH values in the Alaknanda - Bhagirathi basins show pH of less than 9, hence H_4SiO_4 or SiO_2 is the common species in the Alaknanda and Bhagirathi rivers. The Alaknanda mainstream shows average annual concentration of total dissolved silica (SiO_2) of approximately 80 $\mu molL^{-1}$, at Srinagar, whereas it ranges from 34 $\mu molL^{-1}$ (High flow) to 146 (Low flow) $\mu molL^{-1}$. The average annual SiO_2 concentrations were observed to be 68 (21 to 136) $\mu molL^{-1}$ at Maneri village. SiO_2 concentrations observed in the Alaknanda-Bhagirathi Rivers are relatively similar in comparison to the Yamuna river (67-378 $\mu molL^{-1}$; Dalai *et al.* 2002), Amazon river (60-160 $\mu molL^{-1}$; Gaillardet *et al.* 1999), Congo river (140-210 $\mu molL^{-1}$; Dupre *et al.* 1996). The SiO_2 concentrations in the Alaknanda-Bhagirathi rivers are significantly low in comparison to the rivers draining mostly volcanic rocks such as, the Krishna river (91-685 $\mu molL^{-1}$; Das *et al.* 2005), Reunion Island (200-800 $\mu molL^{-1}$; Louvat and Allegre, 1997), Sao Miguel Island (268-1250 $\mu molL^{-1}$; Louvat and Allegre, 1998) Caribbean Island

(213-1000 μmolL$^{-1;}$ Rad *et al.* 2006), Iceland (420-2700 μmolL^{-1}; Gislason *et al.*1996) and the Nyong basin (490-1086 μmolL^{-1}; Viers *et al.* 2000).

Ternary diagram for anions for the Alaknanda and Bhagirathi mainstream (Figure 4.3) shows that most of the samples lie in the zone dominated by HCO^{-}_{3} and SO_4^{2-}.

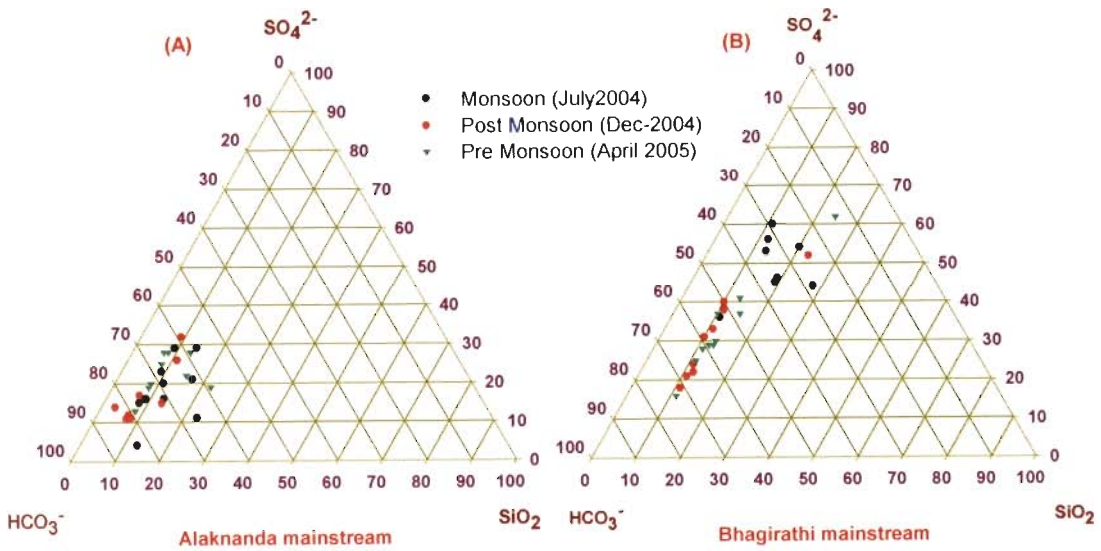

Figure 4.3 Ternary diagram for anions for the (A) Alaknanda and (B) Bhagirathi river

Table 4.1 Major ion compositions of weekly analyzed samples of the Alaknanda and Bhagirathi rivers, during July 2004 to July 2005, (all data in $\mu molL^{-1}$ except pH, TDS and TSM (mgL^{-1}), TZ (μeqL^{-1}) and NICB (%)

S.No.	Code No.	Date	PH	TDS	TSM	Na^{+}	K^{+}	Ca^{+2}	Mg^{+2}	F^{-}	Cl^{-}	NO^{-}_{3}	SO^{-2}_{4}	HCO^{-}_{3}	TZ^{+}	TZ^{-}	NICB	SiO_2
Alaknanda at Srinagar																		
1	SN1	19.07.04	7.78	107	3186	54	49	538	114	10	14	7	85	1153	1406	1355	4	96
2	SN2	26.07.04	7.28	129	4327	49	89	652	130	8	11	23	111	1360	1701	1624	5	104
3	SN3	02.08.04	7.49	111	4558	45	58	561	120	7	9	14	85	1200	1464	1401	4	95
4	SN4	09.08.04	7.45	133	6135	51	82	674	146	15	16	15	93	1442	1771	1674	5	98
5	SN5	16.08.04	7.78	116	3153	52	64	536	183	13	19	14	87	1252	1553	1473	5	98
6	SN6	23.08.04	7.52	92	2851	55	34	406	131	20	15	7	108	953	1161	1211	-4	91
7	SN7	30.08.04	7.51	92	1849	57	42	415	153	16	15	5	81	978	1235	1175	5	90
8	SN8	06.09.04	7.55	89	1026	56	37	386	130	17	14	6	68	984	1123	1158	-3	87
9	SN9	13.09.04	7.65	86	1543	59	36	371	132	16	14	6	64	955	1100	1119	-2	99
10	SN10	20.09.04	7.53	83	976	62	31	359	119	15	18	9	69	899	1050	1080	-3	98
11	SN11	27.09.04	7.49	85	866	58	28	378	142	17	15	5	87	895	1125	1105	2	146
12	SN12	04.10.04	7.32	82	789	60	38	342	128	16	15	4	110	835	1037	1090	-5	115
13	SN13	11.10.04	7.68	88	644	80	33	370	164	17	21	13	129	851	1181	1161	2	136
14	SN14	18.10.04	7.48	112	433	118	46	482	214	15	19	14	213	1005	1556	1479	5	133
15	SN15	25.10.04	7.82	119	325	133	54	509	216	16	19	14	195	1110	1636	1549	5	94
16	SN16	01.11.04	7.56	159	159	242	59	627	299	11	19	16	260	1502	2153	2068	4	68
17	SN17	08.11.04	7.77	136	115	166	58	577	248	8	98	41	214	1219	1873	1793	4	66
18	SN18	15.11.04	7.65	132	99	158	54	544	250	20	76	21	213	1200	1800	1743	3	63
19	SN19	22.11.04	7.67	126	65	134	48	518	234	20	53	19	222	1140	1686	1677	1	63

20	SN20	29.11.04	7.76	138	45	179	51	579	256	17	30	16	240	1261	1899	1804	5	63
21	SN21	20.12.04	7.52	142	36	180	58	591	287	49	84	45	239	1240	1994	1896	5	63
S.No.	**Code No.**	**Date**	**PH**	**TDS**	**TSM**	**Na^{+}**	**K^{+}**	**Ca^{+2}**	**Mg^{+2}**	**F^{-}**	**Cl^{-}**	**NO^{-}_{3}**	**SO^{-2}_{4}**	**HCO^{-}_{3}**	**$TZ^{(+)}$**	**$TZ^{(-)}$**	**NICB**	**SiO_2**
22	SN22	27.12.04	7.57	137	48	155	50	571	278	22	53	46	225	1236	1902	1806	5	63
23	SN23	03.01.05	7.65	204	41	448	113	714	445	2	378	138	303	1619	2879	2742	5	80
24	SN24	10.01.05	7.50	144	39	181	56	585	297	17	60	25	246	1306	2001	1901	5	58
25	SN25	17.01.05	7.62	152	76	198	57	622	301	15	87	100	244	1310	2100	2000	5	47
26	SN26	24.01.04	7.62	142	65	176	59	571	284	13	65	45	183	1366	1945	1854	5	51
27	SN27	31.01.04	7.61	173	48	563	104	608	237	172	31	357	95	1481	2357	2232	5	48
28	SN28	07.02.05	7.63	127	97	163	38	535	231	14	62	53	170	1186	1732	1654	5	34
29	SN29	14.02.05	7.65	125	104	156	36	532	213	30	53	35	168	1200	1682	1655	2	61
30	SN30	21.02.05	7.70	141	88	178	53	580	270	12	75	30	176	1363	1932	1832	5	69
31	SN31	28.02.05	7.65	134	118	164	45	547	228	19	72	36	245	1192	1760	1810	-3	63
32	SN32	07.03.05	7.56	134	99	159	40	559	259	9	59	44	173	1287	1835	1745	5	63
33	SN33	14.03.05	7.49	134	123	102	48	577	255	10	56	33	236	1205	1814	1776	2	63
34	SN34	21.03.05	7.75	134	110	111	62	584	234	11	51	28	223	1224	1810	1760	3	77
35	SN35	28.03.05	7.72	133	227	91	60	604	231	12	53	27	201	1246	1822	1741	4	71
36	SN36	05.04.05	7.78	138	175	106	74	641	204	15	46	17	174	1355	1869	1781	5	48
37	SN37	12.04.05	7.70	139	123	101	83	612	243	16	56	16	179	1362	1896	1809	5	44
38	SN38	19.04.05	7.59	144	268	90	82	666	212	17	44	16	158	1456	1929	1849	4	67
39	SN39	26.04.05	7.62	139	225	80	77	666	194	16	35	11	143	1431	1877	1777	5	101
40	SN40	03.05.05	7.52	145	315	72	85	708	182	17	31	13	153	1476	1936	1842	5	44
41	SN41	10.05.05	7.77	129	522	62	68	627	167	17	30	10	126	1341	1719	1650	4	77
42	SN42	06.06.05	7.71	121	563	72	50	609	136	19	32	16	131	1220	1612	1548	4	116

43	SN43	13.06.05	7.76	126	652	67	58	647	134	13	31	12	125	1291	1687	1596	5	76
44	SN44	5.07.05	7.81	127	2865	56	75	684	83	3	25	9	107	1332	1665	1583	5	96
45	SN45	12.07.05	7.90	119	3238	65	54	599	107	4	25	21	101	1260	1532	1512	1	94
46	SN46	19.07.05	8.02	127	8692	62	39	681	110	3	24	4	82	1399	1682	1594	5	98
S.No.	**Code No.**	**Date**	**PH**	**TDS**	**TSM**	**Na^{+}**	**K^{+}**	**Ca^{+2}**	**Mg^{+2}**	**F^{-}**	**Cl^{-}**	**NO^{-}_{3}**	**SO^{-2}_{4}**	**HCO^{-}_{3}**	**TZ $^{(+)}$**	**TZ $^{(-)}$**	**NICB**	**SiO_2**
							Bhagirathi at Maneri											
47	UK1	19.07.04	7.51	48	6094	18	27	207	89	21	11	12	105	396	636	650	-2.2	21
48	UK2	26.07.04	7.85	60	2863	48	61	259	98	21	11	12	142	472	825	801	2.9	99
49	UK3	02.08.04	7.68	56	4733	50	44	227	88	19	12	12	128	456	723	756	-4.6	101
50	UK4	09.08.04	7.36	70	6030	51	79	287	99	22	14	17	177	538	900	944	-4.9	106
51	UK5	16.08.04	7.65	119	8939	57	89	566	189	19	11	12	379	798	1656	1599	3.4	108
52	UK6	23.08.04	7.24	89	9864	51	36	352	186	14	7	10	217	758	1165	1223	-5.0	83
53	UK7	30.08.04	7.33	202	4753	479	37	794	359	15	10	9	511	1621	2822	2677	5.1	78
54	UK8	06.09.04	7.68	80	1281	57	34	317	155	13	8	7	188	685	1036	1091	-5.3	76
55	UK9	13.09.04	7.85	51	1063	28	22	249	62	14	7	6	114	423	674	679	-0.7	69
56	UK10	20.09.04	7.64	73	976	46	27	336	124	19	9	11	166	610	993	981	1.2	74
57	UK11	27.09.04	7.74	96	645	79	38	414	194	16	10	9	232	789	1332	1287	3.4	94
58	UK12	04.10.04	7.64	99	457	77	36	422	219	14	18	13	250	789	1394	1334	4.3	85
59	UK13	11.10.04	7.66	97	403	79	30	389	190	17	13	11	229	833	1268	1332	-5.0	104
60	UK14	18.10.04	7.85	104	277	138	35	418	196	18	24	14	285	794	1402	1422	-1.4	136
61	UK15	25.10.04	7.89	95	61	31	48	402	193	18	25	14	253	748	1269	1312	-3.4	122
62	UK16	01.11.04	7.78	54	44	47	31	211	90	2	7	6	48	595	680	707	-4.0	133
63	UK17	08.11.04	7.89	50	48	45	34	199	80	3	7	12	44	537	637	647	-1.5	120

64	UK18	15.11.04	7.76	51	56	46	39	204	82	1	11	0	64	514	656	654	0.3	61
65	UK19	22.11.04	7.92	51	51	43	37	209	80	1	10	12	77	494	659	672	-1.9	58
66	UK20	29.11.04	8.05	48	67	44	40	208	70	1	10	1	63	480	640	618	3.4	61
67	UK21	06.12.04	7.92	60	45	49	42	255	97	1	9	10	63	615	794	760	4.3	62
68	UK22	31.01.04	7.70	108	43	216	26	471	171	19	47	0	371	683	1527	1491	2.4	52
69	UK23	07.02.05	7.30	103	49	207	43	434	155	17	56	2	314	711	1430	1413	1.2	61
70	UK24	14.02.05	7.39	113	53	223	47	499	166	18	50	0	348	766	1598	1530	4.3	63

S.No.	Code No.	Date	pH	TDS	TSM	Na^{+}	K^{+}	Ca^{+2}	Mg^{+2}	F^{-}	Cl^{-}	NO^{-}_{3}	SO^{-2}_{4}	HCO^{-}_{3}	$TZ^{(+)}$	$TZ^{(-)}$	NICB	SiO_2
71	UK25	21.02.05	7.69	115	55	223	46	478	189	19	48	1	345	812	1603	1571	2.0	62
72	UK26	28.02.05	7.25	114	62	224	44	486	185	17	60	0	342	793	1609	1554	3.4	53
73	UK27	07.03.05	7.61	108	47	206	52	462	164	22	51	1	316	754	1508	1460	3.2	61
74	UK28	14.03.05	7.68	109	49	209	49	468	163	18	51	0	313	785	1521	1480	2.7	54
75	UK29	21.03.05	7.57	92	56	149	46	364	137	14	38	0	225	741	1199	1244	-3.8	61
76	UK30	28.03.05	7.67	100	63	189	39	435	147	18	40	1	251	780	1391	1342	3.5	59
77	UK31	05.04.05	7.74	84	96	142	36	347	125	13	34	0	202	690	1122	1141	-1.7	58
78	UK32	12.04.05	7.62	102	84	180	44	411	139	15	44	0	241	841	1323	1381	-4.4	58
79	UK33	19.04.05	7.55	100	72	158	58	374	167	15	32	18	236	826	1296	1362	-5.1	54
80	UK34	26.04.05	7.67	94	92	132	41	385	144	1	3	2	122	960	1231	1210	1.7	50
81	UK35	03.05.05	7.46	97	109	114	40	386	190	15	25	26	253	752	1306	1324	-1.4	44
82	UK36	10.05.05	7.71	82	98	109	35	340	122	28	25	48	223	584	1068	1130	-5.8	48
83	UK37	17.05.05	7.56	80	126	98	35	321	147	12	24	22	202	633	1070	1095	-2.3	43
84	UK38	23.05.05	7.66	82	345	109	31	334	153	10	34	23	219	610	1115	1115	0.0	44
85	UK39	30.05.05	7.83	83	141	106	31	328	144	11	29	16	244	600	1082	1145	-5.8	45
86	UK40	06.06.05	7.65	78	393	104	28	327	129	13	23	21	230	555	1044	1073	-2.8	46

87	UK41	13.06.05	7.84	84	631	94	26	341	163	12	20	17	254	612	1127	1170	-3.8	41
88	UK42	21.06.05	7.87	81	783	124	48	335	156	21	31	12	274	496	1152	1108	3.8	45
89	UK43	28.06.05	7.94	61	1082	58	42	248	133	19	12	8	261	312	861	874	-1.5	46
90	UK44	05.07.05	7.76	45	1982	37	19	197	82	9	12	5	108	368	613	610	0.5	57
91	UK45	12.07.05	7.63	64	3474	41	70	317	85	26	11	16	238	335	915	864	5.6	43
92	UK46	19.07.05	7.69	54	8459	40	38	254	84	28	14	22	161	356	756	743	1.7	42

4.1.2 Elemental Flux Rates

Estimation of elemental flux rates is important to understand chemical weathering rates in the Alaknanda and Bhagirathi rivers. Figure 4.5 shows temporal and spatial variation in flux rates of Ca^{2+}, Mg^{2+} and SiO_2 at two different locations, Maneri and Srinagar, respectively along Alaknanda and Bhagirathi rivers, over the time period between July 2005 to July 2006 (the flux rates of Ca^{2+}, Mg^{2+} and SiO_2 are only calculated, since these elements have been selected for calculations of dissolution rates by laboratory experiments, discussed later). A strong seasonal variation is noticed, which indicates the important role of rainfall, snowmelt and temperature on water chemistry. During monsoon period (June-October) flux rates are considerably high as compared to flux rates during pre- or post-monsoon period (November-May). The Himalayan rivers carry 69-83% of their annual flow during the monsoon months (June-October) characterized by heavy and intense rainfall up to 11,000 mm yr^{-1} (Bruijnzeel *et al.* 1989; Sinha *et al.* 2002). Subsequently, these Himalayan rivers, draining through the world's greatest range of relief and extreme climate, carry large sediment loads as they drain through the most active tectonic zones and geologically young, easily erodible foothill rocks. Wasson (2003), observed approximately two thirds of the landslides in the Himalayan region produced in 1999 were caused by human activities and contribute 140 and 1400 t $km^{-2}yr^{-1}$ of river sediment loads. High water discharge and sediment loads in Alaknanda and Bhagirathi rivers are essentially confined to monsoon season. Thus, during the monsoon season, heavy and continuous precipitation augment physical weathering, as a result, dissolution of the solids in the stream increases the concentration of the ionic species and thus contribute towards high chemical flux

rates of the elements. Calcium is a very mobile and easily soluble element and hence shows high seasonal fluctuation, followed by Mg^{2+} and SiO_2. The ratio of average water discharge and basin area of both the rivers at the respective sampling sites is almost the same, which advocates the importance of the concentration of the ionic species in deciding the chemical weathering rates and elemental flux rates. The Ca^{2+} flux rate is ~ 7x compared to Si flux rate in Alaknanda river at Srinagar, whereas at Maneri in Bhagirathi river, it is about 5x high as compared to Si flux rate. On the other hand, Ca^{2+} to Mg^{2+} flux rates are approximately 2.5x high in both the rivers at the respective sites. This is most likely due to dominance of dissolution of carbonates over silicate rocks in both the catchments. Previous studies have indicated that the source waters of Ganga river, namely Alaknanda and Bhagirathi rivers show high chemical and physical denudation rates (Krishnaswami *et al.* 1992; Pegram *et al.* 1992; Sarin *et al.* 1992; Singh *et al.* 1999; Dalai *et al.* 2002), although the water composition is significantly derived from carbonate rock weathering (Krishnaswami *et al.* 1992; Palmer and Edmond, 1992; Blum *et al.* 1998). According to Blum *et al.* (1998), 82% of bicarbonate in Raikhot watershed is derived from weathering of carbonate minerals and only 18% is derived from silicate weathering even though the bedrock is predominantly quartzo-feldspathic gneiss and granite with only ~1% carbonate in the watershed. Both the Alaknanda and Bhagirathi rivers flow over multilithologic terrains. They comprise mainly granitoids, high grade gneisses, schists, metabasics, phyllites, quartzites, black shales and carbonates. Although, these catchment rocks altogether contribute towards the stream chemical flux, they undergo different rates of dissolution depending on the type of constituent minerals and may thus show unique trends in Ca^{2+}, Mg^{2+} and dissolved silica flux

rates. Bluth and Kump (1994) showed the control of lithology and climate over river water chemistry by quantifying the flux rates of bicarbonates and silica of about 101 rivers worldwide. Their study indicated that the dissolved yield of a given drainage basin is determined by a balance between physical and chemical weathering. A warm, wet climate or the presence of abundant vegetation does not necessarily result in high rates of chemical denudation unless accompanied by high rates of physical weathering. In multilithologic terrains, the roles of individual rock types contribute at different rates in the estimation of chemical weathering and flux rates. The Alaknanda and Bhagirathi river waters are mildly alkaline with pH averaging in between 7.5 to 8.5 and average annual temperature fluctuates between 5^0C to 25^0C. Considering the above factors observed from field data, the dissolution experiments were carried out at pH 8.4 and at temperatures of 5^0C and 25^0C. In addition, the experiment was also carried out at pH 4.2 and 2.2 to estimate the role of organic acid and inorganic acid on dissolution rates.

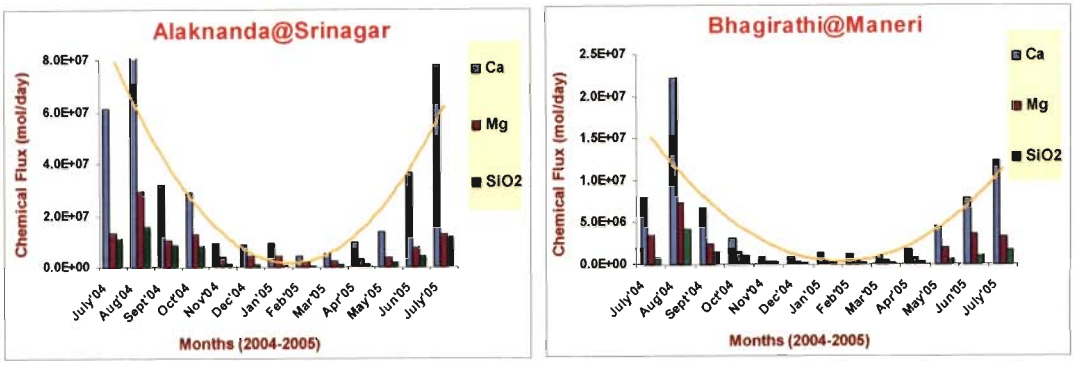

Figure 4.4 Chemical flux of Ca^{2+}, Mg^{2+} and SiO_2 in Alaknanda and Bhagirathi rivers at Srinagar and Maneri respectively during July 2004 through July 2005

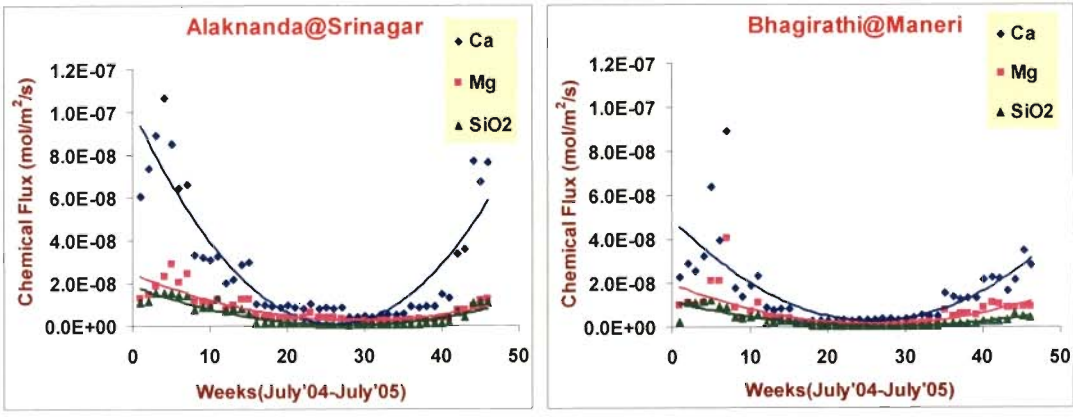

Figure 4.5 Temporal variation in chemical flux rates (w.r.t. Ca^{2+}, Mg^{2+} and SiO_2) of Alaknanda and Bhagirathi rivers at Srinagar and Maneri respectively during July 2004 to July 2005

4.2 DISSOLUTION KINETICS OF CALCITE (CC) AND DOLOMITE (DM)

Dissolution rates of calcite (CC) and dolomite (DM) and the respective activation energies are presented in Table 4.2.

For CC, it is observed that the release rate of Ca is comparatively higher at 25^0C as compared to 5^0C, and the same trend has been observed for DM as well. For CC and DM (Figure 4.6), the progress of dissolution was observed in terms of Ca- and Mg-release as a function of time.

Table 4.2 Experimental conditions and results of CC and DM dissolution

pH	Sample	Element released	ln (dissolution rate) (mol/m^2/s)		Activation Energy E_a (kcal/mol)
			lnR_2 (25^0C)	lnR_1 (5^0C)	
8.4	CC	Ca	-26.85	-27.25	13.98
	DM	Ca	-27.59	-27.69	3.41
		Mg	-28.5	-28.79	9.98

An important aspect of dissolution behavior of CC (with respect to Ca) and DM (with respect to Mg) (Fig. 4.6), is the higher release of both the cations (~1.5x) at 25^0C as compared to 5^0C. The ratio of Ca-release rate of CC and Mg-release rate of DM at 25^0C is 5.2, whereas the ratio of Ca-release rate of CC and Mg-release rate of DM at 5^0C is 4.6.

Experiment for determining dissolution rate was also done in indigenously made Mixed Flow Reactor at controlled temperature (25^0C) and pH (8.4) conditions for 15 days. Higher speed of the magnetic stirrer caused rapid wearing of the CC grains which subsequently resulted in increase in Ca release during the initial phase of the experiment and during course of time it decreased to

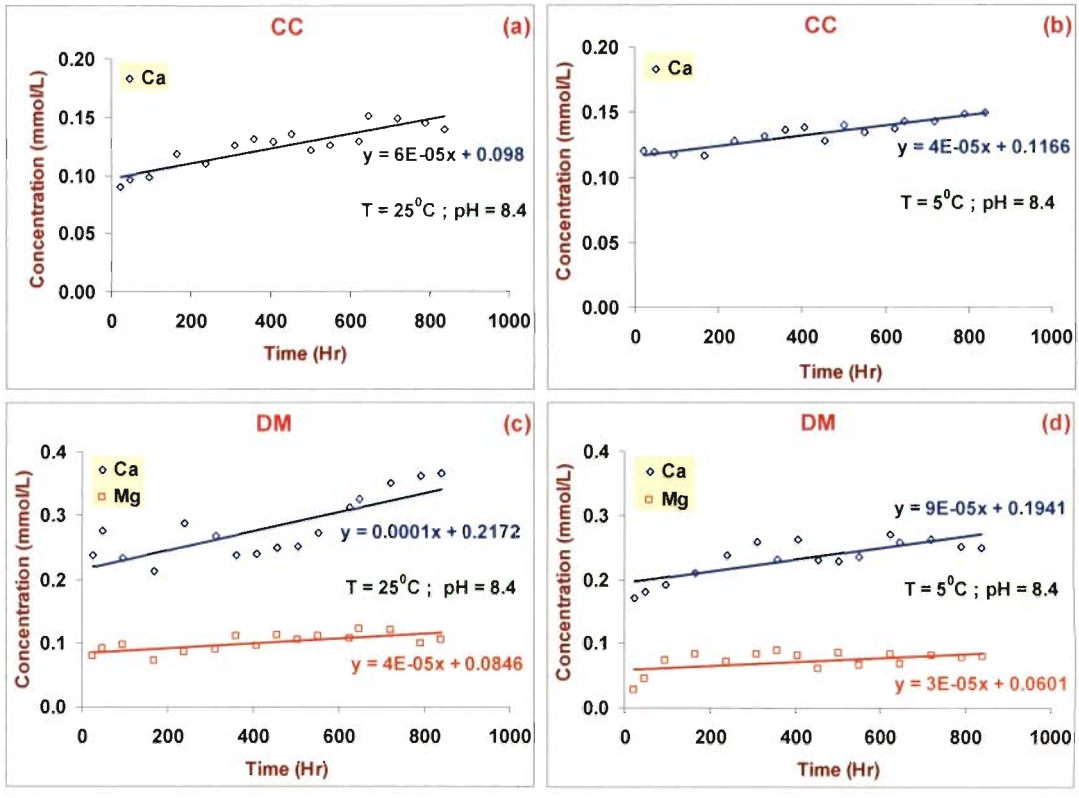

Figure 4.6 Elemental release versus time plots for CC and DM at pH 8.4 and temperature 25^{0}C and 5^{0}C. (a) and (b) show Ca release of CC; (c) and (d) show Ca and Mg release for DM

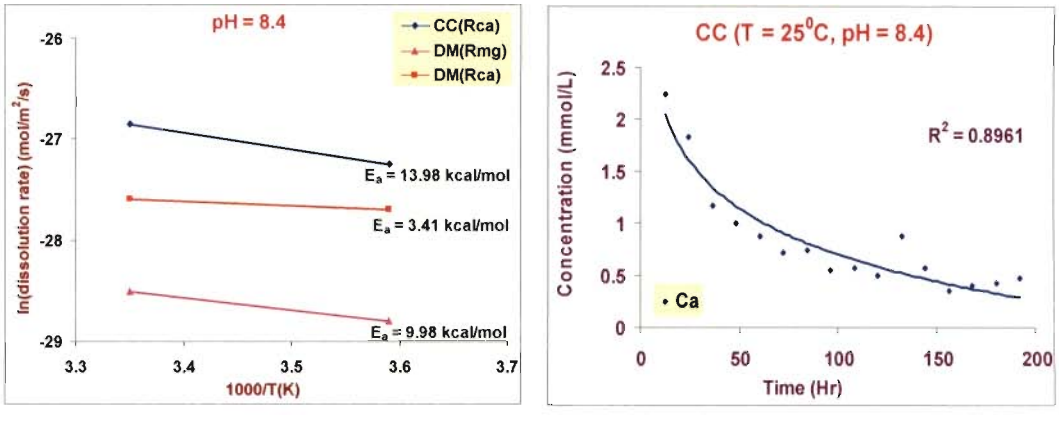

Figure 4.7 Calculated activation energies (E_a) of CC and DM dissolution with respect to temporal release of Ca and Mg at pH = 8.4 (*left hand side*); behavior of CC precipitation in mixed flow reactor (*right hand side*)

minimum which presents a negative trend line when plotted against time (Fig. 4.7, *right hand side*). The negative trend line depicts the precipitation behavior of CC.

Ca and Mg exhibit average apparent activation energies (E_a) of 13.98 and 9.98 kcal/mol respectively at pH 8.4 over the temperature range of 5^0-25^0 C (Table 4.2, Figure 4.7, *left hand side*). The Ca release rate for CC is more sensitive to increase in temperature from 5^0 to 25^0C, as compared to Mg release rate for DM in the same temperature range at pH 8.4. This may be one of the reasons for CC to dissolve faster as compared to DM. The dissolution rates of CC and DM determined in the present study are comparatively less than the summarized calcite dissolution rates observed by Arvidson et al. (2003) and calcite and dolomite dissolution rates observed by Pokrovsky et al. (2005). The differences may be attributed to the differing conditions of experimentation, e.g. we did not use rotating disk for continuous stirring and did not have pCO_2 input. These two factors could substantially alter the dissolution rates. In addition, the experimentation time, equilibrium conditions and ionic-strength of the buffer solutions may also have influenced the slower rates of dissolution of CC and DM.

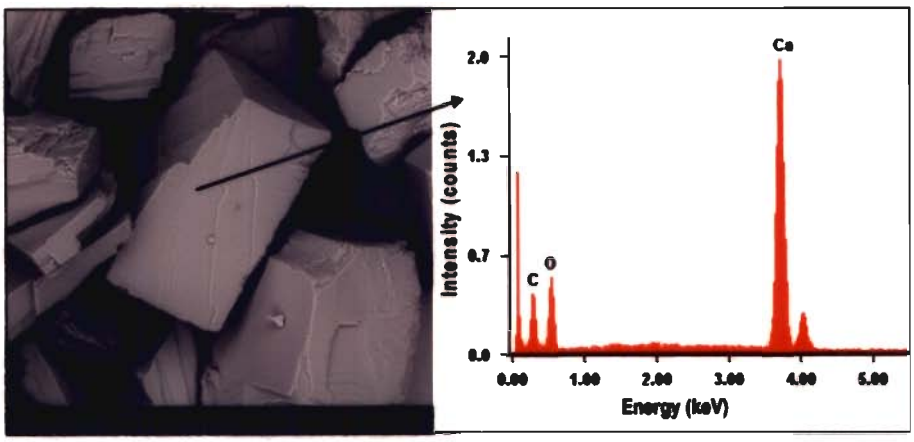

Figure 4.8 SEM microphotograph of CC before dissolution experiment with EDX spectra of its flat surface

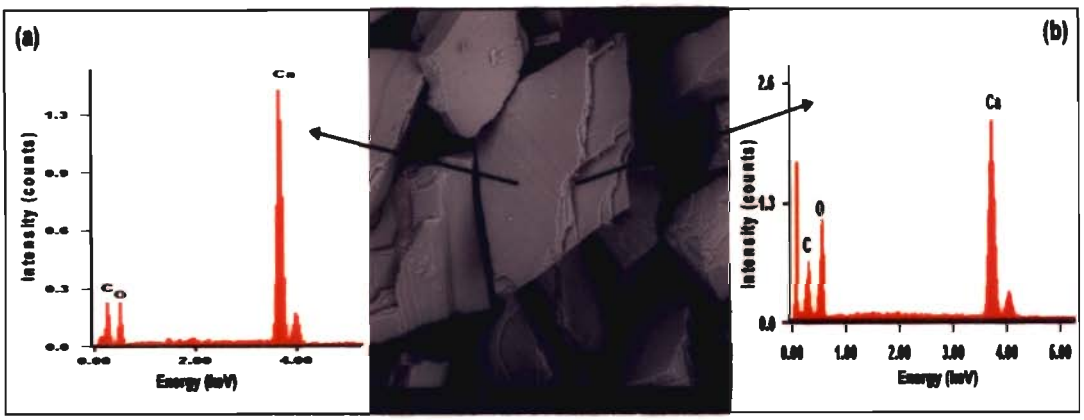

Figure 4.9 SEM microphotograph of CC after dissolution experiment with EDX spectra of its flat surface (a), and dislocation-site (b)

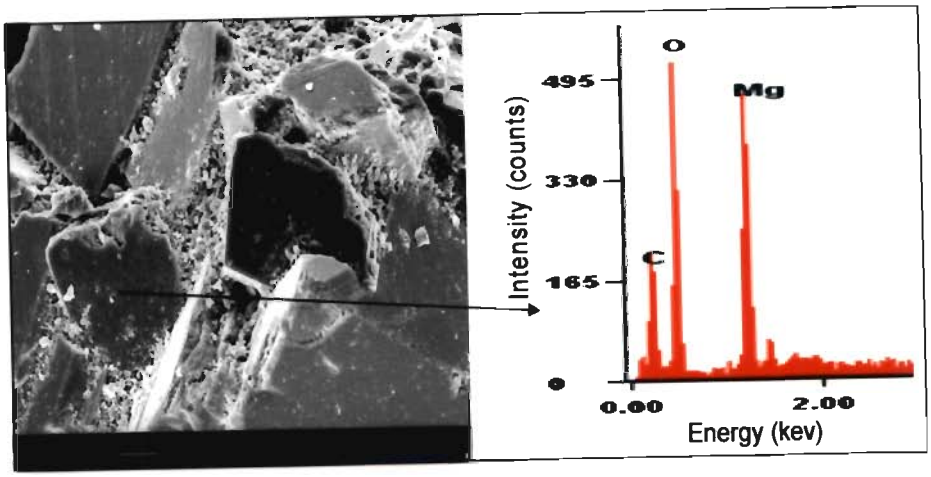

Figure 4.10 SEM microphotograph of DM before dissolution experiment with EDX spectra of its flat surface

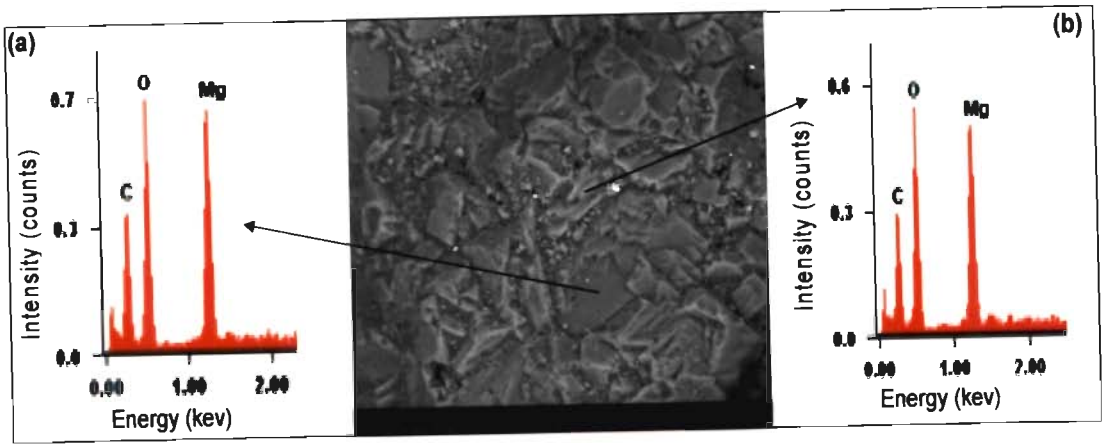

Figure 4.11 SEM microphotograph of DM after dissolution experiment with EDX spectra of (a) flat surface and (b) dislocation-site

Dissolution rates of minerals are most often controlled by their surface imperfections called dislocations (Drever, 1994, 1997; Appelo et al., 2005). Arvidson et al. (2003) discussed the role of grain size and surface topography in the dissolution rate variations in calcite. Pre-experiment SEM images of CC and DM grains (Fig. 4.8, Fig. 4.10) depict the rhombohedral-form with few kinks and steps developed at the grain boundaries. Although, the samples were ultrasonically cleaned prior to experiment, CC-grains may have been attached to very few ultra fine particles and are thus relatively clean as compared to grains of DM adhering many ultra fine particles. The kinks and steps at the crystal edges can be termed as dislocation sites and are characterized by lower binding energy. The atoms of these sites are highly susceptible to detach themselves from the surface and are thus the first to be released upon dissolution. An EDX spectrum of CC (Figure 4.8) and DM (Figure 4.10) show the pre-experiment concentration of Ca-atoms and Mg-atoms on their flat and smooth surfaces respectively. Post-experiment SEM images of the CC grains along with EDX spectra of its flat surface and dislocation site is shown in Figure 4.9 (a,b) and for DM in Figure 4.11(a,b). Table 4.3 presents a summary of pre- and post-experiment SEM-EDAX analysis data. From the SEM-EDAX data, it is observed that the release of cations is higher on the dislocation sites as compared to the flat smooth surfaces. For CC, the decrease in Ca atoms at the dislocation site is 2.25 times more compared to the flat surface. Similarly for DM, the decrease in Mg atoms at the dislocation site is 1.25 times more than that on the flat surface. However, there is a decrease in the release of Ca atoms at the flat surface than at the edges in the case of DM. These differences in elemental release rates indicate the importance of crytstallographic controlled dislocation sites as well as

rough grain boundaries. Thus, the release rates from high step and kink density will be higher, as compared to the smooth flat surfaces. Hence, the overall dissolution rates of CC and DM at experimental conditions given in Table 4.2 may be the average of elementary reaction rates at the rough grain boundaries and flat smooth surfaces.

Table 4.3 Summary of SEM-EDAX data of CC and DM dissolution-experiment at 25^0C

Sample	Element	Before Experiment (Atom %)	After Experiment (Atom %)		After Experiment (% decrease)	
			On Flat Surface	On Edge	On Flat Surface	On Edge
CC	Ca	31.04	27.40	22.85	11.72	26.38
DM	Mg	11.59	09.26	08.68	20.10	25.10
	Ca	15.59	12.43	14.00	20.26	10.19

CC dissolution may be described in terms of destruction of framework bonds involving Ca^{2+}, whereas DM dissolution can be envisaged in terms of detachment of Ca^{2+} and Mg^{2+} from the crystal surface. In both cases, diffusion of the cations and CO_3^{2-} ions away from the crystal surface also can not be ignored and may be minimal because truly diffusion controlled dissolution is limited to highly soluble salt minerals, which results in general rounding of the mineral grains. With increasing pH (alkaline conditions) far from equilibrium (high undersaturation), CC dissolution is controlled by *surface reaction* (as opposed to transport) kinetics (Sjöberg, 1976; Rickard and Sjöberg, 1983). Post-experiment SEM images of CC and DM depict the original rhombohedral form of the crystal without rounding of the grains. It suggests the crystallographic-controlled surface-reaction dissolution. CC and DM belong to the same crystal system and have similar crystal-forms, but framework bond of CC involves only Ca^{2+} and CO_3^{2-},

whereas DM involves Ca^{2+}, Mg^{2+} and CO_3^{2-}. Atomic structure of CC is characterized by layers of Ca analogous to the framework structure of halite. Dolomite shows dense atomic packing as the Ca and Mg are segregated in alternate layers (Deer et al., 1966). Dissimilarity in dissolution behavior of CC and DM can also be linked to the disparity in atomic configuration of their framework structure. Relative to CC, dense atomic packing in DM may retard its dissolution rate.

4.3 DISSOLUTION KINETICS OF ROCK TYPES AND SOIL

Dissolution rates of LG, GN and CQ is determined with respect to the temporal release of Si at the experimental conditions. Dissolution study of PY was carried out at pH 8.4 and the rate was determined with respect to temporal release of the targeted elements Ca, Mg, and Si. Dissolution rate of KS is determined with respect to the temporal release of Ca, Mg and Si at the experimental conditions. The results of the laboratory simulated dissolution rates of these rock types under present study is presented in Table 4.4.

Figures 4.12 (a, b), 4.12 (c, d), 4.13(a, b) demonstrate silica-release trends for LG, GN and CQ respectively at experimental conditions. For PY and KS, the progress of dissolution experiment was followed in terms of Ca-, Mg- and Si-release as a function of time as shown in Figure 4.14 and Figure 4.15 respectively.

It is observed from the respective trend lines of the targeted elements that the rate of dissolution of all lithologies increases with increase in temperature at all pH conditions (refer Table 4.4). Hence, temperature shows direct correlation with the dissolution rates of these lithologies during the short period of experimentation. Average activation energy (E_a) at pH 8.4, 4.2 and 2.2, exhibited by Si during dissolution of LG is 51.8, 37.93, and 3.6 kcal/mol respectively (Figure 4.16a); during dissolution of GN is 41.87, 20.33, and 13.9 kcal/mol respectively (Figure 4.16b); and during dissolution of CQ is 89.35, 23.8, and 10 kcal/mol respectively (Figure 4.17) and hence demonstrate the direct correlation of E_a with pH.

Table 4.4 Experimental conditions and results of rock-dissolution

pH	Sample	Element released	Dissolution Rate R(mol/m^2/s)		ln (dissolution rate)		Activation Energy(E_a)
			R_1(5^{0}C)	R_2(25^{0}C)	lnR_1(5^{0}C)	lnR_2(25^{0}C)	(kcal/mol)
8.4	LG	Si	5.49E-14	2.47E-13	-30.53	-29.03	51.80
	GN	Si	5.20E-14	1.75E-13	-30.58	-29.37	41.87
	CQ	Si	3.67E-14	4.90E-13	-30.93	-28.34	89.35
	PY	Ca	1.80E-14	2.40E-13	-31.63	-29.04	89.35
	PY	Mg	6.10E-14	1.80E-13	-30.43	-29.33	37.95
	PY	Si	6.10E-15	1.80E-14	-32.73	-31.63	37.95
	KS	Ca	1.16E-14	3.87E-14	-32.08	-30.88	41.40
	KS	Mg	3.87E-15	5.81E-15	-33.18	-32.78	13.80
	KS	Si	1.93E-15	1.93E-14	-33.87	-31.57	79.35
4.2	LG	Si	3.30E-14	9.91E-14	-31.04	-29.94	37.93
	GN	Si	3.50E-13	6.31E-13	-28.68	-28.09	20.33
	CQ	Si	2.45E-15	4.90E-15	-33.64	-32.95	23.80
	KS	Ca	6.35E-12	1.48E-11	-25.78	-24.94	28.98
	KS	Mg	2.40E-12	2.79E-12	-26.75	-26.60	05.17
	KS	Si	7.74E-15	3.09E-14	-32.49	-31.10	47.95
2.2	LG	Si	9.91E-13	1.10E-12	-27.64	-27.53	03.60
	GN	Si	1.40E-12	2.10E-12	-27.29	-26.89	13.90
	CQ	Si	3.67E-15	4.90E-15	-33.24	-32.95	10.00
	KS	Ca	6.97E-13	1.31E-12	-27.99	-27.35	22.08
	KS	Mg	2.32E-13	4.64E-13	-29.09	-28.39	24.15
	KS	Si	1.55E-14	3.09E-14	-31.79	-31.10	23.80

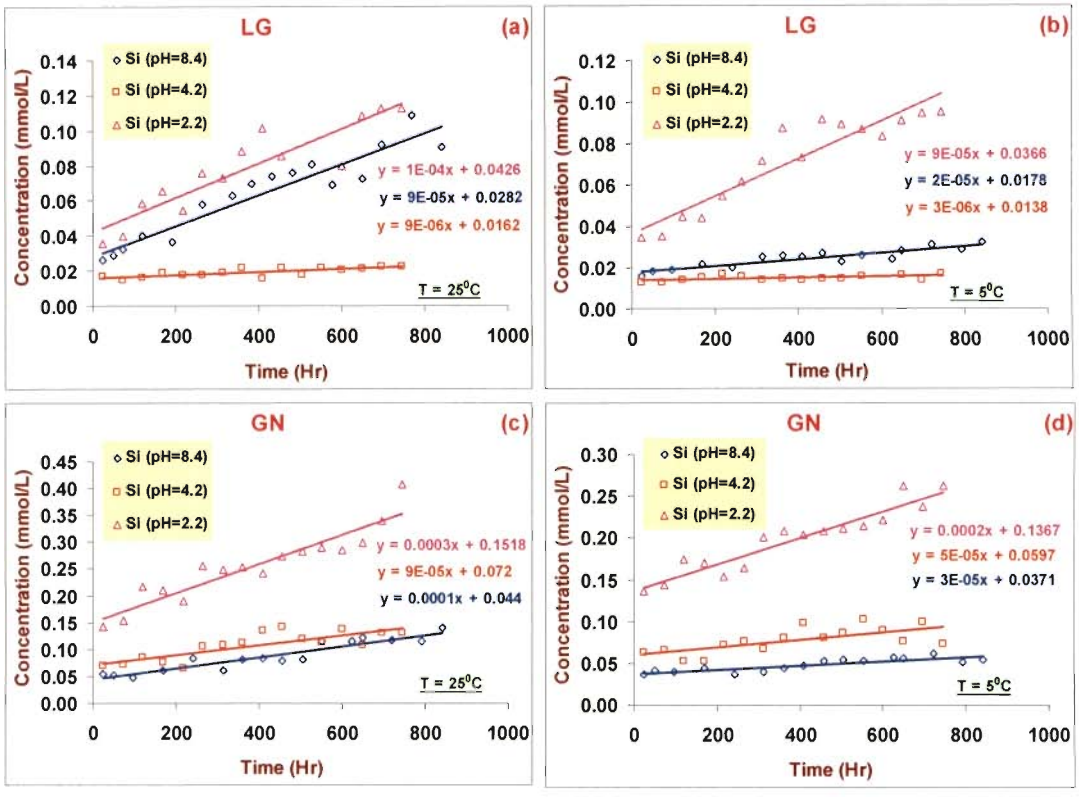

Figure 4.12 Temporal release of silica for LG and GN dissolution at pH = 8.4, 4.2 and 2.2. (a) and (b) show Si release for LG at 25^{0}C and 5^{0}C respectively; (c) and (d) show Si release for GN at 25^{0}C and 5^{0}C respectively

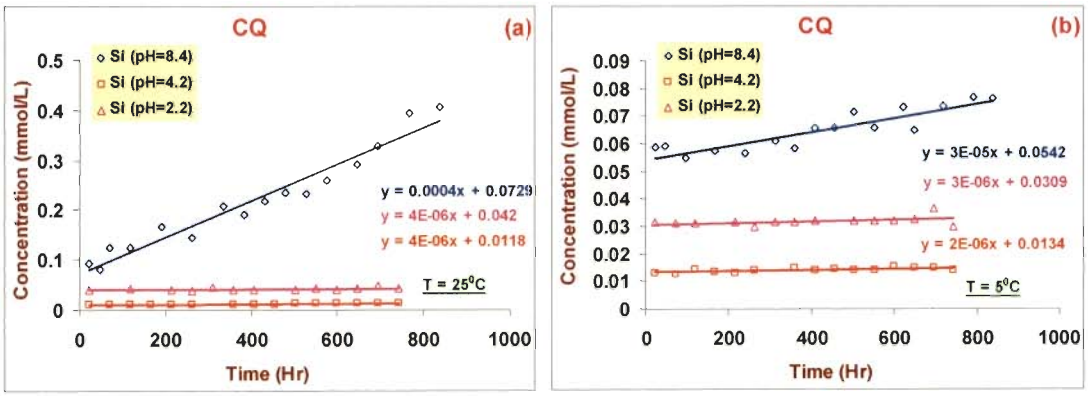

Figure 4.13 Temporal release of silica for CQ dissolution at pH = 8.4, 4.2 and 2.2 respectively at (a) 25^0C and (b) 5^0C

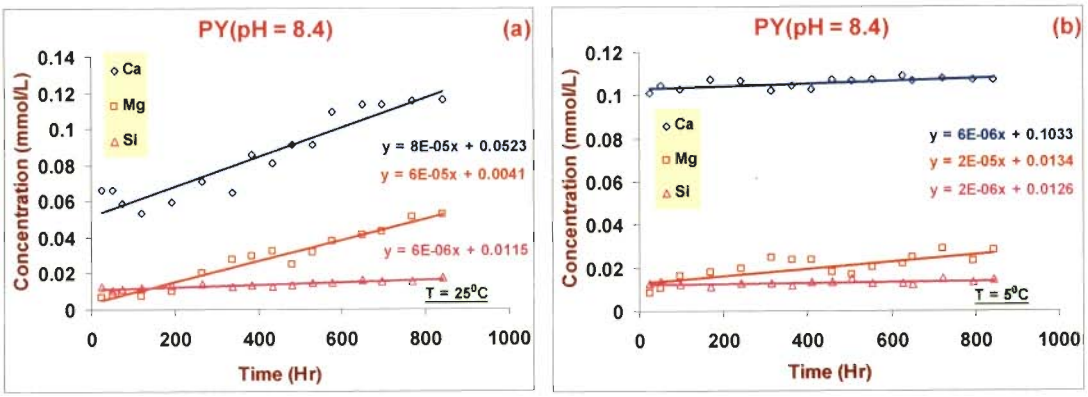

Figure 4.14 Temporal release of Ca, Mg, and Si for PY dissolution at pH = 8.4 respectively at (a) 25^0C and (b) 5^0C

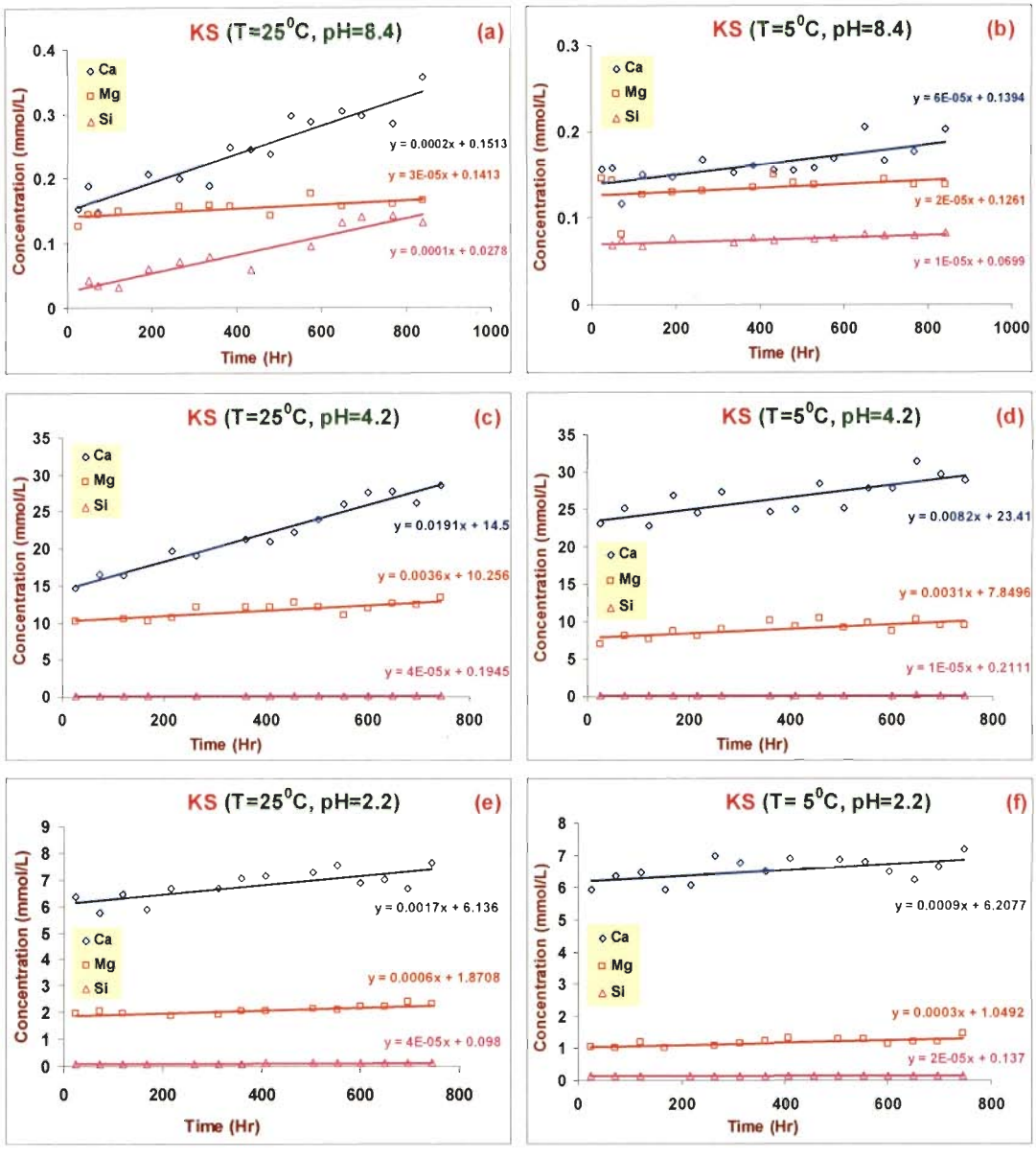

Figure 4.15 Temporal release of Ca, Mg, and Si for KS dissolution at 25°C and 5°C respectively (a,b) at pH = 8.4, (c,d) at pH = 4.2 and (e,f) at pH = 2.2

The average activation energy (E_a) at pH 8.4, 4.2 and 2.2 respectively, exhibited by Si during dissolution of KS is 79.35, 47.95, and 23.8 kcal/mol; for Ca, it is 41.4, 28.98, and 22.08 kcal/mol; and for Mg, it is 13.8, 5.17, and 24.15 kcal/mol (Table 4.4). A direct correlation is observed for E_a with pH. Hence, during dissolution reactions of LG, GN, CQ, and KS, E_a for Si release is high at pH 8.4, moderate at pH 4.0 and low at pH 2.2, suggesting that the release rate of silica is sensitive to pH in a positive way within the experimental temperature range between 5^0C to 25^0C.

In case of PY, it is observed from Figure 4.14 that the release-rate of Ca is comparatively more at 25^0C than at 5^0C. Besides, it reveals the same positive trend for temporal release of Ca, Mg, and Si with time. As shown in Figure 4.14, the progress of dissolution experiment was followed in terms of Ca-, Mg- and Si-release as a function of time. If we compare the rates of PY (Table 4.4) at different experimental conditions, an increase in dissolution-rate at 5^0C to 25^0C is ~13x, ~ 3x, and ~ 3x respectively for Ca, Mg and Si. It indicates the predominant role of temperature as compared to pH in regulating dissolution rate of PY with respect to Ca- release during experimental period at two different temperature conditions, whereas Mg and Si dissolve independently with more or less similar rates during experimental period at two different temperature conditions. It is possible that, Mg and Si are not very much influenced either by pH or temperature. This is evident from the activation energies involved in their respective dissolutions during the experimental conditions (Figure 4.17); Ca exhibits 89.35 kcal/mol, wheras Mg and Si exhibit 37.95 kcal/mol each for their dissolution within the experimental temperature range between 5^0C to 25^0C. The

range in which the amount of Ca is released during the experimental period is extremely high as compared to Mg and Si, both at 5^0C and 25^0C (Fig. 4.14). The rate of PY dissolution with respect to Ca release is dominantly controlled by temperature at pH 8.4.

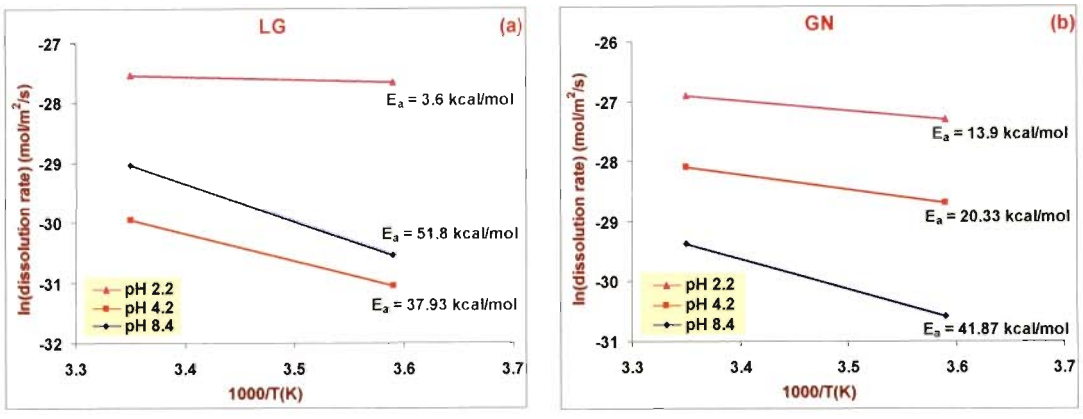

Figure 4.16 Activation energies (E_a) of LG and GN dissolution (a and b respectively) with respect to temporal release of Si at different pH conditions

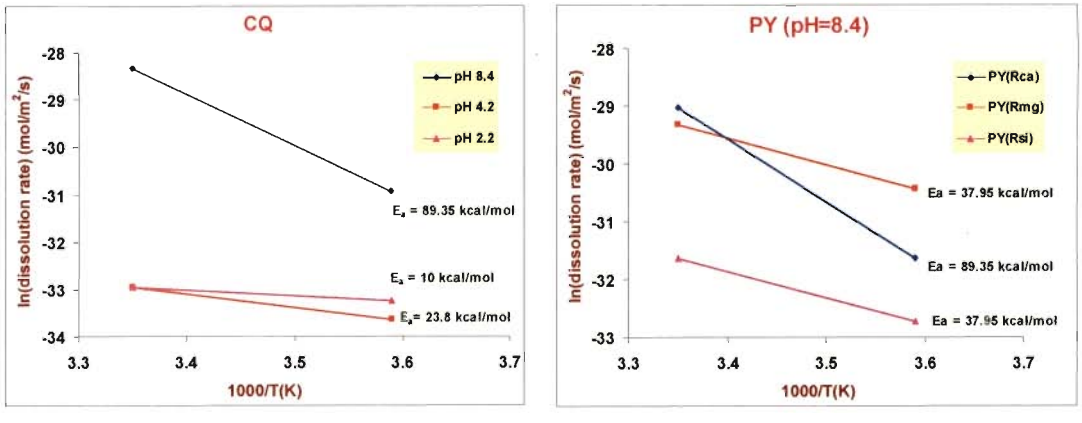

Fig. 4.17 Activation energies (E_a) of CQ (Si release) and PY dissolution (Ca, Mg, Si) at experimental conditions

The buffers of different pH used for the dissolution experiment in the present study contain the following characteristic ionic species as shown in the product side in the following reactions,

$CH_3COOH + CH_3COONa + H_2O = Na^+ + 2H^+ + OH^- + 2CH_3COO^-$ (pH 4.2)

$HCl + KCl + H_20 = K^+ + 2H^+ + OH^- + 2Cl^-$ (pH 2.2)

$NaHCO_3 + H_2O = Na^+ + 2OH^- + H^+ + CO_2 \uparrow$ (pH 8.4)

At pH 4.2 and 2.2 (acidic media), 2 moles of protons (H^+) are released as compared to 1 mole of hydroxyls (OH^-), whereas in alkaline media (pH 8.4), the quantity of hydroxyls (OH^-) is twice of the protons (H^+). CH_3COO^- is the organic-ligand and Cl^- is the inorganic-ligand produced in organic acid (pH 4.2) and inorganic acid (pH 2.2) respectively. pH dependency on dissolution rate of rock types in the present study at temperatures of 25^0C and 5^0C is shown in Figure 4.18. Far from equilibrium, dissolution rate of most silicate minerals is regulated by pH. In general, dissolution rates are pH-independent in the pH range of 5-8 of most natural waters, and increase exponentially both in the acid range and in the alkaline range (Arvidson *et al.* 2003, Berner and Berner, 1987). This pH dependency can be visualized in terms of proton (H^+) promoted dissolution in acid-solutions, hydroxyl (OH^-) promoted dissolution in alkaline-solutions and complex forming ligand assisted dissolution in organic solutions, resulting in adsorption of proton, hydroxyl or ligand to a cation at the surface of a solid and thus facilitating weakening and breaking of framework bonds of the crystal-lattice (Berner and Berner, 1987). Fig. 4.18 *(left hand side)* shows the rate of dissolution of LG with respect to silica is maximum at pH 2.2, moderate at pH 8.4 and low at pH 4.2. However, the dissolution rate of GN is maximum at pH 2.2, moderate at

pH 4.2 and least at pH 8.4. If we compare the dissolution rates of LG and GN (Table 4.4) at different experimental conditions for LG, an increase in release-rate of silica in between 5^0C to 25^0C is ~ 4.5x, ~ 3x, and ~ 1x respectively at pH 8.4, 4.2 and 2.2. Similarly, for GN, an increase in release-rate of silica in the temperature range of 5 - 25^0C is ~ 3.4x, ~ 1.8x and ~ 1.5x at pH 8.4, 4.2, and 2.2 respectively. This suggests the effect of temperature-change on dissolution of LG and GN with respect to Si-release rate, which is high at pH 8.4, moderate at pH 4.2 and low at pH 2.2. It is apparent that the rate of dissolution of CQ with respect to silica release is maximum at pH 8.4, moderate at pH 2.2 and least at pH 4.2 (Fig. 4.18, *left hand side*). However, the rates of CQ dissolution with respect to temporal release of silica as compared to LG and GN is appreciably low at pH 2.2 and 4.2 (acidic range), whereas the rate of CQ is comparable to LG and GN at pH 8.4 at both temperature conditions. The dissolution rates of CQ (Table 4.4) at different experimental conditions show an increase in release-rate of silica in between 5-25^0C is ~13x, ~ 2x and ~ 1.3x at pH 8.4, 4.2, and 2.2 respectively. In case of KS (Table 4.4) at different experimental conditions, the release rates of Si at 5-25^0C is ~ 10x, ~ 4x, and ~ 2.6x respectively at pH 8.4, 4.2, and 2.2. Increase in release-rate of Ca at 5-25^0C is ~ 3.3 x, ~ 2.3x, and ~ 1.8x at pH 8.4, 4.2, and 2.2 respectively. Increase in release-rate of Mg at 5-25^0C is ~ 1.5x, ~ 1x, and ~ 2x respectively at pH 8.4, 4.2, and 2.2. It indicates that the release rate of Ca and Mg does not show much deviation and are more or less similar under all experimental conditions. Only release rate of Si shows some anomaly. Increase in release-rate of Si progressively becomes higher as we move towards higher pH (8.4) from lower pH (2.2). The effect of temperature-change on dissolution of

LG, GN, CQ and KS with respect to Si-release rate is high at pH 8.4, moderate at pH 4.2 and low at pH 2.2.

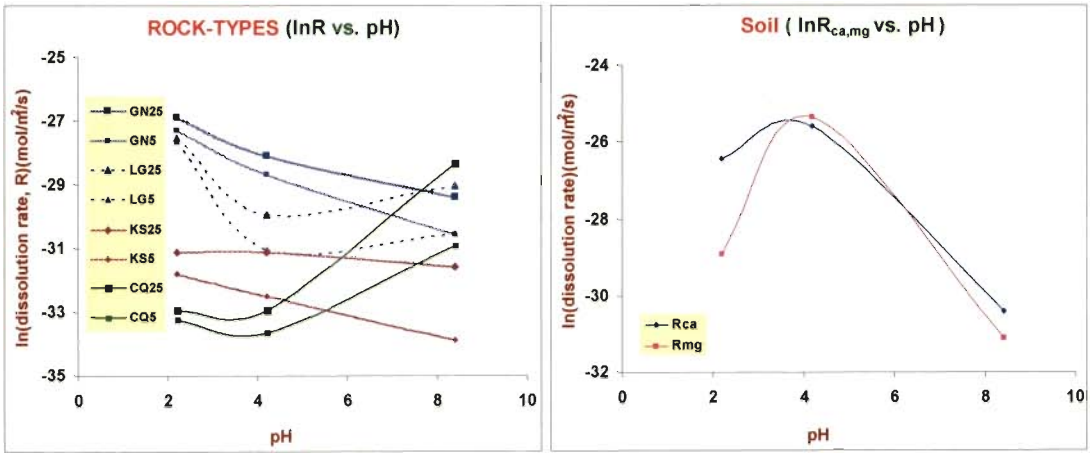

Figure 4.18 Graph showing pH dependency of dissolution rates of rock-types (*left hand side*) and soil (*right hand side*) under study

In acid-range (pH = 2.2 – 4.2), pH is the dominating controlling factor compared to temperature in regulating dissolution rate of LG, GN, CQ and KS with respect to silica release, whereas, in alkaline condition (pH = 8.4), temperature is the dominant controlling factor in regulating dissolution rate of these rock types. It is interesting to observe (Figure 4.18) that the field between the two curves belonging to temperature 5^0C and 25^0C is narrow in pH range 2.2 – 4.2, and gets widened as we move towards higher pH (pH = 8.4). The rates of dissolution at lower pH (2.2 and 4.2) are more or less similar, whereas at higher pH (8.4), the difference in rates calculated at two experimental temperature conditions is appreciable, suggesting that in alkaline media (pH = 8.4), E_a is greatly controlled by temperature change, whereas in acidic media (pH = 2.2 –

4.2), it has negligible effect on temperature change, and thus the rate is mostly pH controlled.

The range in which the amount of Ca, Mg and Si released during KS dissolution is extremely high for KS at pH 4.2, moderate at pH 2.2 and least at pH 8.4, both at 5^0C and 25^0C (Figure 4.15). In all experimental conditions, release of Mg and Ca during KS dissolution is very high as compared to Si because Ca and Mg are more reactive than Si as seen in Figure 4.19. Organic acid (of pH 4.2) significantly attributes in the release of elements during dissolution of KS as compared to solutions of acidic (2.2 pH) and alkaline (8.4 pH) nature. The clay minerals, fine size and organic content in KS may play a crucial role in ligand/chelate formation. When organic acid reacts with clay minerals, they play an active role in chelation process by getting associated with heavy metals and release free H^+ ions which replace cations (Ca and Mg) from the surface releasing Mg and Ca. It is observed that the rate of dissolution of KS with respect to Ca and Mg release is maximum at pH 4.2, moderate at pH 2.2 and least at pH 8.2 Fig. 4.19 (a, b). Figure 4.19 (c) shows that the rate of dissolution of KS with respect to Si release is maximum and somewhat similar at pH 2.2 and 4.2, and least at pH 8.2. In acidic media (pH 2.2-4.2), dissolution of KS is controlled jointly by H^+ and CH_3COO^-, whereas in alkaline media (pH 8.4), dissolution is primarily governed by OH^-. It is commonly accepted that dissolution rates of most primary and secondary minerals are promoted by the presence of protons, hydroxyls and complex forming ligands (Drever, 1994; Drever and Stillings, 1997; Zhang and Bloom, 1999; Chen and Brantley, 2000) and the rate controlling steps in the dissolution of most oxides and aluminosilicates are surface transport processes (e.g. Stumm and Furrer, 1987).

XRD analysis of pre-treated KS indicates that quartz, illite and kaolinite are the primary mineral constituents, with minor amounts of albite, gypsum and iron-oxides. KS dissolution in the present study can be explained in terms of proton-, ligand-, and hydroxyl-assisted together with surface-complexation and ion-exchange mechanism. Clay minerals (illite and kaolinite) of KS greatly contribute towards the increased release-rate of Ca and Mg during KS dissolution at pH 4.2 in organic acid. The main process is through ion exchange (adsorption/desorption) and suface-complexation phenomena. Clay minerals are considered the most common ion exchangers. The cation exchange capacity (CEC) of illite is high as compared to kaolinite as the former provides greater external surface area for adsorption than kaolinite. Carroll-Webb and Walther (1988) interpreted kaolinite dissolution at 25^0C and 60^0C in terms of H^+ adsorption to the ≡ SiOH and ≡ AlOH surface hydroxyl sites. These same two sites, in combination with an ≡ Si-O-Al ≡ site, were used by Wieland and Stumm (1992) and by Ganor *et al.* (1995) to model kaolinite dissolution. During KS dissolution, protonation/adsorption of H^+ to the ≡ SiOH, ≡ AlOH, and ≡ Si-O-Al ≡ surface hydroxyl sites on the outer surface of the clay minerals catalyse the hydrolysis/dissolution reaction by weakening the metal-oxygen bond both in electrolytes of pH 4.2 and 2.2. According to Drever and Stillings (1997), organic acids may accelerate dissolution rate far from equilibrium significantly below a pH of about 5. In the presence of a ligand, the dissolution rate can be seen as the sum of H^+ promoted and ligand promoted rate (Furrer and Stumm, 1986). Surface complexation with metal ions such as Fe^{2+}, Mn^{2+}, Ca^{2+}, and Mg^{2+} and rare earth elements present in the interlayer structure of clay minerals by the organic ligand (CH_3COO^-) in organic acid of pH 4.2 and inorganic ligand (Cl^-) in

inorganic acid of pH 2.2 greatly facilitates the dissolution rate of KS. The quantity of protons (H^+) and organic ligand (CH_3COO^-) produced in organic acid (pH 4.2) and the quantity of protons (H^+) and inorganic ligand (Cl^-) produced in inorganic acid (pH 2.2), is same. However, KS dissolution with respect to Ca and Mg release rate is much higher in organic acid (pH 4.2) than in inorganic acid (pH 2.2). This suggests that the intensity of ligand assisted dissolution is more in organic acid (pH 4.2) than in inorganic acid (pH 2.2), although in both cases dissolution is controlled by proton and ligand together. In addition, organic carbon released during the experiment strengthens the intensity of organic ligand (CH_3COO^-) and thus helps in greater release of Ca and Mg in organic acid of pH 4.2. An increase of dissolution rate in the presence of organic acids has been reported in a number of studies (e.g. Blum and Stillings, 1995; Oelkers and Schott, 1998). However, the role of organic acids for aluminosilicate dissolution has been questioned many times (Drever, 1994; Drever and Stillings, 1997). This is mainly because of the fact that, organic acids formed in nature are a variety of high molecular weight compounds collectively called as humic and fulvic acids (Berner and Berner, 1987), whereas the organic acids used in laboratory experiments are highly concentrated low molecular weight compounds, for example citric and oxalic acid (Lundström and Öhman, 1990; Ochs, 1996). In the present study, buffer (pH 4.2) of acetic acid and sodium acetate was used in order to simulate the dissolution experiment at the same pH encountered in most of the soil solutions and derived mainly from the decay and decomposition of micro-fauna and -flora in addition to their respiratory processes.

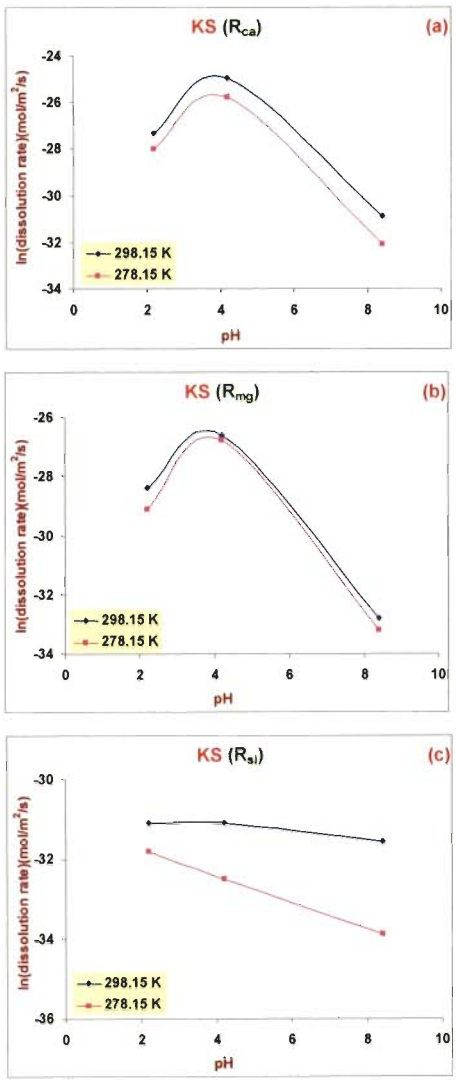

Figure 4.19 Graph showing pH dependency of dissolution rate for KS with respect to (a) Ca release, (b) Mg release, and (c) Si release at temperatures 5^0 C (278.15K) and 25^0C (298.15K)

Dissolution rate of soils with respect to temporal release of major cations (Ca^{2+}, Mg^{2+}) were calculated from a one month simulated soil column leaching experiment at room temperature in different pH (8.4, 4.2, 2.2) conditions.

Estimation of soil dissolution rate is needed to compare it with the dissolution rate of the other rock types discussed earlier. The soil studied is essentially derived from the rock types constituting Alaknanda-Bhagirathi catchment. Table 4.5 represents the result of dissolution rates of soil with respect to temporal release of Ca and Mg at experimental conditions. The slopes of the Ca- and Mg-release trend-lines are shown in Figure 4.20. Average BET surface area of the soil column is used in calculation of dissolution rate estimation of the soils.

Table 4.5 Result of dissolution rates of soils with respect to temporal release of Ca and Mg at room temperature (20-25^{0}C) under different pH conditions

pH	Dissolution Rate (mol/m^2/s)	
	Ca	Mg
8.4	6.20E-14	3.10E-14
4.2	7.56E-12	9.83E-12
2.2	3.25E-12	2.77E-13

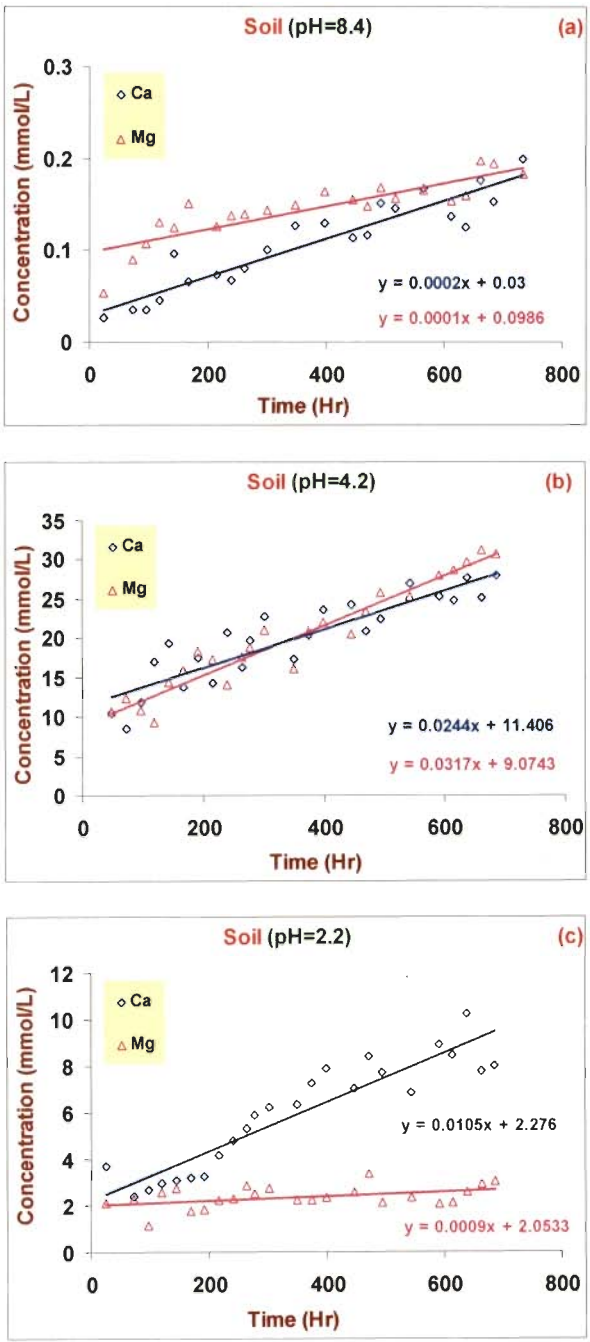

Figure 4.20 Temporal release of major cations (Ca, Mg) during soil-column leaching experiment at room temperature in three different pH conditions; (a) 8.4, (b) 4.2, (c) 2.2

Figure 4.18 (*right hand side*) shows pH dependency of dissolution rate of soil with respect to release rate of Ca (R_{ca}) and release rate of Mg (R_{mg}). The rate of dissolution (with respect to Ca and Mg release) of soil at room temperature is ~ 100x high in acidic media (pH 2.2 – 4.2) as compared to the alkaline media (pH 8.4) (Table 4.5). However, R_{ca} is higher than R_{mg} at all pH conditions. Figure 4.18 (*right hand side*) shows that the difference in release rate of Ca and Mg is negligible at pH 8.4 and 4.2, whereas at pH 2.2, R_{ca} is about 10 times greater than R_{mg}. This indicates that at room temperature, pH dominantly controls the dissolution of Ca than Mg.

4.4 POST-EXPERIMENT SURFACE AREA

Post-experiment BET surface areas of some treated samples were measured to explore the effect of dissolution on mineral / rock initial surface area. Table 4.6 shows post-experiment BET surface areas of selected samples at 25^0 C. It is observed that, the BET surface area of the treated samples significantly decreased compared to the fresh samples with the exception of CC. For CC, an increase in the surface area was observed for the treated samples. Initial grinding of the samples to get grains of desired size-range for experimentation produces ultra fine particles and numerous strained regions (etch pits), which are sites of weak atomic bonding and excess surface free energy (Drever, 1997; Appelo *et al.* 2005). Some amount of ultra fine particles continue to adhere to the mineral surfaces even after ultrasonic cleaning aimed to completely remove fine particles (Drever, 1997). This suggests that decrease in the specific surface areas of DM, LG, GN and KS is most likely due to rapid preferential dissolution of fine particles and other highly soluble phases during the short experimentation period. During

the experimentation period, the attack of the solution was specific to irregular surface of the grains, except for CC where it was crystal controlled. In the case of CC, advancement of dissolution occurs mostly via dislocation sites, which may act as a precursor. During the course of the experiment, rhombohedral etch-pits as visible in SEM images (Figure 4.8, 4.9) grow and eventually coalesce. The diffusion controlled reaction may have resulted in the formation of micro- to nano-pores on the surface. These processes may result in a substantial increase in the initial BET surface area of CC. Decrease in surface area of LG, GN and KS is considerably higher compared to DM (Table 4.6), which may be attributed to the presence of high energy lattice defects and strains in the grains of LG, GN and KS as compared to DM. Also, precipitation of some secondary minerals such as kaolinite in LG and GN, may be a possible reason for the increased surface area after the experiment. Drastic increase in the initial surface area of CC can be suggestive of its higher dissolution rate (~ 5x) compared to DM.

Table 4.6 Post-experiment BET surface areas of selected samples at 25^0 C

Sample Code	pH	BET surface area (m^2/g)		% decrease /increase
		Initial	Final	
CC	8.4	0.037	0.128	71.10%I
DM	8.4	0.322	0.222	31.05%D
LG	4.2	0.491	0.087	82.28%D
	2.2	0.491	0.174	64.56%D
GN	4.2	0.77	0.244	68.31%D
KS	4.2	6.972	2.617	62.46%D
	2.2	6.972	3.226	53.72%D

*I = Increase; D = Decrease

CHAPTER 5

CONCLUSION

In the present study, dissolution rates of the major lithologies and soil collected from the Alaknanda and Bhagirathi river basins have been calculated by conducting laboratory dissolution-experiments at selected pH and temperature conditions and with different leaching solutions. The water chemistry of the Alaknanda and Bhagirathi rivers have been studied by analyzing the daily water samples collected during July'2004 to July'2005. The flux rates of Ca, Mg, and SiO_2 in these two rivers at their respective sampling locations have been calculated to observe the seasonal variations in the composition and flux rates. The water chemistry established that composition of water is primarily controlled by variable rates of dissolution of the lithologies of the catchment and the basin and thus prompting to study the dissolution rates of the rocks, minerals and soils by laboratory experiments.

The present study dealt with laboratory-simulated dissolution kinetics of minerals (CC and DM), rocks (LG, GN, PY, CQ and KS), and soil. Dissolution rates were calculated with respect to release of Ca, Mg and Si and activation energies involved in the respective dissolution reactions were calculated. Temperature and pH dependency on the dissolution rates of the samples were examined along with the morphochemical analysis of the minerals due to chemical alteration after dissolution experiments. Post- experiment analysis of the surface areas of the minerals and rocks were carried out to find the effect of dissolution on the initial surface areas of the samples. The major conclusions from the study are,

1. High Ca/Si flux ratio in both Alaknanda and Bhagirathi river indicates predominance of carbonate weathering.

2. Average Ca-flux rate (2.92E-08 mol/m^2/s in Alaknanda and 1.60E-08 mol/m^2/s in Bhagirathi) is much higher compared to the carbonate dissolution rate in laboratory at pH 8.4 and temperature 25^0C, whereas the average SiO_2-flux (range 10^{-8}-10^{-9} mol/m^2/s) is much higher compared to the dissolution rate of LG, GN, CQ, PY, and KS with respect to Si-release. Laboratory derived dissolution rate of the lithologies at pH 8.4 and temperature 25^0C indicate that CQ dissolution is faster followed by LG, GN, PY and KS. The low rates of dissolution of PY and KS with respect to Si-release might be due to the presence of clay minerals which show low solubility.

3. At pH 8.4 and temperature 25^0C, dissolution rate of soil in soil column experiment is about 23 times slower compared to carbonate dissolution rate derived experimentally. The slow rate of dissolution of soil during the experimental period might be due to abundance of highly resistant quartz grains and relatively insoluble clay minerals as compared to the dissolution of pure and homogeneous carbonate mineral fragments.

4. Carbonate (calcite and dolomite) dissolution (~10^{-12}) is higher than the dissolution rate of rock types LG, GN, CQ, PY, and KS (range 10^{-14}-10^{-15}) under laboratory simulated conditions.

5. CC is dissolving ~ 5x faster as compared to DM with respect to the release of their respective cations Ca and Mg. This is supported by drastic increase in surface area of CC after the completion of experiment. During CC dissolution, advancement of dissolution occurs mostly via dislocation sites which act as a precursor. During the course of the CC dissolution-experiment, rhombohedral

etch-pits as visible in SEM images grow as a result of diffusion controlled reaction and eventually coalesce leading to increase in post experiment surface area.

6. Unlike CC and DM, there is decrease in the specific surface areas of DM, LG, GN and KS is most likely due to rapid preferential dissolution of fine particles and other highly soluble phases during the short experimentation period.

7. The effect of temperature-change on dissolution of LG, GN, CQ and KS is high at pH 8.4, moderate at pH 4.2 and low at pH 2.2. In acid-range (pH = 2.2–4.2), pH is the major controlling factor compared to temperature in regulating dissolution rate of LG, GN, CQ and KS whereas, in alkaline condition (pH = 8.4), temperature is the dominant controlling factor in regulating dissolution rate.

8. For dissolution reaction of each of these rock types under experiment, Ea for Si release is highest at pH 8.4, moderate at pH 4.0 and least at pH 2.2 showing that, Si release rate is sensitive to temperature change within the experimental pH range 2.2 – 8.4. In alkaline media (pH = 8.4), Ea is highly controlled by temperature change, whereas in acidic media (pH = 2.2 – 4.2), it has negligible effect on temperature change. In other words,

Low E_a = pH dependency on rate is more or temperature dependency on rate is less

High E_a = temperature dependency on rate is more or pH dependency on rate is less

BIBLIOGRAPHY

1. **Abbas, N. and Subramanian, V. (1984).** Erosion and sediment transport in the Ganga river basin. *Jour. Hydrol.* **69**: 173-184.

2. **Amrhein, C. and Suarez, D.L. (1988).** The use of a surface complexation model to describe the kinetics of ligand-promoted dissolution of anorthite. *Geochim. Chosmochim. Acta* **52**: 2785-2793.

3. **Appelo, C.A.J. and Postma, D. (2005).** Geochemistry, groundwater and pollution, A.A. Balkema Publishers, Netherlands.

4. **Arvidson, R.S., Ertan, I.E., Amonette, J.E. and Luttge, A. (2003).** Variation in calcite dissolution rates: a fundamental problem? *Geochim. Cosmochim. Acta* **67**: 1623-1634.

5. **Auden, J.B. (1934).** The Geology of the Krol belt. *Geol. Surv. India* **67**: 357-454.

6. **Auden, J.B. (1949).** General report of G.S.I. for 1939. *Rec. Geol. Surv. India* **78**: 74-78.

7. **Bennett, P.C., Melcer, M.E., Siegel, D.I. and Hassett, J.P. (1988).** The dissolution of quartz in dilute aqueous solutions of organic acids at 25^0C. *Geochim. Chosmochim. Acta* **52**:1521-1530.

8. **Berner, E.K. and Berner, R.A. (1987).** Soil water and groundwater: weathering. In: The global water cycle: geochemistry and environment, Prentice-Hall, Englewood cliffs, New Jersey, pp. 142-173.

9. **Berner, R.A. (1981).** Kinetics of weathering and diagenesis. In: Lasaga, A.C., Kirkpatrick, R.J. (Eds.), Kinetics of Geochemical Processes, Reviews in Mineralogy. *Min. Soc. of Am.* **8**: 111-134.

10. **Berner, R.A., Lasaga, A.C. and Garrels, R.M. (1983).** The carbonate-silicate geochemical cycle and its effect on atmospheric carbon dioxide over the past 100 million years. *Am. J. Sci.* **284**: 641-683.

11. **Bickle, J.M., Bunbury, J., Chapman, J.H., Harris, B.W.N., Fairchild, J.I. and Ahmad, T. (2003).** Fluxes of Sr into the headwaters of the Ganges. *Geochim. Cosmochim. Acta* **67**: 2567 – 2584.

12. **Blum, A.E. and Lasaga, A.C. (1991).** The role of surface speciation in the dissolution of albite. *Geochim. Chosmochim. Acta* **51**: 2193-2201.

13. **Blum, A.E. and Stillings, L.L. (1995).** Feldspar dissolution kinetics. *In* White, A.F. and Brantley, S.L., (Eds.), Chemical Weathering Rates of Silicate Minerals. *Min. Soc. Am. Rev. Mineral.* **31**: 291-346, Washington, DC.

14. **Blum, J.D., Gazis, C.A., Jacobson, A.D. and Chamberlain, C.P. (1998).** Carbonate versus silicate weathering in the Raikhot watershed within the Higher Himalayan Crystalline Series. *Geology* **26**: 411- 414.

15. **Bluth, G.J.S. and Kump, L.R. (1994).** Lithologic and climatologic controls of river chemistry. *Geochim. Cosmochim. Acta* **58**: 2341-2359.

16. **Brady, P.V. and Carroll, S.A. (1994).** Direct effects of CO_2 and temperature on silicate weathering: possible implications for climate control. *Geochim. Cosmochim. Acta* **58**:1853-1863.

17. **Brady, P.V. and Walther, J.V. (1992).** Surface chemistry and silicate dissolution at elevated temperatures. *Am. J. Sci.* **292**: 639-658.

18. **Brantley, S.L. (2003).** In: Reaction kinetics of primary rock-forming minerals under ambient conditions. *Treatise on Geochemistry* **5:** 1-44.

19. **Braun, I., Ravindra Kumar, G.R. and Raithi, M. (1996)**. Dehydration—melting phenomena in leptynitic gneisses and the generation of leucogranites: a case study from the kerala khondalite belt, southern India. *J. of Petro.* **37**: 1285-1305.

20. **Bruinzeel, L.A. and Bremmer, C.N., (1989).** Highland – lowland interactions in the Ganga Brahmputra river basin review of published literature. ICIMOD Occasional Paper No. 11, Kathmandu, Nepal, **136.**

21. **Cama, J., Metz, V. and Ganor, J. (2002).** The effect of temperature and pH on kaolinite dissolution rate under acidic conditions. *Geochim. Cosmochim. Acta* **66**: 3913-3926.

22. **Carroll-Webb, S.A. and Walther J.V. (1988).** A surface complex reaction model for the pH-dependence of corundum and kaolinite dissolution rates. *Geochim. Cosmochim. Acta* **52:** 2609-2623.

23. **Chen, Y. and Brantley, S.L. (1996).** Temperature and pH-dependence of albite dissolution rate at acid pH. *Chem. Geol.* **135**:275-290.

24. **Chen, Y. and Brantley, S.L. (1997).** Temperature and pH dependence of albite dissolution rate at acid pH. *Chem.Geol.* **135**: 275-290.

25. **Chen, Y. and Brantley, S.L. (2000).** Dissolution of forsteritic olivine at 65°C and 2<pH<5. *Chem.Geol.* **65**: 267-281.

26. **Chin, P.F. and Mills, G.L. (1991).** Kinetics and mechanisms of kaolinite dissolution: Effects of organic ligands. *Chem. Geol.* **90**: 307-317.

27. **Clesceri, L.S., Greenberg, A.E. and Eaton, A.D. (1998).** (Eds): Standard methods for the examination of water and wastewater.

28. **Cornell, R.M. and Schwertmann, U. (1996).** The iron oxides. VCH Publishers, Weinheim, 573 pp.

29. **Dalai, T.K., Krishnaswami, S., and Sarin, M.M. (2002).** Major ion chemistry in the headwaters of the Yamuna River system: Chemical weathering, its temperature dependence and CO_2 consumption in the Himalya. *Geochim. Cosmochim. Acta* **66**: 3397-3416.

30. **Das, A., Krishnaswami, S., Sarin, M.M. and Pande, K. (2005).** Chemical weathering in the Krishna basin and the western ghats of the Deccan Traps: Rates of weathering and their control. *Geochim. Cosmochim. Acta* **69**: 2067-2084.

31. **Deer, W.A., Howie, R. A. and Zussman, J. (1966)**. An Introduction to the rock-forming minerals. ELBS/Longman, England, 473-503.

32. **Drever, J .I. and Stillings, L.L. (1997).** The role of organic acids in mineral weathering. *Colloids and Surfaces*, **120**: 167-181.

33. **Drever, J .I. and Stillings, L.L. (1997).** The role of organic acids in mineral weathering. *Colloids and Surfaces*, **120:** 167-181.

34. **Drever, J. I. (1994).** The effect of land plants on weathering rates of silicate minerals. *Geochim. Cosmochim. Acta* **58:** 2325-2332.

35. **Drever, J. I. (1997).** Kinetics. In: The Geochemistry of Natural Waters: Surface and Groundwater Environments, Prentice Hall, New Jersey, pp. 215-234.

36. **Dupre, B., Dessert, C., Oliva P., Godderis, Y., Viers, J., Francois, L., Millot, R. and Gaillardet, J. (2003).** Rivers, chemical weathering and Earth's climate. *C. R. Geoscience* **335**: 1141-1160.

37. **Dupre, B., Gaillardet, J., Rousseau, D. and Allegre, C. J. (1996).** Major and trace elements of river borne material: The Congo Basin. *Geochim. Cosmochim. Acta* **60**: 1301-1321.

38. **English, N.B., Quade, J., Decelles, P. G. and Garzionne C. N. (2000).** Geologic control of Sr and major element chemistry in Himalayan Rivers, Nepal. *Geochim. Cosmochim. Acta* **64:** 2549-2566.

39. **Furrer, G. and Stumm, W. (1986).** The coordination chemistry of weathering: I. Dissolution kinetics of δAl2O3 and BeO. *Geochim. Cosmochim. Acta* **50**:1847-1860.

40. **Gaillardet, J., Dupre,B and Allegre, C.J. (1999).** Geochemistry of large river suspended sediments: silicate weathering or recycling tracer? *Geochim. Cosmochim. Acta* **63**: 4037-4051.

41. **Ganor, J., Mogollon, J. L. and Lasaga, A. C. (1995).** The effect of pH on kaolinite dissolution rates and on activation energy. *Geochim. Cosmochim. Acta* **59**: 1037-1052.

42. **Garrels, R.M. and Mackenzie, F. (1971).** *Evolution of sedimentary rocks*: W.W. Norton, New York, 397p.

43. **Gautlier, M., Oelkers, E.H. and Schott J. (1999).** An experimental study of dolomite dissolution rates as a function of pH from -0.5 to 5 and temperatures from 25^0 to 80^0C. *Chem. Geol.* **157**: 13-26.

44. **Gislason, S.R., Arnorsson, S. and Armannsson, H. (1996).** Chemical weathering of basalt in southwest Iceland: Effects of runoff, age of rocks and vegetative/glacial cover. *Am. J. Sci.* **296:** 837-907.

45. **Gopendra Kumar and Agrawal, N.C. (1975).** Geology of Srinagar – Nandprayag area (Alaknanda Valley), Chamoli, Garhwal and Tehri Garhwal Districts, Uttar Pradesh. *Himalayan Geology* **5:** 29-59.

46. **Gopendra Kumar, (2005).** Geology of Uttar Pradesh and Uttaranchal. Aditya Printers, Bangalore pp135-266.

47. **Hees, P.A.W. van, Lundstrom, U.S. and Morth, C. M. (2002).** Dissolution of microcline and labradorite in a forest O horizon extract: the effect of naturally occurring organic acids. *Chem. Geol.* **189:**199-211.

48. **Hering, J.G. and Stumm, W. (1990).** Oxidative and Reductive Dissolution of Minerals. In: *M.F. Hochella Jr. and A.F. White (Editors), Mineral-water interface*. Reviews in Mineralogy. Mineralogical society of America.

49. **Huang, W.H. and Kiang, W.C. (1972).** Laboratory dissolution of plagioclase feldspars in water and organic acids at room temperature. *Am. Mineral.* **57**: 1849-1859.

50. **Huh, Y. (2003).** Chemical weathering and climate-a global experiment: A review. *Geosciences Journal,* **7**: 277-288.

51. **Krishnaswami, S., Trivedi, J.R., Sarin, M.M., Ramesh, R. and Sharma K.K. (1992).** Strontium isotopes and rubidium in the Ganga-Brahmaputra river system: weathering in the Himalaya, fluxes to the Bay of Bengal and contributions to the evolution of oceanic $^{87}Sr/^{86}Sr$. *Ear. Planet. Sci. Lett.* **109:** 243-253.

52. **Lasaga, A.C. (1984).** Chemical kinetics of water-rock interactions. *J. Geophys. Res.* **89:** 4009-4025.

53. **Lasaga, A.C. and Kirkpatrick, R.J. (1981).** (Eds): "Kinetics of Geochemical Processes", Reviews in Mineralogy. *Min. Soc. Am.* **8**: 135-169.

54. **Lasaga, L.C., Soler, J.M., Ganor, J., Burch, T. E. and Nagy, K. L. (1994).** Chemical weathering rate laws and global geochemical cycles. *Geochim. Cosmochim. Acta* **58:** 2361-2386.

55. **Louvat, P. and Allegre, C.J. (1997).** Present denudation rates at Reunion island determined by river geochemistry: basalt weathering and mass budget between chemical and mechanical erosions, *Geochim. Cosmochim. Acta* **61**: 3645-3669.

56. **Louvet, P. and Allegre, C.J. (1998).** Present denudation rates on the island of Reunion determined by river geochemistry: Basalt weathering and mass budget between chemical and mechanical erosions. *Geochim. Cosmochim. Acta* **61**: 3645-3669.

57. **Lundström, U. and Öhman, L.O. (1990).** Dissolution of feldspars in the presence of natural, organic solutes. *J. Soil Sci.* **41**: 359-369.

58. **Manley, E.P. and Evans, L.J. (1986).** Dissolution of feldspar by low-molecular-weight aliphatic and aromatic acids. *Soil Sci.* **141**:106-112.

59. **Mast, M.A. and Drever, J.I. (1987).** The effect of oxalate on the dissolution rates of oligoclase and tremolite. *Geochim. Chosmochim. Acta* **51**: 2559-2568.

60. **Meybeck, M. (1987).** Global chemical weathering of surficial rocks estimated from river dissolved loads. *Am. J. Sci.* **287**: 401-428.

61. **Morel, F.M.M. and Hering, J.G. (1993).** Principles and applications of aquatic chemistry. John Wiley and sons Inc., New York.

62. **Nater, E.A. and Huang, P.M. (1988).** The effects of organic acids on the kinetics of microcline weathering. Agronomy abstracts. Madison, WI.

63. **Ochs, M. (1996).** Influence of humified and non-humified natural organic compounds on mineral dissolution. *Chem. Geol.* **131**:119-124.

64. **Oelkers, E.H. and Schott, J. (1998).** Does organic acid adsorption affect alkali- feldspar dissolution rates? *Chem. Geol.* **151**: 235-246.

65. **Palmer, M.R. and Edmond, J .M. (1992).** Controls over the strontium isotope composition of river water. *Geochim. Cosmochim. Acta* **56**: 2099-2111.

66. **Pande, K., Sarin, M.M., Trivedi, J.R., Krishnaswami, S. and Sharma, K.K. (1994).** The Indus river system (India-Pakistan): major-ion chemistry, uranium and strontium isotopes. *Chem. Geol.* **116**: 245-259.

67. **Pegram, W.J., Krishnaswami, S., Ravizza, G.E. and Turekian, K.K. (1992).** Record of seawater $^{187}Os/^{188}Os$ variation through the Cenozoic. *Ear. Planet. Sci. Lett.* **91**: 63-79.

68. **Pokrovski, O.S. and Schott, J. (2000).** Kinetics and mechanism of forsterite dissolution at 25° C and pH from 1 to 12. *Geochim. Cosmochim. Acta* **64**: 3313-3325.

69. **Pokrovsky, O. S., Golubev, S. V. and Schott, J. (2005).** Dissolution kinetics of calcite, dolomite and magnesite at 25^0C and 0 to 50 atm pCO_2. *Chem. Geol.* **217**: 239–255.

70. **Rad, S., Louvat, P., Gorge, C., Gaillardet, J. and Allegre, C.J. (2006).** River dissolved and solid loads in the Lesser Antilles: New insight into basalt weathering processes. *J. of Geochem. Expl.* **88**: 308– 312.

71. **Raymo, M.E. and Ruddiman, W.F. (1992).** Tectonic forcing of late Cenozoic climate. *Nature* **359**: 117-122.

72. **Rickard, D.T. and Sjöberg, E.L. (1983).** Mixed kinetic control of calcite dissolution rates. *Am. J. Sci.* **283**: 815-830.

73. **Sarin, M. M. and Krishnaswami, S. (1984).** Major ion chemistry of the Ganga-Brahmaputra river systems. *Nature* **312**: 538–541.

74. **Sarin, M.M. (2001).** Biogeochemistry of Himalayan rivers as an agent of climate change. *Curr. Sci.* **81**: 1446-1450.

75. **Sarin, M.M., Krishnaswami, S., Sharma, K.K. and Trivedi, J.R. (1992).** Uranium isotopes and rubidium in the Bhagirathi-Alaknanda river system: evidence for high uranium mobilisation in the Himalaya. *Curr. Sci.* **62**: 801-805.

76. **Singh, S.K., Trivedi, J.R. and Krishnaswami, S. (1999).** Re-Gs isotope systematics in black shales from the Lesser Himalaya: Their chronology and role in the $^{187}Os/^{188}Os$ evolution of seawater. *Geochim. Cosmochim. Acta* **63**: 2381-2392.

77. **Sinha, R., Khanna, M., Jain, V. and Tandon, S.K. (2002).** Megageomorphology and sedimentation history of parts of the Ganga-Yamina plains. *Curr. Sci.* **84**: 562– 566.

78. **Sjöberg, E.L. (1976)**. A fundamental equation for calcite dissolution kinetics. *Geochim. Cosmochim. Acta* **40**: 441-447.

79. **Sposito, G. (1989).** The chemistry of soils. Oxford University press, Newyork. 277pp.

80. **Stallard, R.F. and Edmond, J.M. (1983).** Geochemistry of the Amazon. The influence of the geology and the weathering environment on the dissolved load. *Jour. Geophys. Res.* **88**: 9671-9688.

81. **Stillings, L.L., Drever, J.I. and Poulson, S.R. (1998).** Oxalate adsorption at a plagioclase (An (47)) surface and models for ligand-promoted dissolution. *Environ. Sci. Technol.* **32**: 2856-2864.

82. **Stumm, W. and Furrer, G. (1987).** The dissolution of oxides and aluminum silicates: examples of surface coordination controlled kinetics. pp. 197-219. *In* Stumm, W. (ed.) Aquatic surface chemistry chemical processes at the particle-water interface. Wiley Interscience, New York.

83. **Stumm, W.,Furrer, G., Wieland, E. and Zinder, B. (1985).** The effects of complex-forming ligands on the dissolution of oxides and aluminosilicates. *In* The chemistry of weathering (ed. J.I. Drever), pp. 55-74. Reidel Pub. Co.

84. **Valdiya, K.S. (1980).** Geology of Kumaun Lesser Himalaya. Himachal Times Press, Dehradun, 291pp.

85. **Velbel, M.A. (1993).** Temperature dependence of silicate weathering in nature: How strong a negative feedback on long-term accumulation of atmospheric CO_2 and global greenhouse warming? *Geology* **21:** 1059-1062.

86. **Velbel, M.A. (2004).** Laboratory and Homework exercises in the Geochemical Kinetics of Mineral-Water Reaction: Rate Law, Arrhenius Activation Energy, and the Rate-Determining Step in the Dissolution of Halite. *J. Geosci. Edu.* **52:** 52-59.

87. **Viers, J., Dupre, B., Braun, J., Deberdt, S., Angeletti, B., Ngoupayou, J. N. and Michard, A. (2000).** Major and trace elements abundances and strontium isotopes in the Nyong river basin (Cameroon): Constraints transport mechanism in humid tropical environments. *Chem. Geol.* **169:** 211-241.

88. **Walker, J.C.G., Hays, P.B., and Kasting, J.F. (1981).** A negative feedback mechanism for the long term stabilization of the earth's surface temperatures. *J. Geophys. Res.* **86:** 9776-9782.

89. **Wasson, R. J. (2003)**. A sediment budget for the Ganga-Brahmaputra catchment. *Curr. Sci.* **84:** 1041-1047.

90. **Weiland, E., Wehrl, B. and Stumm. W. (1988).**The coordination chemistry of weathering: III. A generalization on the dissolution of minerals. *Geochim. Chosmochim. Acta* **52**: 1969-1981.

91. **Welch, S.A. and Ullman, W. J. (2000).** The temperature dependence of bytownite feldspar dissolution in neutral aqueous solutions of inorganic

and organic Ligands at low temperature (5-35^{0}C). *Chem. Geol.* **167:** 337-354.

92. **Welch, S.A. and W.J. Ullman (1996).** Feldspar dissolution in acidic and organic acid solutions: Compositional and pH dependence of dissolution rate. *Geochim. Cosmochim. Acta* **60**: 2939-2948.

93. **Wellman, D., M., Icenhower, J. P.,Gamerdinger, A. P., Forrester and S. W. (2006).** Effects of pH, temperature, and aqueous organic material on the dissolution kinetics of meta-autunite minerals, (Na, $Ca)_{2-1}[(UO_2)(PO_4)]_2.3H_2O$. *Am. Mineralogist* **91**: 143-158.

94. **White, A.F. and Brantley, S.L. (2003).** The effect of time on weathering of silicate minerals: why do weathering rates differ in the laboratory and field? *Chem. Geol.* **202**: 479-506.

95. **White, A.F. and Brantley, S.L. (2003).** The effect of time on weathering of silicate minerals: why do weathering rates differ in the laboratory and field? *Chem. Geol.* **202**: 479-506.

96. **White, A.F., Blum, A.E., Bullen, T.D., Vivit, D.V., Schulz, M. and Fitzpatrick, J. (1999).** The effect of temperature on experimental and natural chemical weathering rates of granitoid rocks. *Geochim. Cosmochim. Acta* **63**: 3277-3291.

97. **Wieland, E. and Stumm, W. (1992).** Dissolution kinetics of kaolinite in acidic aqueous solutions at 25°C. *Geochim. Cosmochim. Acta* **56**: 3339-3355.

98. **Wogelius, R. A. and Walther, J. V. (1991).** Olivine dissolution at 25^0C: effects of pH, CO_2, and organic-acids. *Geochim. Cosmochim. Acta* **55**: 943-954.

99. **Wogelius, R.A. and Walther J.V. (1992).** Olivine dissolution kinetics at near-surface conditions. *Chem. Geol.* **97**: 101-112.

100. **Wollast, R. (1967).** Kinetics of the alteration of K-feldspar in buffered solutions at low temperature. *Geochim. Cosmochim. Acta* **31**: 635-648.

101. **Yadav, S.K. and Chakrapani, G. J. (2006).** Dissolution kinetics of rock-water interactions and its implications. *Curr. Sci.* **90**: 932-937.

102. **Yadav, S.K., Chakrapani, G. J. and Gupta, M.K.** An experimental study of dissolution kinetics of Calcite, Dolomite, Leucogranite and Gneiss in buffered solutions at temperature 25^0C and 5^0C. *Env. Geol.* (In Press)

103. **Zhang, H. and Bloom, R. (1999).** Dissolution kinetics of hornblende in organic acid solutions. *Soil Sci. Soc. Am. J.* **63**: 815-822.

Appendix A: Tables

(refer chapter 4)

A1. Chemical flux of Ca, Mg, and SiO_2 in Alaknanda River at Srinagar during July'2004 to July'2005.

Date	Dissolved Elements (µmol/L)			Discharge (10^{12}L/month)	FLUX (mol/day)		
	Ca	Mg	SiO_2		Ca	Mg	SiO_2
19.07.04	537.6	114.1	95.6	3.45	6.12E+07	1.30E+07	1.09E+07
16.08.04	535.9	182.7	97.8	4.86	8.59E+07	2.93E+07	1.57E+07
20.09.04	359.0	119.2	97.8	2.65	3.14E+07	1.04E+07	8.55E+06
18.10.04	481.6	214.3	133.1	1.80	2.86E+07	1.27E+07	7.90E+06
22.11.04	517.8	234.0	63.0	0.51	8.71E+06	3.94E+06	1.06E+06
20.12.04	590.9	286.8	63.4	0.43	8.39E+06	4.07E+06	8.99E+05
17.01.05	621.7	301.2	46.7	0.43	8.82E+06	4.27E+06	6.62E+05
21.02.05	580.3	270.0	69.5	0.23	4.40E+06	2.05E+06	5.27E+05
21.03.05	583.9	234.4	76.6	0.28	5.39E+06	2.17E+06	7.08E+05
19.04.05	666.3	212.0	67.4	0.43	9.45E+06	3.01E+06	9.57E+05
10.05.05	627.2	167.3	77.1	0.65	1.35E+07	3.59E+06	1.65E+06
13.06.05	647.3	133.9	75.6	1.69	3.61E+07	7.47E+06	4.22E+06
19.07.05	680.9	109.6	97.7	3.45	7.75E+07	1.25E+07	1.11E+07

A2. Chemical flux of Ca, Mg, and SiO_2 in Bhagirathi River at Maneri during July'2004 to July'2005.

Date	Dissolved Elements (µmol/L)			Discharge (10^{12}L/month)	FLUX (mol/day)		
	Ca	Mg	SiO_2		Ca	Mg	Si
19.07.04	207.4	88.5	20.6	1.17	7.99E+06	3.41E+06	7.92E+05
16.08.04	565.5	189.4	108.5	1.19	2.22E+07	7.42E+06	4.25E+06
20.09.04	336.2	123.8	74.5	0.60	6.65E+06	2.45E+06	1.47E+06
18.10.04	418.3	196.2	135.6	0.22	3.00E+06	1.41E+06	9.71E+05
22.11.04	209.2	80.3	57.9	0.13	9.04E+05	3.47E+05	2.50E+05
06.12.04	255.4	96.7	62.0	0.10	8.65E+05	3.28E+05	2.10E+05
31.01.04	471.4	171.3	52.1	0.08	1.25E+06	4.56E+05	1.39E+05
21.02.05	478.4	188.7	62.0	0.07	1.10E+06	4.35E+05	1.43E+05
21.03.05	364.5	137.0	61.0	0.09	1.07E+06	4.03E+05	1.79E+05
19.04.05	373.7	166.8	53.6	0.14	1.73E+06	7.70E+05	2.47E+05
17.05.05	321.3	147.0	42.9	0.42	4.50E+06	2.06E+06	6.01E+05
21.06.05	334.8	155.7	44.5	0.70	7.78E+06	3.62E+06	1.03E+06
12.07.05	317.3	84.8	43.3	1.17	1.22E+07	3.27E+06	1.67E+06

A3. Chemical flux rates of Ca, Mg, and SiO_2 in Alaknanda River at Srinagar during July'2004 to July'2005.

Date	Ca	Mg	SiO_2	Discharge (10^{12}L/month)	Area (10^3km^2)	Elemental release rate (mol/m^2/s)		
						Ca	Mg	SiO_2
19.07.04	537.6	114.1	95.6	3.45	11.8	6.07E-08	1.29E-08	1.08E-08
26.07.04	651.8	129.8	103.6	3.45	11.8	7.36E-08	1.46E-08	1.17E-08
02.08.04	560.7	119.6	95.3	4.86	11.8	8.91E-08	1.90E-08	1.52E-08
09.08.04	673.6	145.8	97.8	4.86	11.8	1.07E-07	2.32E-08	1.55E-08
16.08.04	535.9	182.7	97.8	4.86	11.8	8.52E-08	2.90E-08	1.55E-08
23.08.04	405.6	130.7	91.2	4.86	11.8	6.45E-08	2.08E-08	1.45E-08
30.08.04	415.3	152.8	89.6	4.86	11.8	6.60E-08	2.43E-08	1.42E-08
06.09.04	385.6	129.7	87.3	2.65	11.8	3.34E-08	1.12E-08	7.56E-09
13.09.04	370.9	131.9	99.4	2.65	11.8	3.22E-08	1.14E-08	8.62E-09
20.09.04	359.0	119.2	97.8	2.65	11.8	3.11E-08	1.03E-08	8.48E-09
27.09.04	377.8	141.8	145.6	2.65	11.8	3.27E-08	1.23E-08	1.26E-08
04.10.04	342.2	127.7	115.1	1.80	11.8	2.01E-08	7.52E-09	6.77E-09
11.10.04	370.2	163.8	135.6	1.80	11.8	2.18E-08	9.65E-09	7.98E-09
18.10.04	481.6	214.3	133.1	1.80	11.8	2.84E-08	1.26E-08	7.84E-09
25.10.04	508.6	216.2	94.1	1.80	11.8	2.99E-08	1.27E-08	5.54E-09
01.11.04	626.9	298.8	68.1	0.51	11.8	1.05E-08	4.99E-09	1.14E-09
08.11.04	576.9	247.7	66.1	0.51	11.8	9.62E-09	4.13E-09	1.10E-09
15.11.04	544.1	250.0	62.7	0.51	11.8	9.08E-09	4.17E-09	1.05E-09
22.11.04	517.8	234.0	63.0	0.51	11.8	8.64E-09	3.90E-09	1.05E-09
29.11.04	578.7	256.1	62.5	0.51	11.8	9.65E-09	4.27E-09	1.04E-09
20.12.04	590.9	286.8	63.4	0.43	11.8	8.31E-09	4.03E-09	8.91E-10
27.12.04	570.8	277.6	62.7	0.43	11.8	8.03E-09	3.90E-09	8.81E-10
03.01.05	713.8	445.3	79.7	0.43	11.8	1.00E-08	6.26E-09	1.12E-09
10.01.05	584.9	297.1	58.2	0.43	11.8	8.23E-09	4.18E-09	8.19E-10
17.01.05	621.7	301.2	46.7	0.43	11.8	8.74E-09	4.24E-09	6.56E-10
24.01.05	571.2	283.5	51.4	0.43	11.8	8.03E-09	3.99E-09	7.23E-10
31.01.05	608.4	236.7	48.4	0.43	11.8	8.56E-09	3.33E-09	6.80E-10
07.02.05	534.5	230.9	33.7	0.23	11.8	4.02E-09	1.74E-09	2.54E-10
14.02.05	532.0	212.8	61.3	0.23	11.8	4.00E-09	1.60E-09	4.61E-10
21.02.05	580.3	270.0	69.5	0.23	11.8	4.37E-09	2.03E-09	5.23E-10
28.02.05	546.6	228.3	63.0	0.23	11.8	4.11E-09	1.72E-09	4.74E-10
07.03.05	559.1	258.9	63.4	0.28	11.8	5.12E-09	2.37E-09	5.80E-10
14.03.05	577.2	255.3	63.4	0.28	11.8	5.29E-09	2.34E-09	5.80E-10
21.03.05	583.9	234.4	76.6	0.28	11.8	5.35E-09	2.15E-09	7.02E-10
28.03.05	604.0	231.3	70.9	0.28	11.8	5.53E-09	2.12E-09	6.49E-10
05.04.05	640.8	203.9	48.0	0.43	11.8	9.01E-09	2.87E-09	6.75E-10
12.04.05	612.5	243.4	43.9	0.43	11.8	8.61E-09	3.42E-09	6.18E-10
19.04.05	666.3	212.0	67.4	0.43	11.8	9.37E-09	2.98E-09	9.49E-10
26.04.05	666.1	193.8	101.2	0.43	11.8	9.37E-09	2.73E-09	1.42E-09
03.05.05	708.0	181.6	44.3	0.65	11.8	1.51E-08	3.86E-09	9.42E-10
10.05.05	627.2	167.3	77.1	0.65	11.8	1.33E-08	3.56E-09	1.64E-09
06.06.05	608.9	136.0	116.4	1.69	11.8	3.37E-08	7.52E-09	6.43E-09
13.06.05	647.3	133.9	75.6	1.69	11.8	3.58E-08	7.40E-09	4.18E-09
05.07.05	684.3	82.8	95.7	3.45	11.8	7.72E-08	9.34E-09	1.08E-08
12.07.05	599.3	107.1	93.9	3.45	11.8	6.76E-08	1.21E-08	1.06E-08
19.07.05	680.9	109.6	97.7	3.45	11.8	7.68E-08	1.24E-08	1.10E-08

A4. Chemical flux rates of Ca, Mg, and SiO_2 in Bhagirathi River at Maneri during July'2004 to July'2005.

Date	Ca	Mg	SiO_2	Discharge (10^{12}L/month)	Area(10^3km^2)	Elementai reiease rate (mol/m^2/s)		
						Ca	Mg	SiO_2
19.07.04	207.4	88.5	20.6	1.17	4.071	2.30E-08	9.80E-09	2.28E-09
26.07.04	259.5	98.3	99.4	1.17	4.071	2.87E-08	1.09E-08	1.10E-08
02.08.04	227.2	87.6	101.1	1.19	4.071	2.56E-08	9.86E-09	1.14E-08
09.08.04	286.7	98.7	106.0	1.19	4.071	3.23E-08	1.11E-08	1.19E-08
16.08.04	565.5	189.4	108.5	1.19	4.071	6.36E-08	2.13E-08	1.22E-08
23.08.04	352.0	186.5	83.0	1.19	4.071	3.96E-08	2.10E-08	9.34E-09
30.08.04	793.6	359.5	78.1	1.19	4.071	8.93E-08	4.05E-08	8.78E-09
06.09.04	317.3	155.0	76.4	0.60	4.071	1.80E-08	8.81E-09	4.34E-09
13.09.04	249.4	62.0	69.0	0.60	4.071	1.42E-08	3.52E-09	3.92E-09
20.09.04	336.2	123.8	74.5	0.60	4.071	1.91E-08	7.03E-09	4.23E-09
27.09.04	414.1	193.5	93.7	0.60	4.071	2.35E-08	1.10E-08	5.32E-09
04.10.04	421.6	218.8	85.5	0.22	4.071	8.67E-09	4.50E-09	1.76E-09
11.10.04	388.7	190.4	104.4	0.22	4.071	8.00E-09	3.92E-09	2.15E-09
18.10.04	418.3	196.2	135.6	0.22	4.071	8.61E-09	4.04E-09	2.79E-09
25.10.04	402.2	193.0	122.5	0.22	4.071	8.28E-09	3.97E-09	2.52E-09
01.11.04	211.1	89.5	133.1	0.13	4.071	2.62E-09	1.11E-09	1.65E-09
08.11.04	198.8	80.0	120.4	0.13	4.071	2.47E-09	9.94E-10	1.49E-09
15.11.04	204.0	81.5	60.6	0.13	4.071	2.53E-09	1.01E-09	7.53E-10
22.11.04	209.2	80.3	57.9	0.13	4.071	2.60E-09	9.97E-10	7.19E-10
29.11.04	207.7	70.3	61.3	0.13	4.071	2.58E-09	8.73E-10	7.61E-10
06.12.04	255.4	96.7	62.0	0.10	4.071	2.49E-09	9.42E-10	6.03E-10
31.01.04	471.4	171.3	52.1	0.08	4.071	3.61E-09	1.31E-09	3.98E-10
07.02.05	434.5	155.1	61.3	0.07	4.071	2.87E-09	1.03E-09	4.05E-10
14.02.05	498.6	165.5	62.7	0.07	4.071	3.30E-09	1.10E-09	4.14E-10
21.02.05	478.4	188.7	62.0	0.07	4.071	3.16E-09	1.25E-09	4.10E-10
28.02.05	485.8	185.3	53.1	0.07	4.071	3.21E-09	1.23E-09	3.51E-10
07.03.05	461.9	163.5	61.0	0.09	4.071	3.90E-09	1.38E-09	5.14E-10
14.03.05	467.9	163.3	54.2	0.09	4.071	3.95E-09	1.38E-09	4.57E-10
21.03.05	364.5	137.0	61.0	0.09	4.071	3.08E-09	1.16E-09	5.14E-10
28.03.05	435.1	146.7	58.8	0.09	4.071	3.67E-09	1.24E-09	4.96E-10
05.04.05	346.7	125.5	58.2	0.14	4.071	4.60E-09	1.66E-09	7.71E-10
12.04.05	410.5	138.9	58.5	0.14	4.071	5.45E-09	1.84E-09	7.75E-10
19.04.05	373.7	166.8	53.6	0.14	4.071	4.96E-09	2.21E-09	7.10E-10
26.04.05	385.3	143.8	50.1	0.14	4.071	5.11E-09	1.91E-09	6.64E-10
03.05.05	385.8	190.1	44.3	0.42	4.071	1.55E-08	7.64E-09	1.78E-09
10.05.05	340.0	122.1	48.0	0.42	4.071	1.37E-08	4.91E-09	1.93E-09
17.05.05	321.3	147.0	42.9	0.42	4.071	1.29E-08	5.91E-09	1.72E-09
23.05.05	334.2	152.9	44.3	0.42	4.071	1.34E-08	6.15E-09	1.78E-09
30.05.05	328.1	144.1	44.8	0.42	4.071	1.32E-08	5.79E-09	1.80E-09
06.06.05	326.6	129.3	45.6	0.70	4.071	2.18E-08	8.63E-09	3.05E-09
13.06.05	341.0	162.5	40.9	0.70	4.071	2.28E-08	1.09E-08	2.73E-09
21.06.05	334.8	155.7	44.5	0.70	4.071	2.24E-08	1.04E-08	2.97E-09
28.06.05	247.6	132.9	46.3	0.70	4.071	1.65E-08	8.87E-09	3.09E-09
05.07.05	196.5	82.4	57.2	1.17	4.071	2.18E-08	9.13E-09	6.33E-09
12.07.05	317.3	84.8	43.3	1.17	4.071	3.51E-08	9.39E-09	4.79E-09
19.07.05	254.4	84.5	42.2	1.17	4.071	2.82E-08	9.35E-09	4.67E-09

A5. Temporal release of Calcium (Ca) and Magnesium (Mg) during dissolution of CC and DM at 25^0C and 5^0C (pH = 8.4).

Time (Hour)	(CC) Ca (mmol/L)		(DM) Ca (mmol/L)		(DM) Mg (mmol/L)	
	25^0C	5^0C	25^0C	5^0C	25^0C	5^0C
24	0.090	0.120	0.237	0.170	0.081	0.029
48	0.096	0.119	0.276	0.181	0.091	0.045
96	0.098	0.117	0.234	0.192	0.097	0.074
168	0.118	0.116	0.213	0.211	0.073	0.083
240	0.110	0.128	0.287	0.236	0.086	0.073
312	0.126	0.131	0.268	0.258	0.089	0.084
360	0.131	0.136	0.238	0.232	0.111	0.089
408	0.129	0.138	0.240	0.262	0.096	0.082
456	0.135	0.127	0.248	0.230	0.113	0.061
504	0.121	0.140	0.251	0.228	0.106	0.085
552	0.126	0.134	0.271	0.235	0.112	0.066
624	0.129	0.137	0.311	0.269	0.108	0.083
648	0.151	0.143	0.326	0.258	0.123	0.068
720	0.149	0.143	0.351	0.261	0.120	0.082
792	0.144	0.148	0.361	0.251	0.100	0.078
840	0.140	0.149	0.366	0.249	0.105	0.080

A6. Temporal release of Calcium (Ca) during dissolution of CC in mixed flow reactor at 25^0C (pH = 8.4).

Time (Hr)	Ca (mmol/L)
12	2.250
24	1.825
36	1.175
48	1.000
60	0.875
72	0.725
84	0.750
96	0.550
108	0.575
120	0.500
132	0.875
144	0.575
156	0.350
168	0.400
180	0.425

A7. Temporal release of Silica (Si) during dissolution of LG at 25^0C and 5^0C (pH = 8.4, 4.2, and 2.2).

Time (Hour)	Si release at 25^0C (mmol/L)			Si release at 5^0C (mmol/L)		
	pH = 8.4	pH = 4.2	pH = 2.2	pH = 8.4	pH = 4.2	pH = 2.2
24	0.026	0.017	0.036	0.016	0.013	0.035
48	0.029	-	-	0.018	-	-
72	0.033	0.015	0.04	-	0.013	0.036
96	-	-	-	0.019	-	-
120	0.04	0.017	0.059	-	0.014	0.045
168	-	0.019	0.066	0.022	0.015	0.044
192	0.037	-	-	-	-	-
216	-	0.018	0.055	-	0.017	0.055
240	-	-	-	0.02	-	-
264	0.058	0.018	0.077		0.016	0.062
312	-	0.019	0.073	0.025	0.014	0.072
360	-	0.022	0.089	0.026	0.015	0.088
336	0.063	-	-	-	-	-
384	0.07	-	-	-	-	-
408	-	0.016	0.102	0.025	0.014	0.074
432	0.074	-	-	-	-	-
456	-	0.022	0.086	0.027	0.015	0.092
480	0.076	-	-	-	-	-
504	-	0.018	-	0.023	0.015	0.089
528	0.081	-	-	-	-	-
552	-	0.022	-	0.026	0.016	0.087
576	0.069	-	-	-	-	-
600	-	0.021	0.08	-	-	0.084
624	-	-	-	0.024	-	-
648	0.073	0.022	0.109	0.028	0.017	0.091
696	0.092	0.023	0.113	-	0.014	0.095
720	-	-	-	0.031	-	-
744	-	0.023	0.113	-	0.017	0.095
768	0.109	-	-	-	-	-
792	-	-	-	0.029	-	-
840	0.091	-	-	0.032	-	-

A8. Temporal release of Silica (Si) during dissolution of GN at 25^0C and 5^0C (pH = 8.4, 4.2, and 2.2).

Time (Hour)	Si release at 25^0C (mmol/L)			Si release at 5^0C (mmol/L)		
	pH = 8.4	pH = 4.2	pH = 2.2	pH = 8.4	pH = 4.2	pH = 2.2
24	0.055	0.070	0.143	0.037	0.063	0.136
48	0.051	-	-	0.041	-	-
72	-	0.072	0.154	-	0.066	0.143
96	0.048	-	-	0.039	-	-
120	-	0.086	0.218	-	0.053	0.175
168	0.062	0.078	0.210	0.044	0.053	0.170
216	-	0.065	0.189	-	0.072	0.154
240	0.084	-	-	0.037	-	-
264	-	0.106	0.255	-	0.076	0.164
312	0.062	0.108	0.250	0.040	0.067	0.200
360	0.081	0.113	0.253	0.044	0.080	0.207
408	0.083	0.135	0.242	0.047	0.098	0.204
456	0.079	0.142	0.273	0.052	0.080	0.208
504	0.082	0.119	0.282	0.055	0.086	0.210
552	0.116	0.112	0.289	0.053	0.103	0.214
600	-	0.138	0.285	-	0.089	0.221
624	0.116	-	-	0.057	-	-
648	0.122	0.108	0.298	0.056	0.077	0.261
696	-	0.130	0.338	-	0.099	0.236
720	0.118	-	-	0.062	-	-
744	-	0.130	0.407	-	0.073	0.262
792	0.116	-	-	0.051	-	-
840	0.140	-	-	0.054	-	-

A9. Temporal release of Silica (Si) during dissolution of CQ at 25^0C and 5^0C (pH = 8.4, 4.2, and 2.2).

Time (Hour)	Si release at 25^0C (mmol/L)			Si release at 5^0C (mmol/L)		
	pH = 8.4	pH = 4.2	pH = 2.2	pH = 8.4	pH = 4.2	pH = 2.2
24	0.093	0.013	0.042	0.059	0.013	0.031
48	0.082	-	-	0.059	-	-
72	0.124	0.012	-	-	0.013	0.031
96	-	-	-	0.055	-	-
120	0.124	0.012	0.045	-	0.014	0.031
168	-	0.013	-	0.057	0.014	-
192	0.168	-	-	-	-	-
216	-	0.012	0.043	-	0.013	0.032
240	-	-	-	0.056	-	-
264	0.145	0.012	0.040	-	0.014	0.029
312	-	-	0.045	0.061	-	0.032
336	0.207	-	-	-	-	-
360	-	0.013	0.042	0.058	0.015	0.032
384	0.191	-	-	-	-	-
408	-	0.013	0.043	0.066	0.014	0.032
432	0.219	-	-	-	-	-
456	-	0.013	-	0.066	0.015	-
480	0.235	-	-	-	-	-
504	-	0.014	0.042	0.072	0.014	0.032
528	0.234	-	-	-	-	-
552	-	0.014	0.043	0.066	0.014	0.032
576	0.259	-	-	-	-	-
600	-	0.015	0.042	-	0.016	0.032
624	-	-	-	0.073	-	-
648	0.292	0.014	0.043	0.065	0.015	0.033
696	0.329	0.014	0.049	-	0.015	0.036
720	-	-	-	0.074	-	-
744	-	0.014	0.044	-	0.014	0.030
768	0.394	-	-	-	-	-
792	-	-	-	0.077	-	-
840	0.407	-	-	0.076	-	-

A10. Temporal release of targeted elements during dissolution of PY at temperature 25^0C and 5^0C (pH = 8.4).

Time (Hour)	Element released at 25^0C (mmol/L)			Time (Hour)	Element released at 5^0C (mmol/L)		
	Ca	Mg	Si		Ca	Mg	Si
24	0.066	0.007	0.013	24	0.102	0.008	0.013
48	0.066	0.008	0.011	48	0.105	0.011	0.014
72	0.059	0.010	0.012	96	0.103	0.017	0.012
120	0.053	0.007	0.013	168	0.108	0.018	0.012
192	0.060	0.010	0.013	240	0.107	0.020	0.013
264	0.071	0.021	0.014	312	0.102	0.025	0.013
336	0.065	0.028	0.013	360	0.105	0.024	0.012
384	0.086	0.029	0.013	408	0.103	0.024	0.014
432	0.081	0.033	0.013	456	0.108	0.018	0.014
480	0.091	0.025	0.014	504	0.107	0.017	0.015
528	0.091	0.032	0.015	552	0.107	0.020	0.013
576	0.110	0.038	0.015	624	0.109	0.022	0.013
648	0.113	0.041	0.016	648	0.107	0.025	0.012
696	0.114	0.044	0.016	720	0.108	0.029	0.015
768	0.116	0.051	0.016	792	0.108	0.023	0.014
840	0.116	0.052	0.017	840	0.107	0.028	0.015

A11. Temporal release of Ca, Mg, and Si during dissolution of KS at 25^0C and 5^0C (pH= 8.4).

Time (Hour)	Element released at 25^0C (mmol/L)			Element released at 5^0C (mmol/L)		
	Ca	Mg	Si	Ca	Mg	Si
24	0.153	0.126	-	0.156	0.147	-
48	0.190	0.145	0.044	0.159	0.144	0.069
72	0.148	0.145	0.036	0.116	0.081	0.075
120	-	0.149	0.033	0.150	0.127	0.068
192	0.207	-	0.062	0.148	0.130	0.077
264	0.200	0.156	0.072	0.167	0.131	-
336	0.189	0.159	0.079	0.153	-	0.071
384	0.248	0.157	-	0.161	0.135	0.077
432	0.245	-	0.060	0.155	0.150	0.075
480	0.237	0.143	-	0.156	0.140	-
528	0.298	-	-	0.158	0.138	0.076
576	0.289	0.177	0.095	0.169	-	0.077
648	0.304	0.156	0.131	0.206	-	0.081
696	0.297	-	0.140	0.166	0.145	0.080
768	0.285	0.160	0.142	0.177	0.138	0.080
840	0.356	0.166	0.131	0.202	0.138	0.082

A12. Temporal release of Ca, Mg, and Si during dissolution of KS at 25^0C and 5^0C (pH= 4.2).

Time (Hour)	Element released at 25^0C (mmol/L)			Element released at 5^0C (mmol/L)		
	Ca	Mg	Si	Ca	Mg	Si
24	14.613	10.185	0.189	23.123	7.041	0.186
72	16.546	-	0.204	25.163	8.123	0.221
120	16.384	10.519	0.199	22.880	7.716	0.221
168	-	10.296	0.201	26.870	8.777	0.214
216	19.665	10.652	-	24.510	8.074	0.217
264	19.138	12.199	0.203	27.363	9.001	0.218
360	21.338	12.080	0.191	24.750	10.218	0.225
408	20.925	12.202	0.220	25.038	9.418	0.222
456	22.225	12.720	0.225	28.425	10.432	0.211
504	24.013	12.159	0.214	25.125	9.165	0.212
552	25.980	11.029	0.206	27.740	9.802	-
600	27.610	11.947	0.216	27.780	8.815	0.228
648	27.750	12.630	0.225	31.338	10.296	0.239
696	26.163	12.416	0.220	29.763	9.568	0.208
744	28.550	13.465	0.217	28.863	9.560	0.211

A13. Temporal release of Ca, Mg, and Si during dissolution of KS at 25^0C and 5^0C (pH= 2.2).

Time (Hour)	Element released at 25^0C (mmol/L)			Element released at 5^0C (mmol/L)		
	Ca	Mg	Si	Ca	Mg	Si
24	6.387	1.944	0.100	5.933	1.049	0.145
72	5.785	2.049	0.107	6.377	1.010	0.135
120	6.470	1.963	0.109	6.495	1.194	0.145
168	5.915	-	0.102	5.946	1.024	-
216	6.680	1.870	-	6.080	-	0.129
264	-	-	0.103	6.988	1.094	0.133
312	6.675	1.916	0.105	6.763	1.167	0.140
360	7.063	2.057	0.105	6.513	1.245	0.151
408	7.150	2.051	0.113	6.913	1.309	0.151
456	-	-	-	-	-	0.156
504	7.313	2.137	0.125	6.888	1.252	0.149
552	7.550	2.113	0.122	6.820	1.284	0.158
600	6.890	2.230	0.126	6.500	1.116	0.150
648	7.040	2.237	0.126	6.260	1.205	0.149
696	6.690	2.383	0.126	6.670	1.202	0.150
744	7.650	2.326	0.127	7.210	1.432	0.150

A14. Temporal release of Ca and Mg at room temperature (pH = 8.4, 4.2, 2.2) during soil column dissolution experiment. (values in mmol/L)

Time (Hour)	Temporal release of major cations at room temeprature					
	8.4pH		4.2pH		2.2pH	
	Ca	Mg	Ca	Mg	Ca	Mg
24	0.027	0.054	-	-	3.700	2.107
48	-	-	10.520	10.765	-	-
72	-	-	8.470	12.354	2.380	2.284
74	0.035	0.090	-	-	-	-
96	0.035	0.108	11.875	10.947	2.670	1.148
120	0.045	0.131	16.925	9.342	2.970	2.543
144	0.097	0.126	19.350	14.436	3.075	2.716
168	0.066	0.151	13.790	16.016	3.210	1.778
192	-	-	17.465	18.329	3.285	1.827
216	0.072	0.126	14.270	17.407	4.190	2.210
240	0.068	0.138	20.780	14.041	4.785	2.280
264	0.080	0.140	16.315	17.695	5.320	2.864
278	-	-	19.640	18.856	5.890	2.535
302	0.100	0.144	22.850	20.996	6.255	2.741
350	0.127	0.150	17.280	16.058	6.330	2.218
374	-	-	20.395	20.979	7.260	2.214
398	0.130	0.164	23.615	22.008	7.875	2.325
446	0.113	0.156	24.225	20.593	7.055	2.560
470	0.116	0.148	20.965	23.424	8.425	3.358
494	0.151	0.169	22.385	25.893	7.725	2.111
518	0.146	0.158	-	-	-	-
542	-	-	26.935	25.370	6.840	2.366
566	0.168	0.166	-	-	-	-
590	-	-	25.355	27.971	8.905	2.029
614	0.136	0.154	24.870	28.782	8.470	2.115
638	0.126	0.160	27.695	29.650	10.225	2.576
662	0.177	0.199	25.160	31.317	7.785	2.905
686	0.153	0.195	28.075	30.704	8.010	3.050
734	0.199	0.184	-	-	-	-

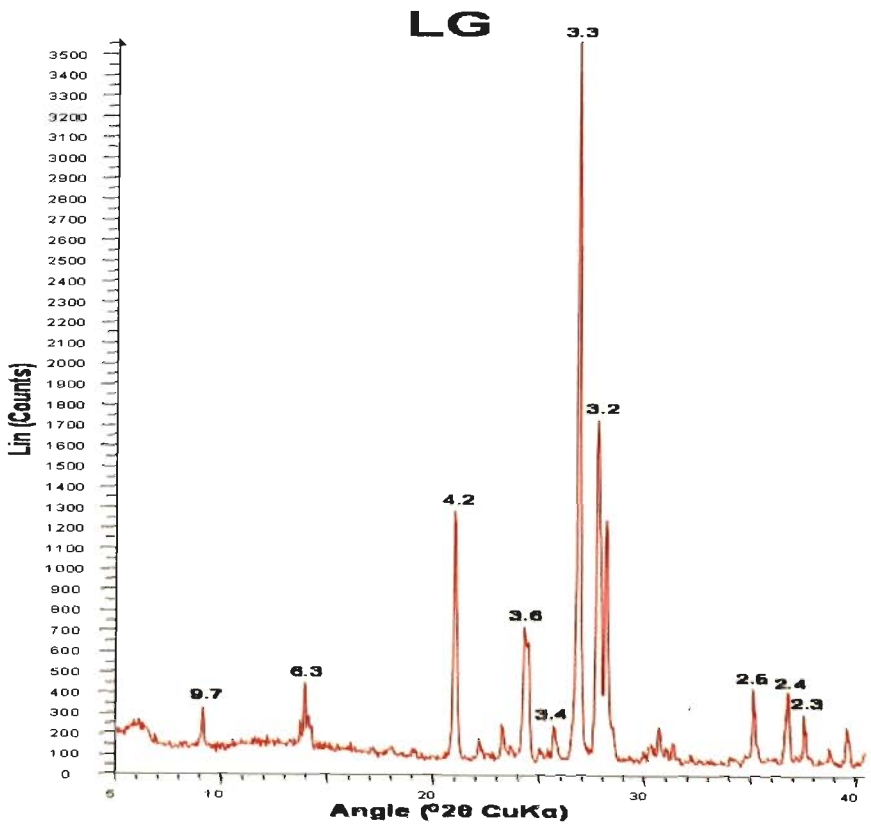

B1. This diffractogram represents sample of LG. The values written above the peaks refer to their d-spacing values in angstroms (A^0). The 9.7, 3.4 and 2.4 peaks suggest the presence of mica, the peak 6.3 indicates tourmaline, the peak 4.2 is either orthoclase or quartz, the peak 3.3 indicates quartz, the peak 3.6 is iron oxide, 3.2 suggest albite and the peak 2.5 is either hornblende or hypersthene.

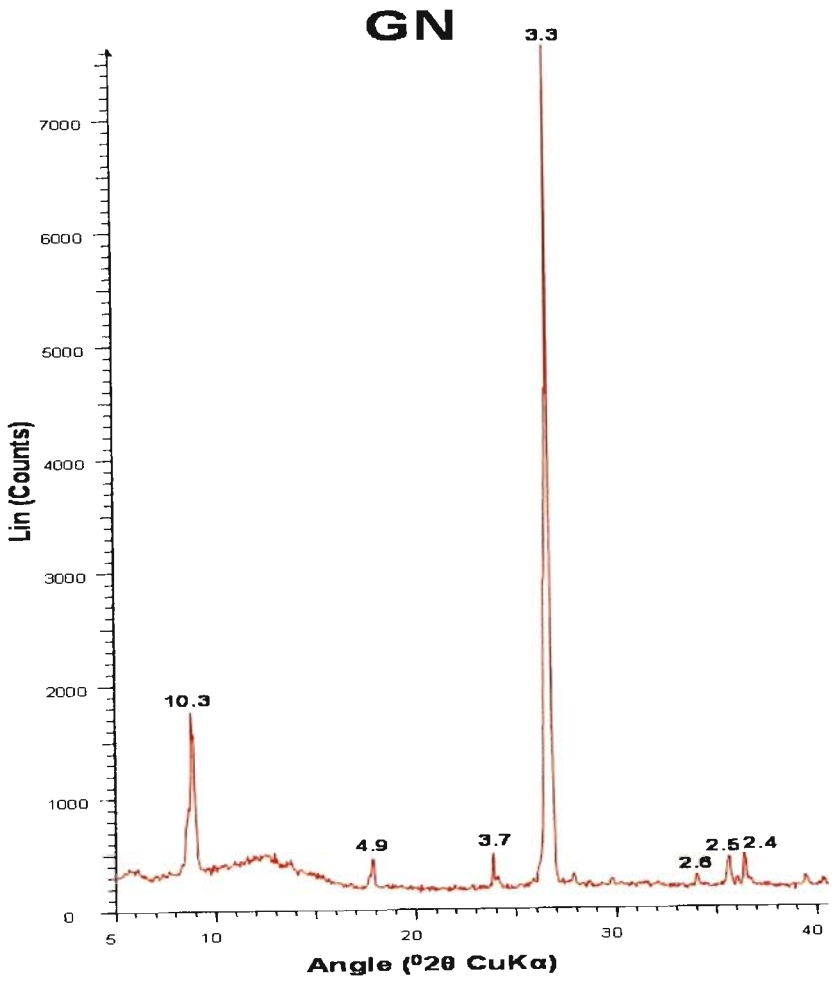

B2. This diffractogram represents sample of GN. The values written above the peaks refer to their d-spacing values in angstroms (A^0). The peaks 10.3, 4.9 and 3.7 suggest the presence of mica, the peaks 3.3 and 2.4 indicate quartz, 2.6 suggest garnet, and the peak 2.5 is kyanite.

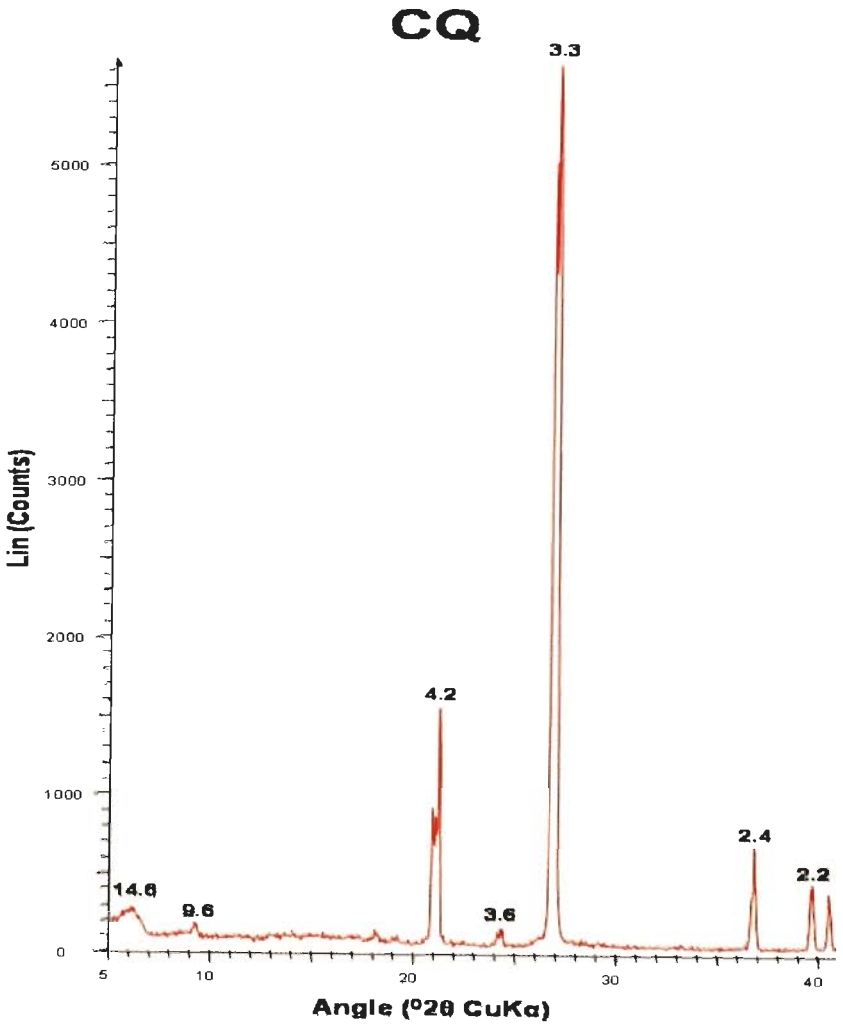

B3. This diffractogram represents sample of CQ. The values written above the peaks refer to their d-spacing values in angstroms (A^0). The peak 14.6 represents the presence of chlorite, the peak 9.6 indicates mica, the peaks 3.3, 4.2, 2.4 and 2.2 indicate quartz, and the peak 3.6 is iron oxide.

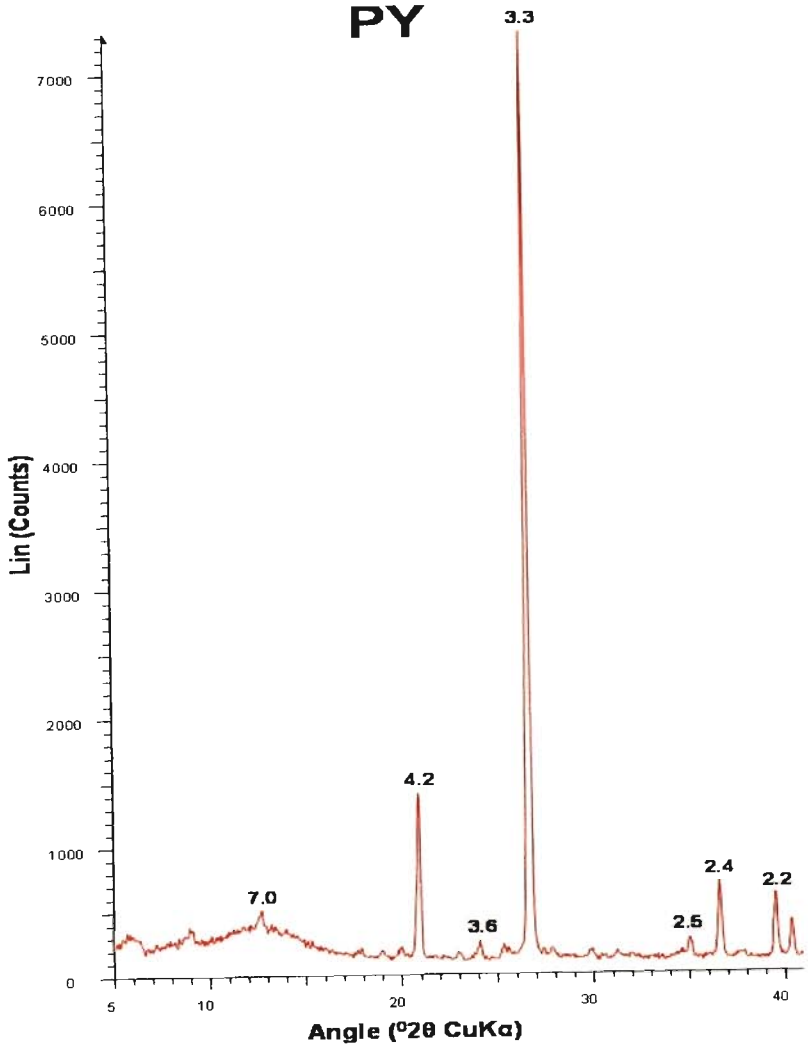

B4. This diffractogram represents sample of PY. The values written above the peaks refer to their d-spacing values in angstroms (A^0). The peak 7.0 represents either kaolinite, chamosite or chlorite, the peak 4.2 represents either orthoclase or quartz, the peaks 2.4 and 2.2 indicate quartz, 3.6 is iron oxide, and the peak 2.5 suggests augite.

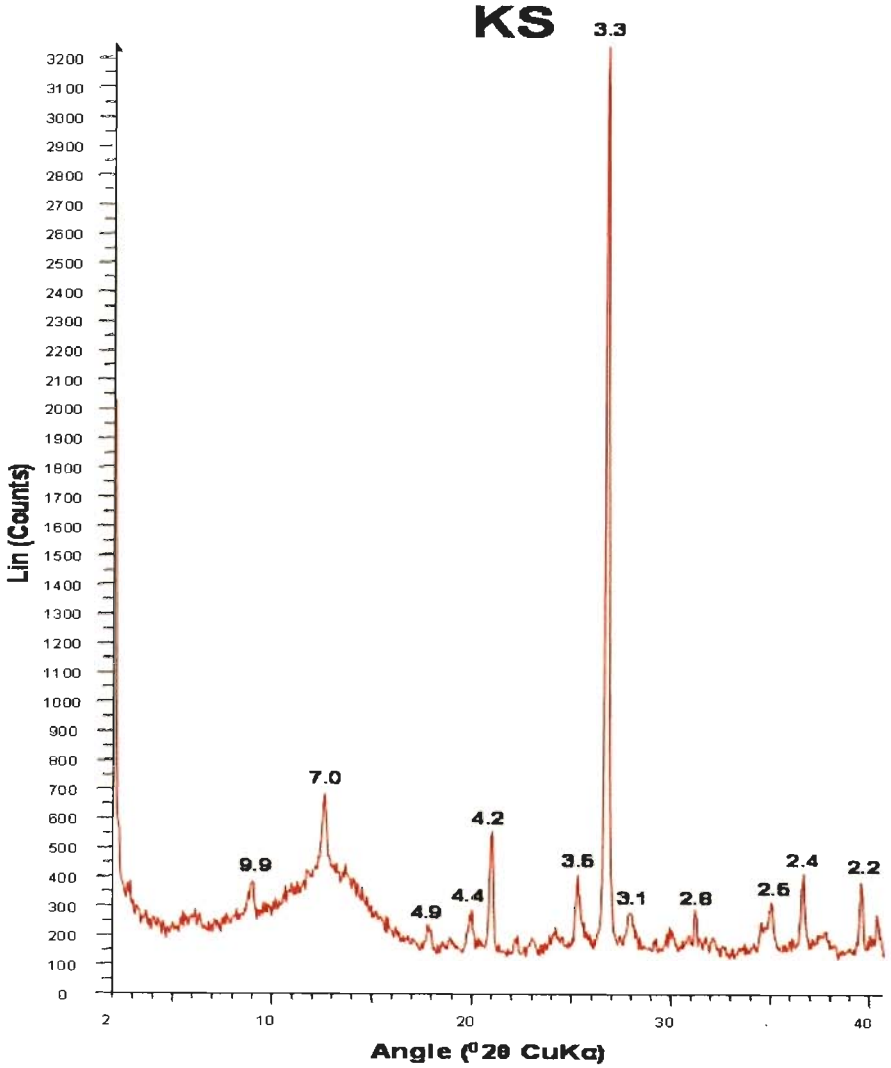

B5. This diffractogram represents sample of KS. The values written above the peaks refer to their d-spacing values in angstroms (A^0). The peaks 9.9, 4.9, and 4.4 suggest the presence of illite, the peaks 7.0, 3.5, and 2.5 indicate kaolinite, the peak 4.2 represents either orthoclase or quartz, the peaks 3.3, 2.4 and 2.2 indicates quartz, the peak 3.1 is albite and the peak 2.8 is gypsum.

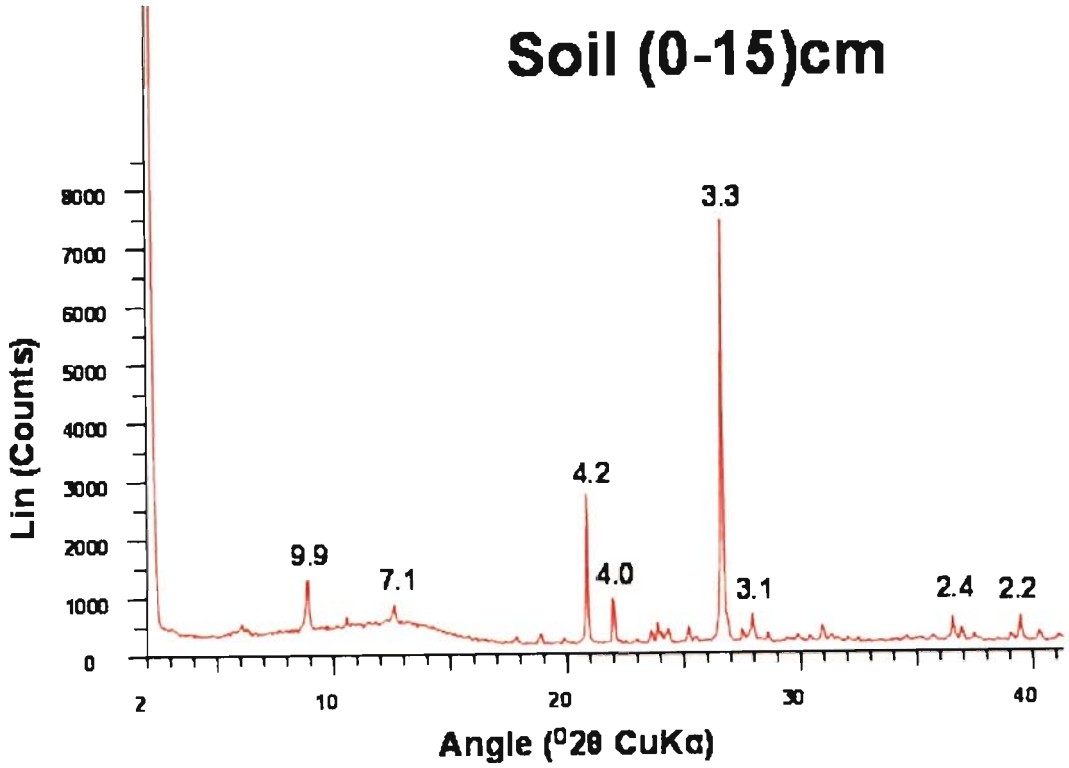

B6. This diffractogram represents sample of soil at top layer (0-15 cm). The values written above the peaks refer to their d-spacing values in angstroms (A^0). The peak 9.9 represents either illite or mica, the peak 7.1 suggests either kaolinite or chamosite, the peak 4.2 is either orthoclase or quartz, peaks 4.0 and 3.1 is albite, the peaks 3.3 and 2.2 indicate quartz, and 2.4 represents iron oxide.

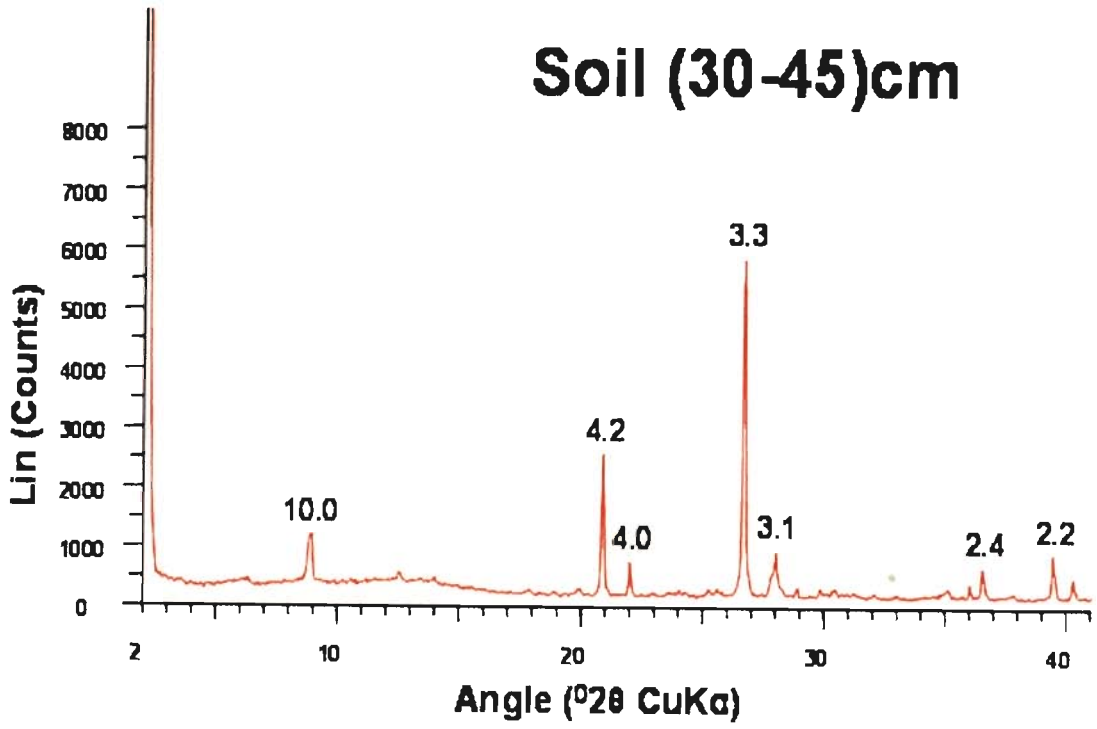

B7. This diffractogram represents sample of soil in middle layer (30-45 cm). The values written above the peaks refer to their d-spacing values in angstroms (A^0). The peak 10.0 represents either illite or mica, the peak 4.2 is either orthoclase or quartz, peaks 4.0 and 3.1 is albite, the peaks 3.3 and 2.2 indicate quartz, and 2.4 represents iron oxide.

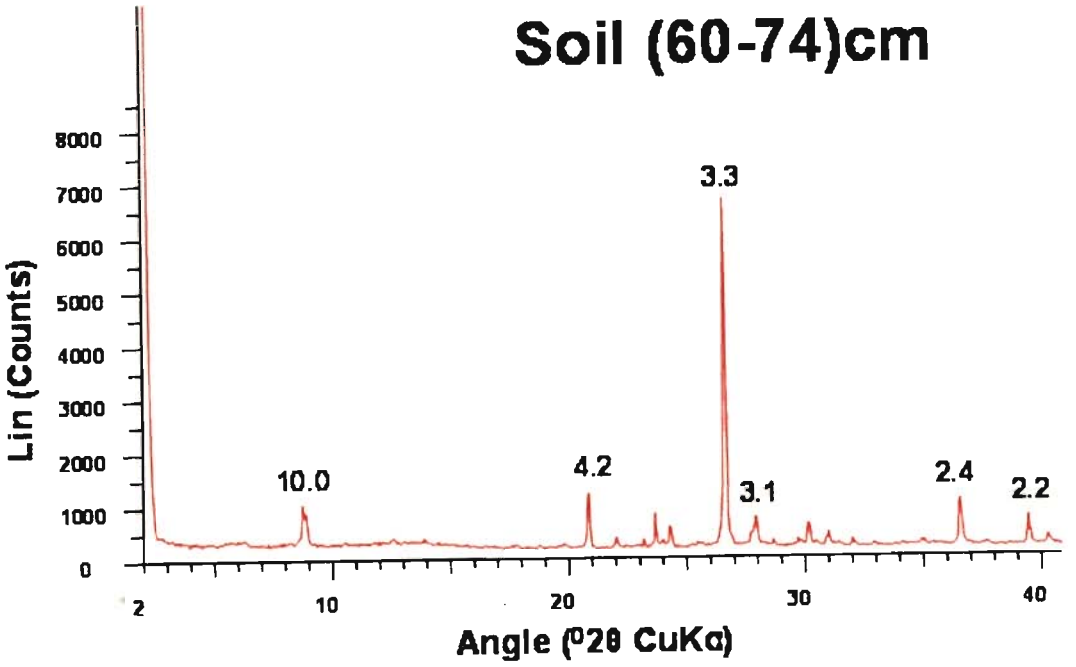

B8. This diffractogram represents sample of soil at bottom layer (60-74 cm). The values written above the peaks refer to their d-spacing values in angstroms (A^0). The peak 10.0 represents either illite or mica, the peak 4.2 is either orthoclase or quartz, peak 3.1 is albite, the peaks 3.3 and 2.2 indicate quartz, and 2.4 represents iron oxide.